TARGETING MUTANT *KRAS* IN PANCREATIC CANCER

Tikvah Katheryn Hayes

A dissertation submitted to the faculty of the University of North Carolina at Chapel Hill in partial fulfillment of the requirements for the degree of Doctor of Philosophy in the Curriculum in Genetics and Molecular Biology.

Chapel Hill
2015

Approved by:

Albert S. Baldwin

Christopher M. Counter

Channing J. Der

Gary L. Johnson

William Y. Kim

ABSTRACT

Tikvah Katheryn Hayes: Targeting mutant *KRAS* in pancreatic cancer
(Under the direction of Channing Der)

The development of pharmacologic inhibitors of the KRAS oncoprotein, which is mutated in ~30% of all human cancers, has been at the forefront of drug discovery for the last three decades. Despite intensive efforts by the pharmaceutical industry, no effective anti-KRAS strategies have reached the cancer patient. While many approaches to achieve this are being pursued, arguably inhibition of mutant *KRAS* effector signaling is considered the most promising to block KRAS-driven cancer growth. The best-validated downstream effector of KRAS is a three-tiered protein kinase cascade, the Raf-MEK-ERK protein kinase cascade, where KRAS activates Raf, which then activates MEK, and MEK then activates ERK. Activated ERK then activates a complex spectrum of signaling events that then drive cancer growth. Unfortunately, inhibitors of the first two levels, targeting Raf or MEK, have proven ineffective in mutant *KRAS* cancers. The ineffectiveness of anti-Raf and –MEK therapies has been attributed to inhibitor-induced resistance mechanisms, where the majority cause reactivation of ERK signaling to bypass the action of these inhibitors. Our studies sought to determine whether pharmacological inhibition of the last step at ERK will be more efficacious than treatment with either MEK or Raf inhibitors in mutant *KRAS* cancers.

In our studies, we first determined that pharmacologic inhibition of ERK suppressed the growth of a subset of *KRAS*-mutant pancreatic cancer cell lines by inducing both cycle cell arrest and apoptosis. Interestingly, we found that concurrent PI3K inhibition, another well-established KRAS effector, modulated ERK inhibitor sensitivity by enhancing the apoptotic phenotype. Next, we

employed a drug sensitivity screen to identify novel inhibitor combinations that enhanced ERK inhibitor sensitivity. We identified the PI3K-AKT-mTOR signaling cascade as a potent modulator of ERK inhibitor sensitivity, which was consistent with our previous finding where concurrent PI3K inhibition combination enhanced ERK inhibitor sensitivity. We unexpectedly found that long-term treatment of sensitive cell lines caused cellular senescence, a type of irreversible growth arrest, mediated in part by causing degradation of Myc and activation of the p16-RB tumor suppressor pathway. Next, we performed a novel genetic gain-of-function screen to identify mechanisms of acquired resistance to ERK inhibition. Interestingly, we identified, once again, the PI3K-AKT signaling cascade, as modulator of ERK inhibitor sensitivity. We also found p38 to be an important modulator or ERK inhibitor sensitivity. Finally, to investigate *de novo* resistance to ERK inhibition, we used a loss-of-function screen to identify kinases whose inhibition in combination with ERK inhibitor treatment resulted in sensitivity. Future studies will be needed to elucidate the mechanisms behind these modulators of pharmacological ERK inhibition. Collectively, our findings not only revealed distinct consequences of inhibiting this kinase cascade at the level of ERK, but identified inhibitor combinations that will be informative for potential clinical trials.

ACKNOWLEDGEMENTS

First, I would like to thank Channing J. Der and the Der Lab members, past and present, for supporting my scientific development over the last 6 years. Specifically, I would like to acknowledge Jeran S. Stratford, Timothy D. Martin, Tai-Young Kim, David J. Reiner, and Nicole F. Neel for guidance and support, without which I would not be the scientist I am today. Additionally, I would like to acknowledge Kirsten L. Bryant, Samuel D. George, and Swapnil Kher for their enthusiasm and willingness to collaborate, which significantly improved the Der Lab work environment during the later half of my graduate studies. I would also like to recognize members of the Baldwin, Davis, Kim, and Yeh labs for letting me dig through their freezers and supplies to in order to attain reagents. My extensive network of collaborators really perpeled by Furthermore, I would like to thank my committee members Albert S. Baldwin, Christopher M. Counter, Gary L. Johnson, and William Y. Kim for their time, interest, and insightful discussion.

Next, I would like to acknowledge IMSD (Initiative for Maximizing Student Diversity) for support me during my graduate studies. As a part of this organization I was fortunate enough to make some awesome friends that pushed me through the highs and lows of graduate school. I would like to acknowledge Jasmyn Adams, Samira A. Brooks, Raquel Burger-Calderon, LeShara M. Fulton, Megan and Nicholas C. Gomez, Grace O. Silva, and Kimberly S. Williams for their contributions to my success. I would also like to recognize the members of Pharm Club, Rebecca N. Bauer, Melissa Ellermann, Kimberly Maxfield, Ernesto Perez-Chanona, and Kenton T. Woodard for embarking on interesting adventures in North Carolina with me, and for constant support and entertainment during graduate school. Finally, I would like to thank Kate E. Coleman and Crystal A. Waters for making graduate school a more enjoyable experience.

I would like to acknowledge all the administrative support I received from IMSD, GMB (Curriculum in Genetics and Molecular Biology), and Lineberger Comprehensive Cancer Center (LCCC). Each of these organizations made it easier for me to focus solely on my science.

Chapel Hill is home to a vibrant rugby community. The last 5 years I have been privileged to be part of the University of North Carolina Woman's Rugby Football Club (UNCWRFC). There really aren't words that can accurately capture what the members and this experience have meant to me, and my development as a person and a professional. I would like to specifically recognize the members that have been here with me from the beginning: Johnathan R. Atkeison, Ariel Esperancilla, Cameron Gunn, Brittany N. Lademann, D'Chante McKenzie, and H. James Morrison. I would also like to acknowledge 2016 four year graduating seniors: Lindsey J. Broadwell, Nicole R. Davis, Tanya K. Houston, Katherine D. Lutton, Lindsey C. Oliver, and Naya E. Tapper. I would also like to acknowledge members of the the Chapel Hill Warriors and Highlanders for filling my summers with touch rugby.

I would not have been successful without the support of my friends outside of UNC Chapel Hill community. I would like to acknowledge my friends from California, Leanna R. Corpus, Kristen Driskell, Victoria Gargiso, Nancy H. Godsk, Sarah Harstrom, Emily Ogata, and Katielee S. Pallis for all their love and support throughout the years. I would also like to recognize the Raleigh crew, Brie Butler, Kira Cervenka, Erin Gillikin, Kacy L. Hunt, Deanna Tesch, and Katie Wrigglesworth for our many adventures. Their love and support helped me to adjust to North Carolina living and made it a place I could call home. Anaiah L. Younger and Amber B. Cardenas have been my best friends for the better part of two decades, their constant love and unwavering support has been instrumental through this process.

Finally, I would like to thank my mom, Sarajane Hayes. She truly is the wind beneath my wings.

TABLE OF CONTENTS

LIST OF TABLES

LIST OF FIGURES

LIST OF ABRREVIATIONS AND SYMBOLS

A-Raf, A- rapidly accelerated fibrosarcoma

AKT (PKB), protein kinase b

AML, acute myeloid leukemia

ATP, adenosine triphosphate

AURKB, aurora kinase b

B-Raf, B- rapidly accelerated fibrosarcoma

C-terminal, carboxy-terminal

CDKN2A/INK4A (p16), cyclin dependent kinase inhibitor 2A

CFP, cyan fluorescent protein

CK2, casein kinase 2

COSMIC, catalogue of somatic mutations in cancer

COT (Tpl2 or MAP3K8), cancer osaka thyroid

CRD, cysteine-rich domain

CRISPR, clustered regularly interspaced short palindromic repeats

DMBA, 7,12-dimethylbenz[*a*]anthracene

DNAseq, deoxyribonucleic acid sequencing

DSS, drug sensitivity screen

DUSP, dual specificity phosphatase

EGFR, epidermal growth factor receptor

ELK-1, ETS-like gene 1

ERK1/2, extracelluar signal-regulated kinases

ETS, E26 transformation-specific

FFTase, farnesyltransferase enzyme

FOLFIRINOX, combination of folinic acid (FOL), fluorouracil (F), irinotecan (IRIN), and oxaplatin

(OX)

FOS, FBJ murine osteosarcoma viral oncogene homolog

FTI, farnesyltransferase inhibitor

GEMM, genetically engineered mouse model

GFP, green fluorescent protein

GGTase, geranylgeranyltransferase-I enzyme

GI_{50}, growth inhibition at 50%

GSK3β, glycogen synthase kinase 3 beta

GDP, guanine diphosphate

GTP, guanine triphosphate

GTPase, guanine triphosphate enzyme

HRAS, Harvey Rat sarcoma

HVR, hypervariable region

ICMT, isoprenylcysteine carboxyl methyltransferase

JAK, janus kinase

JNK, c-Jun N-terminal protein kinase

KPC, K-Ras $^{LSLG12D/+}$ $p53^{R172H/+}$ Pdx1:Cre

KRAS, Kirsten Rat sarcoma

K-Ras4A, KRAS splice variant

K-Ras4B, KRAS splice variant

KSR-1, kinase suppressor of Ras 1

MAPK, mitogen activated protein kinase

MAP2K, mitogen activated protein kinase kinase

MAP3K, mitogen activated protein kinase kinase kinase

MEK1/2, mitogen/extracellular signal-regulated kinase

MiB, multiplex inhibitior beads

MLK-3 (MAP3K11), mitogen activated protein kinase kinase kinase 11

MNK (ATP7A), menkes

MOS, moloney murine sarcoma

mRNA, messenger ribonucleic acid

M/S, mass spectrometry

MSK, mitogen and stress activated protein kinase

mTOR, mammalian target of rapamycin

MTT, 3-(4,5-dimethylthiazol-2-yl)-2,5-diphenyltetrazolium bromide

MYC, avian myelocytomatosis viral oncogene homolog

NFκB, nuclear factor kappa b

NRAS, Neuroblastoma Rat sarcoma

p21, protein 21

p27, protein 27

p38, protein 38

PAK, p21 associated kinase

PanINs, pancreatic intraepithelial neoplasia

PARP, poly ADP ribose polymerase

PDAC, pancreatic ductal adenocarcinoma

PDK, phosphoinositide-dependent protein kinase

PDX, patient derived xenograft

PI3K (PIK3CA), class I phosphatidylinositol-4,5-bisphosphate 3-kinases

PLCε, phospholipase C epsilon

PTEN, phosphatase and tensin homolog

PRKCH, protein kinase eta

RA, Ras association domain

Rac1, Ras-related C3 botulium toxin substrate 1

Raf, rapidly accelerated fibrosarcoma

Raf-1 (c-Raf), rapidly accelerated fibrosarcoma 1

Ral, Ras-related protein

RalGDS, ral guanine nucleotide dissociation stimulator

RAS, Rat Sarcoma

RasGAP, Ras GTP activating protein

RasGEF, Ras guanine exchange factor

RB, retinoblastoma

RBD, Ras binding domain

Rce1, Ras converting CAAX endopeptidase 1

RFP, red fluorescent protein

RNAi, ribonucleic acid interference

RNAseq, ribonucleic acid sequencing

RPPA, reverse phase protein array

RSK, ribosomal S6 kinase

RT-PCR, real-time polymerase chain reaction

RTK, receptor tyrosine kinase

shRNA, short hairpin ribonucleic acid

siRNA, small interfering ribonucleic acid

SMAD4 (DPC4), deleted in pancreatic carcinoma, locus 4

SOS1, Son of Sevenless protein

SRC, rous sarcoma

Tiam1, T-cell lymphoma invasion and metastasis-inducing protein 1

TP53, tumor protein 53

TPA, phorbol ester 12-O-tetradecanoylphorbol 13-acetate

YAP1, yes-associated protein 1

YFP, yellow fluorescent protein

β beta

μ, mu

γ, gamma

CHAPTER 1: INTRODUCTION

1.1 RAS genes and Ras proteins

The three human *RAS* genes encode four highly related 188-189 amino acid 21 kDa small GTPases (Figure 1.1). K-Ras4A and K-Ras4B are splice variants encoded by alternative exon 4 usage and differ primarily at their C-terminal sequences. The *RAS* genes comprise one the most frequently mutated gene family in human cancer (Cox and Der, 2010). In cancer and various developmental disorders (referred to as Rasolopaties), *RAS* genes harbor missense mutations that encode mutant proteins that are altered in their biochemical properties (Prior et al., 2012; Rauen, 2013).

Ras proteins act as binary switches regulating a number of biological processes that include cellular proliferation, survival and differentiation. Ras proteins share 90% sequence identity in the G domain (1-164), which is important for guanine nucleotide binding and GTP hydrolysis, and interaction with regulators and effectors. In contrast, the C-terminal 24/25 residues exhibit significant sequence divergence (8% amino acid identity) and is therefore referred to as the hypervariable region (HVR).

Ras activity is regulated by two distinct classes of regulatory proteins: Ras-selective guanine exchange factors (RasGEFs) and GTPases activating proteins (RasGAPs) (Figure 1.2) (Vigil et al., 2010). RasGEFs (e.g., Sos1) accelerate the slow intrinsic guanine nucleotide exchange rate of Ras proteins. Since the intracellular concentration of GTP is 10 times more abundant than GDP, this favors formation of the active Ras-GTP complex. Once bound to GTP, Ras is considered activated and can bind to a number of catalytically distinct downstream

effectors to regulate a diversity of cytoplasmic signaling networks. In order to terminate Ras signal transduction, RasGAPs (e.g., neurofibromin, p120 RasGAP) bind to Ras and accelerate its weak intrinsic GTP hydrolysis activity, returning Ras to the inactive GDP-bound form. However, when Ras proteins are mutated, they display altered intrinsic and GAP-stimulated GTPase activity, favoring a GTP-bound state and promotion of aberrant signal transduction.

The C-terminal sequence is crucial for Ras membrane association and subcellular localization (Figure 1.3). The terminal four residues comprise the CAAX motif (C = cyteine, A = aliphatic amino acid, X = terminal amino acid), which signals for three sequential posttranslational modifications that increase hydrophobicity and promote membrane association (Ahearn et al., 2012). The sequences immediately upstream of the CAAX motif contain a second membrane targeting signal. For H-Ras, K-Ras4A and N-Ras, cysteine residues signal for covalent addition of a palmitate fatty acid, whereas K-Ras4B has a polybasic stretch that serves a similar role. K-Ras4B additionally contains a serine residue (S181) that is phosphorylated by protein kinase C. This modification regulates a dynamic trafficking between the plasma and endomembranes. In addition to association with the plasma membrane, Ras proteins are also found in other cellular endomembrane compartments that include the Golgi, endoplasmic reticulum, mitochondria, and endosomes.

1.2 Ras and cancer

In 1982, the *RAS* genes became the first mutated genes identified in human cancers (Cox and Der, 2010). In this chapter we discuss the role of *RAS* gene mutations in cancer. In particular, we focus on the *RAS* gene most commonly mutated in human cancers, the *KRAS* oncogene (Prior et al., 2012). Although *KRAS* mutations are found in many cancer types, the highest frequency is found in pancreatic ductal adenocarcinoma (PDAC) at ~95% (Bass et al., 2011; Biankin et al., 2012; Jones et al., 2008; Seshagiri et al., 2012; Wood et al., 2007).

PDAC is the fourth leading cancer related death in the United States (Siegel et al., 2014). Among 45,220 individuals diagnosed with PDAC in 2014, approximately 38,000 died of the disease (Siegel et al., 2014). While the mortality rate for most cancers is declining, PDAC is projected to become the second most common cause of cancer-related death by 2020. Given the vague clinical symptoms and the lack of effective screening methods, only 10-20% of PDAC patients are candidates for curative resection at the time of diagnosis. Even with surgical resection followed by adjuvant therapy, the median overall survival of those patients is around two years (Conroy et al., 2011; Neoptolemos et al., 2010; Oettle et al., 2007). Among the rest of the PDAC patients who are not candidates for resection, half of them have localized disease (borderline resectable and locally-advanced disease) and half have metastatic disease at the time of diagnosis. Patients with local disease are most often treated with chemotherapy with or without radiation, and their median overall survivals are around 15 months (Huguet et al., 2007). In patients with metastatic PDAC, the prognosis is extremely dismal. With the recent development of chemotherapy regimens such as FOLFIRINOX (Conroy et al., 2011) and gemcitabine plus nab-paclitaxel (Von Hoff et al., 2013), the survival of metastatic PDAC has moved beyond 6 months (Burris et al., 1997), but remains less than one year. At present, targeted therapies have not provided any meaningful clinical benefit for PDAC patients despite the approval of the EGFR inhibitor erlotinib (Moore et al., 2007). The poor prognosis associated with PDAC reflects an urgent need for novel drug development.

1.3 RAS mutations are early events in cancer development and progression

Ras mutations are generally early events in cancer development and progression (Figure 1.4). For pancreatic cancer, *KRAS* mutations are the initiating genetic event, followed by a progression of mutations in three tumor suppressor genes. The early onset of *RAS* mutations in cancer emphasizes their key role in promoting the initiation and progression of cancer. This role is supported by genetically engineered mouse model studies where tissue restricted *Kras*

mutational activation initiates the early stages of cancer development (Hingorani et al., 2003b). However, when coupled with additional mutations in tumor suppressors, *Kras*-initiated tumor formation was accelerated and advanced to invasive and metastatic disease. For example, *Kras* (G12D) activation alone induced ductal lesions that recapitulated the full spectrum of human pancreatic intraepithelial neoplasias (PanINs), the putative precursors to invasive pancreatic cancer (Hingorani et al., 2003b). At low frequency, these lesions also progressed to invasive and metastatic adenocarcinomas. However, when combined with a mutation in the *Tp53* (R172H) tumor suppressor, rapid onset of invasive and widely metastatic carcinoma was seen (Hingorani et al., 2005). Decreased latency and acceleration of metastatic PDAC was seen when mutational activation of *Kras* (G12D) was coupled with the deletion of either of the other two key tumor suppressor lesions in this cancer (*CDKN2A/INK4A* and *SMAD4*) (Bardeesy et al., 2006a; Bardeesy et al., 2006b; Waddell et al., 2015).

Despite their clear role in tumor initiation and progression, continued expression of mutant *KRAS* is still required for maintenance of the primary and advanced metastatic cancer. For pancreatic cancer, this was first demonstrated by RNA interference suppression of mutant *KRAS* (G12V) expression in the *KRAS* mutant Capan-1 human PDAC cell line, causing loss of loss of anchorage-independent growth in vitro and impaired tumorigenic growth in vivo (Brummelkamp et al., 2002). Subsequently, it was shown that induction of RNAi suppression of *KRAS* in vivo impaired the growth of Capan-1 PDAC cell line xenograft tumors (Lim and Counter, 2005). Subsequent studies showed that shRNA suppression of KRAS expression impaired the growth of other *KRAS* mutant PDAC cell lines (Singh et al., 2009). More recently, two groups independently showed that continued mutant *Kras* G12D expression was required for the maintenance of PDAC growth in *Kras* G12D/*Tp53* null mouse models of PDAC (Collins et al., 2012a; Collins et al., 2012b; Ying et al., 2012).

1.4 RAS mutations in human cancers

Data in COSMIC shows that the *RAS* genes are mutated in 33% of all cancers evaluated, making it the most frequently mutated oncogene family in cancer (http://cancer.sanger.ac.uk/cancergenome/projects/cosmic/). There are three common sites for Ras mutational activation, residues G12, G13, and Q61, which together account for >95% of identified mutations (Cox and Der, 2010). Mutational activation at G12 and G13 interferes with the ability of Ras to be stimulated by GAPs, as any other residue aside from glycine creates steric hindrance (Scheffzek et al., 1997). However, mutational activation at Q61 disrupts the coordination of the water molecule necessary for GTP-hydrolysis (Scheidig et al., 1999). Once mutated at G12, G13, or Q61 Ras becomes constitutively active, leading to aberrant activation of downstream effectors. Of the Ras isoforms, *KRAS* is the most frequently mutated accounting for ~85% of all *RAS* mutations found in cancer (Cox and Der, 2010).

The frequency of mutation of the three *RAS* genes varies significantly with *KRAS* is the most commonly mutated isoform. Mutation data available in COSMIC v68 (http://cancer.sanger.ac.uk/cancergenome/projects/cosmic/) shows that *KRAS* mutations were found in 29,557 of 139, 474 unique samples analyzed (21.2%), followed by *NRAS*, found in 3,587 of 62,609 samples (5.7%), with *HRAS* mutations relatively rare, found in 1,127 of 35,366 samples (3.2%) (Table 1.1). The simple summation of these data is the basis for the ~30% *RAS* mutation frequency found in all human cancers. Mutation frequencies from other databases (e.g., cBioPortal; (http://www.cbioportal.org/public-portal/), representing a smaller dataset, although with more accurate data restricted to deep sequencing studies, come up with a reduced frequency. Since the cancers represented in each database are different, no one source provides a truly accurate determination of the frequency of *RAS* mutations in cancer.

There is preferential mutation of a specific isoform in different cancers, with near exclusive mutation of *KRAS* in PDAC. In contrast, *NRAS* is the predominant isoform mutated in melanoma and acute myelogenous leukemias, whereas *HRAS* is the predominant isoform mutated in bladder and head and neck squamous cell carcinomas. The majority of missense mutations found in *RAS* occur at G12, G13 and Q61. This pattern contrasts with *RAS* mutations found in developmental disorders. There are also *RAS* isoform distinct frequencies in these mutations, with Q61 mutations rare in *KRAS*, yet the predominant mutation seen in NRAS. Finally, the mutation spectrum found in *KRAS* varies widely in different cancers. For example, the G12C is the predominant mutation found in lung cancer, it is rarely seen in PDAC.

1.5 Ras Effectors

There are at least 11 catalytically-distinct classes of Ras effectors (Vigil et al., 2010). Ras effectors typically possess either a Ras binding (RBD) or Ras association (RA) domain that facilitates preferential binding to activated GTP-bound Ras. Of these effector classes, six have been validated roles in Ras-mediated oncogenesis: Raf serine/threonine kinases, class I phosphatidylinositol-4,5-bisphosphate 3-kinases (PI3K), and GEFs for the Ral (RalGEFs) and Rac1 (Tiam1) small GTPases (Figure 1.5) (Cox et al., 2014). Of these, Raf and PI3K are the best validated, in part, because of their frequent mutational activation in human cancer (Davies et al., 2002; Karakas et al., 2006). In addition to their mutational prevalence in cancer, both Raf and PI3K possess catalytic activities that represent tractable drug targets. Furthermore, downstream components of both Raf and PI3K signaling cascades have been targeted for drug discovery with some success. Taken together these findings have placed Raf and PI3K at the forefront of drug discovery as the two key downstream effectors of Ras.

1.6 The Raf-MEK-ERK kinase cascade

The Raf-MEK-ERK three-tiered protein kinase cascade is one of three major MAPK kinase kinase (MAPKKK/MAP3K)- MAPK kinase (MAPKK/MAP2K)-MAPK modules involved in cytoplasmic signaling downstream of active cell surface receptors. The other two MAPKs, p38 and JNK, have less significant roles in oncogenesis and are not known to be directly activated downstream of Ras. Therefore, in this thesis, we focus on the Raf-MEK-ERK cascade in Ras signaling.

1.6.1 Raf serine/threonine kinases

There are three distinct Raf (MAPKKK/MAP3K) isoforms: A-Raf, B-Raf, and Raf-1 (c-Raf). Like Ras isoforms, Raf isoforms share similar sequence identity and conserved domain topology (Figure 1.6). The N-terminal region contains an RBD followed by a cysteine-rich domain (CRD/C1), while the C-terminal region contains the serine/threonine kinase domain. Generally, N-Ras, H-Ras, and K-Ras activate Raf-1 and B-Raf similarly, whereas A-Raf is only weakly activated by Ras (Rodriguez-Viciana et al., 2004). Ras-GTP binding to the RBD relieves the N-terminal auto-inhibitory activity and additionally recruits Raf to the plasma membrane, where additional phosphorylation events and interactions facilitate activation of Raf catalytic function (Figure 1.7). How Ras causes activation of Raf is complex and still not completely understood, with most studies focused on Raf-1, the isoform found originally transduced and activated in the 3611-MSV oncogenic retrovirus that caused *r*apidly *a*ccelerated *fi*brosarcomas (Matallanas et al., 2011)

Inactive Raf-1 exists in a closed confirmation stabilized by the 14-3-3 complex interacting with residues S259 in the N-terminal region and S621 in the C-terminal region (Roskoski, 2010).

RTKs recruit the Sos1 RasGEF to the plasma membrane where it catalyzes the formation of Ras-GTP (Figure 1.8). PP1 and PP2A phosphatases dephosphorylate Raf-1 at residue S259 permitting Ras-GTP to bind the Raf-1 RBD effectively resulting in an open yet inactive confirmation. Several known (PAK, CK2, Raf, Src, and Jak) and unknown kinases phosphorylate the C-terminal region of Raf-1 at residues S338 and Y341. Once activated, Raf proteins either homo- or heterodimerize, which is stabilized by either the 14-3-3 complex, KSR-1, or MLK-3, all well validated scaffolds.

Once Raf-1 is activated, it can phosphorylate its only known physiological downstream substrates, the closely related MEK1 and MEK2 dual specificity protein kinases. Raf kinases phosphorylate MEK1 and MEK2 at two sites (S218 and S222), which are located in the activation loop. Once active MEK1/2 phosphorylate ERK, which also has two distinct isoforms. As a consequence, the field has relied heavily on changes to levels of phosphorylated ERK1 and ERK2 to determine Ras-Raf signaling activation.

B-Raf activation is similar to Raf-1 activation, though several observations have suggested that B-Raf activation may require fewer components (Matallanas et al., 2011). Currently, the model for B-Raf activation is thought to require Ras and 14-3-3 complex interactions for activation. Unlike Raf-1, B-Raf contains a negatively charged N-terminal domain due to the presence of both aspartate at the position corresponding to Raf-1 residue Y341 (D448/449) and constitutive phosphorylation of B-Raf at residue S446, which corresponds to Raf-1 S338. Together these residues promote the stabilization of the 3-dimensional catalytic domain. Like Raf-1, active B-Raf also phosphorylates the MEK1 and MEK2 kinases leading to ERK1 and ERK2 phosphorylation.

Of the Raf kinases, A-Raf is most poorly understood, as it is not mutated in cancer nor has it been identified as a resistance mechanism to any targeted therapies. A-Raf association with mutated Ras is weak as a consequence of the presence of a lysine at position 22, located within the A-Raf RBD (Matallanas et al., 2011). Consistent with this observation, A-Raf seems to be only weakly activated by Ras. Furthermore, there are several non-conserved acidic amino

residues found in the N-terminal domain of A-Raf, most important being Y296, which if mutated results in a constitutively active kinase. This residue, in particular, is thought to stabilize the N-terminal domain interaction with the catalytic domain promoting a closed kinase confirmation. In the C-terminal domain, residue S432, located between the ATP-binding motif and the activation loop, is crucial for both MEK activation and A-Raf signaling. Unlike B-Raf, A-Raf contains a cluster of phosphorylation sites between residues 248 and 267, which, once activated, contribute to dissociation from the plasma membrane. Thus, A-Raf signaling has been found at several subcellular compartments, including the Golgi apparatus, endosomes and mitochondria.

1.6.2 MEK dual specificity kinases

MEK1 and MEK2 (MAP/ERK kinase; MAPKK/MAP2K) are highly related dual specificity kinases that catalyze the phosphorylation of both threonine and tyrosine residues in the TxY motif their only known substrates, ERK1 and ERK2 (Roskoski, 2012b)(Figure 6). MEK1/2 structure can be split into three distinct functional domains: N-terminal domain, protein kinase domain, and a short C-terminal domain (Fischmann et al., 2009). The N-terminal region consists of an inhibitory domain, a nuclear export domain, and a domain that aids in the ability to bind the ERK kinases. The kinase domain comprises the majority of MEK1/2 structure and includes the activation segment and the proline-rich segment. Raf activates MEK1/2 by dual phosphorylation at tandem serine residues (Figure 1.6). Two other known activators of MEK1/2 are the COT/Tpl2 and Mos serine/threonine kinases. Like Raf, Tpl2 and Mos were also identified originally as retroviral oncogenes and act as MAPKKK/MAP3Ks (Moloney, 1966; Salmeron et al., 1996). The PAK1 serine/threonine kinase can phosphorylate and modulate MEK1 at S298, promoting Raf activation of MEK (Coles and Shaw, 2002; Slack-Davis et al., 2003).

1.6.3 ERK serine /threonine kinases

The only well-established MEK1 and MEK2 substrates are the highly related ERK1 and ERK2 serine/threonine kinases (Figure 1.6). Phosphorylation of the ERK kinases is the most common readout for Ras activation of the Raf-MEK-ERK signaling cascade (Roskoski, 2012a). Like many protein kinases ERK1 and ERK2 have short N-terminal and C-terminal domains, with the protein kinase domain making up the largest region. All known cellular activators of ERK1 and ERK2 lead to phosphorylation and activation of both kinases in parallel (Lefloch et al., 2009). To become active MEK1/2 phosphorylate ERK1 and ERK2 at residues T202 and Y204, starting with the tyrosine residue.

Whether ERK1 and ERK2 have unique biological functions has been under evaluation for the last decade. There is evidence that genetic ablation of *Erk2* but not *Erk1* causes embryonic lethality (Hatano et al., 2003; Pages et al., 1999; Saba-El-Leil et al., 2003; Yao et al., 2003). Furthermore, ERK2 but not ERK1 was necessary for H-Ras-induced epithelial-to-mesenchymal transformation in MCF-10A breast epithelial cells (Shin et al., 2010). RNAi silencing of either *ERK1* or *ERK2* impaired the growth of *BRAF* mutant melanoma cells (Qin et al., 2012). Together these observations suggest that ERK1 and ERK2 have distinct biological functions. Future studies will be needed to further characterize these distinct biological functions.

Unlike the highly restricted substrates of the Raf and MEK isoforms, the ERK1 and ERK2 (extracellular-signal regulated kinase) kinases are thought to share up to 200 substrates, in both nuclear and cytosolic compartments (Yoon and Seger, 2006). Once activated ERK1 and ERK2 can phosphorylate cytoplasmic substrates and additionally translocate into the nucleus and phosphorylate nuclear substrates.

Multiple ERK substrates can contribute to the essential role of ERK in cancer growth. Key cytoplasmic substrates include the 90 kDa RSK (ribosomal S6 kinases) serine/threonine kinases (Romeo et al., 2012). RSK proteins (RSK1-4) are regulators of diverse cellular processes, including cell proliferation, survival and motility. Other ERK substrates include the cytoplasmic MNK and nuclear MSK family kinases (Hauge and Frodin, 2006; Hou et al., 2012). ERKs also

phosphorylate many nuclear transcription factors that include Ets family transcription factors (e.g., Elk-1), Fos and Myc. ERK phosphorylation of Myc at S62 stabilizes Myc and prevents FBW7 E3 ligase-mediated proteasomal degradation (Farrell and Sears, 2014).

1.7 Raf-MEK-ERK target validation in Ras mutant cancers

The Raf-MEK-ERK signaling cascade has been rigorously validated as a necessary effector for Ras transformation (Cuadrado et al., 1993; Khosravi-Far et al., 1995; Khosravi-Far et al., 1996; White et al., 1995). In early focus formation and clonogenic growth assays, several laboratories observed that dominant-negative mutants of Raf, MEK, or ERK effectively inhibited Ras-driven transformation (Cowley et al., 1994; Kolch et al., 1991; Schaap et al., 1993). Consistent with the importance of Raf-MEK-ERK signaling, it was also demonstrated that the Ras effector domain mutant T35G, which preferentially impairs Ras-Raf interaction relative to PI3K and RalGEF, inhibited H-Ras transforming capabilities in NIH 3T3 mouse fibroblasts (White et al., 1995). Expression of activated Raf-1 could overcome growth inhibition associated with loss of Ras or expression of Ras dominant negative mutant S17N (Feig and Cooper, 1988). Finally, genetic loss of all three *RAS* isoforms causes growth cessation of mouse embryo fibroblasts and only activated Raf (and not PI3K and/or RalGEF) could rescue the growth defect of “Rasless” cells (Drosten et al., 2010). Activated MEK or ERK could also partially restore growth. Together these initial observations demonstrated that the Raf-MEK-ERK signal cascade was both downstream of Ras in mammalian cells and necessary for Ras transformation.

Raf has been validated extensively in human cancer cell lines as a target for therapies (Hingorani et al., 2003a; Hoeflich et al., 2006; Karasarides et al., 2004; Sharma et al., 2005; Sumimoto et al., 2006). This is a direct consequence of its mutational activation, as well as, mutual exclusivity from Ras mutations in cancers (Davies et al., 2002; Karasarides et al., 2004; Rajagopalan et al., 2002; Sieben et al., 2004; Singer et al., 2003). The non-overlapping occurrence of Raf and Ras mutations in some cancer types (e.g., melanoma, colorectal cancer)

suggests that Raf is likely the most significant downstream effector in these Ras mutant cancers. This contrasts with activating mutations in *PIK3CA* (encodes p110α that can occur together with *RAS* mutations. Consistent with this observation, several studies have validated the role of Raf downstream of mutant Ras in colorectal, pancreatic and lung tumor cell lines (Campbell et al., 2007; Li et al., 2013; Subramanian and Yamakawa, 2012). Together these data suggest that therapies for Ras mutant cancer treatments should be, at least partially, focused on targeting the Raf-MEK-ERK signaling cascade.

While RNAi use in cell culture is a strong tool for validating the importance of a cancer target, there are several caveats associated with genetic manipulation and its translation into actual cancer therapies. First, *in vivo* RNAi targeting is still under investigation and far from use as an effective therapy. As such, our most effective tools for cancer treatment are still targeted small molecule inhibitors. Inhibitors, generally, block catalytic function or prevent protein-protein activation, however RNAi targets the entire protein for depletion, which is vastly distinct from catalytic or allosteric inhibition. Though RNAi is far from ideal, it still remains a powerful tool for targeted drug discovery.

Raf has also been sufficiently validated as an *in vivo* target for mutant Ras-driven cancer initiation and progression. The two-stage chemical carcinogenesis model, where a single treatment with the mutagen 7,12-dimethylbenz[*a*]anthracene (DMBA) is followed by repeated applications of a pro-inflammatory phorbol ester 12-O-tetradecanoylphorbol 13-acetate (TPA) causes *Hras* Q61L-induced squamous cell carcinomas has been widely used to assess the role of Ras effectors (e.g., Tiam1, RalGDS, PLCε, and p110α) in cancer formation (Bai et al., 2004; Gupta et al., 2007; Malliri et al., 2002; Slack-Davis et al., 2003). Using this mouse model, Baccarini and colleagues showed that conditional loss of one *Craf* in the epidermal tissue reduced the number of tumors as well as tumor size, with complete inhibition of tumor formation upon loss of both *c-Raf* alleles (Ehrenreiter et al., 2009). Extending this to *Kras*-driven cancers, two separate

studies observed that *Craf* but not *Braf* deficiency impaired *Kras* G12D-induced lung tumor formation (Blasco et al., 2011; Karreth et al., 2011). However, in contrast to these studies, *Craf* was found to be dispensable for *Kras* G12D-induced pancreatic cancer formation (Eser et al., 2013). While a role for *Braf* was not addressed in this study, the finding by McMahon and colleagues that activated *Braf* V600E alone could phenocopy activated *Kras* G12D and induce pancreatic cancer formation suggests that different *RAF* isoforms may drive *KRAS*-driven cancer development in different tissues (Collisson et al., 2012).

The studies above provide validation that Raf is necessary for tumor initiation and progression. However, whether Raf plays a role in mutant Ras tumor maintenance remains partially answered. Counter and colleagues observed that ERK plays a role in tumor maintenance of Ras transformed cells, as an inducible dominant-negative MEK prevented continued tumor growth in a xenograft mouse model (Lim and Counter, 2005). However, their key finding was that a membrane-targeted, activated, variant of p110α, not *c-Raf*, was sufficient to maintain tumorigenic growth of *KRAS* mutant human colon and pancreatic cancer cell lines when *KRAS* expression was ablated. This result suggests that PI3K rather than Raf inhibition will be required to block the *KRAS* mutant tumor growth.

Use of genetic knockout mouse models where effector function is ablated concurrently with *RAS* activation addresses the role of that effector in tumor initiation and progression but not maintenance. Additionally, genetic ablation of an effector, resulting in loss of protein expression, is not an accurate modeling of the consequences of pharmacologic inhibition of the catalytic function of the effector. With the development of potent and selective pharmacologic inhibitors of the Raf-MEK-ERK cascade, the limitations in these studies can be overcome. However, they still face the limitations of our current mouse models of cancer (Colvin and Scarlett, 2014). Orthotopic tumors induced by implantation of human tumor cells into immunocompromised mice provide another model. However, with the obvious importance of the immune system in host response to tumor growth, these studies cannot evaluate drug response in the context of an intact immune

response. Genetically engineered mouse models overcome these limitations. However, since tumor develop is initiated by one or two genetic alterations, they are genetically less complex than bona fide human cancers.

1.8 Targeting RAS for cancer Treatment

As indicated above, the current therapeutic options for PDAC are limited and ineffective. With the high frequency of *KRAS* mutations in this cancer and strong preclinical evidence that disruption of KRAS function will impair cancer growth, the development of effective anti-KRAS inhibitors has been actively pursued. However, despite more than three decades of intensive effort by the pharmaceutical industry and academia, to date, no effective therapeutic strategies have reached the clinic (Bryant et al., 2014; Stephen et al., 2014). In this section, we provide a summary of past and ongoing efforts to develop anti-Ras therapeutic strategies (Figure 1.9).

As described above, the Ras C-terminal CAAX motif signals for posttranslational modifications that promote Ras membrane association. That mutation of the cysteine residue to serine (SAAX) to prevent the addition of the farnesyl isoprenoid lipid or truncation of the AAX residues results in completely inactive Ras proteins supported the rationale to target farnesyltransferase as a therapeutic strategy (Berndt et al., 2011). Numerous companies successfully developed potent and selective farnesyltransferase inhibitors (FTIs), with two (tipifarnib and lonafarnib) advancing to Phase III clinical evaluation (Basso et al., 2006). Despite promising cell culture and mouse model observations with FTIs, FTIs failed to show any clinical benefit in pancreatic and colorectal cancer patients. Their failure was attributed to the earlier finding that the K-Ras and N-Ras proteins, when FTase activity is blocked, can then serve as a substrate for the related geranylgeranyltransferase-I enzyme (GGTase-I), and be modified by the related geranylgeranylgeranyl isoprenoid lipid (Figure 1.3). Since geranylgeranylgeranyl-modified Ras retains the ability to be membrane-associated and transforming, this bypass mechanism prevented the effectiveness of FTIs for *KRAS* mutant cancers.

Currently, alternative strategies to disrupt Ras membrane association are being considered. These include targeting the other two CAAX motification enzymes, ICMT and Rce1 (Figure 1.3). Another approach are farnesyl lipid mimics, salirasib, that act apparently by competing for Ras membrane association (Bustinza-Linares et al., 2010). More recently, inhibitors of a chaperone protein, the prenyl-binding protein phosphodiesterase 6 delta that modulates Ras trafficking to the plasma membrane have been described (Chandra et al., 2012; Zimmermann et al., 2013).

The most aggressively pursued anti-Ras strategy involves inhibition of Ras downstream effector signaling. However, these efforts are complicated by the fact that Ras uses multiple effectors to promote cancer growth (Mitin et al., 2005). Of these effector pathways, the Raf (A-Raf, B-Raf and C-Raf) and class I phosphatidylinositol-3 kinases (PI3K; p110α, γ and δ) effector pathways have attracted the greatest interest (Fritsch et al., 2013; Nissan et al., 2013), with multiple inhibitors of components of each pathway currently under clinical evaluation. That these effector pathways have driver functions in *KRAS*-dependent cancer growth is supported by their frequent mutational activation in cancer: *BRAF* (20%) and *PIK3CA* (encodes p110α; 12%) (COSMIC). However, when applied as monotherapies, these inhibitors have shown limited to no clinical activity in *RAS* mutant cancers. There are numerous ongoing clinical trials evaluating whether concurrent inhibition of Raf and PI3K effector signaling will be more effective (http://clinicaltrials.gov/).

An approach once thought impossible involves direct inhibition of mutant Ras. Initial efforts to disrupt GTP binding were not successful, due to the picomolar affinity of GTP binding to Ras. This contrasts with the low micromolar binding affinity of ATP to protein kinases, where effective ATP-competitive protein kinase inhibitors have been developed successfully. Similarly, efforts to identify small molecules that can act as a GAP for mutant Ras proteins did not succeed. Recently, small molecules that directly bind Ras and perturb either RasGEF activation or effector

binding have been described (Maurer et al., 2012; Ostrem et al., 2013; Sun et al., 2012). Whether these early stage Ras binders can be advanced to more potent and selective Ras binding molecules and whether they can effectively block the critical functions of Ras to have a clinical consequence remains to be determined.

Other directions considered for anti-Ras drug discovery include targeting the metabolic changes in glucose and glutamine metabolism found in *RAS* mutant cancers (Ahearn et al., 2012; Sun et al., 2012). RNAi targeting of RAS gene expression is also being pursued. Here, whether these can be effectively delivered to the cancer, and whether sufficient suppression of *RAS* gene expression can be achieved, are the current uncertainties in these directions. Finally, unbiased RNA interference screening has been applied to search for synthetic lethal interactors of mutant *RAS*. However, these studies have been hampered by the lack of reproducibility in the findings (Luo et al., 2012; Weiwer et al., 2012).

1.8.1 Pharmacologic Inhibition of Raf-MEK-ERK signaling in mutant RAS cancers

Pharmacologic inhibitors of Raf have not been effective against *RAS* mutant cancers. Their ineffectiveness is due to the paradoxical activation rather than inactivation of ERK signaling (Figure 1.10A). Studies in cell culture and mouse models determined that Raf inhibitor treatment caused the formation of B-Raf/C-Raf heterodimers that are dependent on activated Ras (Heidorn et al., 2010). Ras activation promotes Raf dimerization, primarily B-Raf/C-Raf heterodimers. In the Raf dimmer, B-Raf is inhibited, but it then causes activation of the non-inhibited C-Raf molecule. Only at high inhibitor concentrations that cannot be achieved in the patient are both Raf molecules inhibited and ERK signaling is blocked. To date, the most successful Raf inhibitor is vemurafenib (*Zelboraf*), which targets mutant B-Raf V600E in melanoma (Flaherty et al., 2010). A second Raf inhibitor, dabrafenib (*Tafinlar*), was later approved for the same patient population. However, its success has been complicated by the re-occurrence of tumors harboring Ras mutations (Nazarian et al., 2010). In one study, vemurafenib inhibition caused accelerated ERK signaling resulting in aberrant growth and tumor formation in tissues, which harbored mutant *RAS*.

Although developed originally as a C-Raf inhibitor, sorafenib is a multi-kinase inhibitor that also inhibitors RTKs involved in tumor angiogenesis. Therefore, its clinical activity is not attributed to its Raf inhibitory activity. A number of additional Raf inhibitors are currently under clinical evaluation (Figure 1.11). Currently, efforts to develop Raf inhibitors that do not promote Raf dimerization or have more pan-Raf inhibitory activities, or inhibitors of Raf dimerization, are being pursued to overcome the limitation of first generation Raf inhibitors.

MEK inhibitors have also shown limited to no anti-tumor efficacy in *RAS* mutant cancers. For example, Rosen and colleagues found that MEK inhibitor treatment was effective against *BRAF* but not *RAS* mutant human cancer cell lines (Daouti et al., 2010; Solit et al., 2006). MEK inhibition alone was not effective in a mouse model of *Kras*-driven lung cancer formation (Engelman et al., 2008). The ineffectiveness of MEK inhibition is attributed to the loss of ERK activation induced feedback inhibitory mechanisms (Figure 1.10B). Flux through the Raf-MEK-ERK cascade requires critical regulation, with high levels of activated ERK causing growth suppression; ERK activation induces feedback inhibition mechanisms that dampen upstream activators of the pathway (Figure 6). These mechanisms include ERK phosphorylation of Raf to dampen Ras activation of Raf (Dougherty et al., 2005). Other feedback mechanisms include ERK phosphorylation of Sos1 or the EGFR, or transcription factor-mediated induction of gene expression of negative regulators such as DUSP protein phosphatases (Little et al., 2011; Pratilas et al., 2009; Wagle et al., 2014) or Sprouty (Roskoski, 2010). In a recent unbiased approach to define mechanisms that drive resistance to MEK inhibition, Johnson and colleagues showed that MEK inhibition of *KRAS* mutant breast cancer cell lines resulted in the activation of multiple RTKs (Duncan et al., 2012). They further showed that concurrent inhibition of RTK activation then enhanced the anti-tumor activity of MEK inhibition *in vitro* and *in vivo.* One MEK1/2 inhibitor (trametinib/*Mekinist)* has been approved for use alone, or together with the Raf inhibitor dabrafenib, for *BRAF* mutant melanoma (Figure 1.11). Trametinib is an allosteric, non-ATP competitive inhibitor that prevents activated MEK1/2 phosphorylation of its substrates. There are

at least 16 additional MEK1/2 inhibitors under clinical evaluation (Figure 8), many also allosteric non-ATP competitive inhibitors. One unique inhibitor, RO5126766, inhibits MEK and additionally Raf, making it less susceptible to the feedback activation of Raf caused by ERK inhibition.

With the ineffectiveness of anti-Raf and –MEK therapies in *RAS* mutant cancers due largely to kinome reprogramming mechanisms that caused reactivation of ERK, it prompted studies to address whether inhibition of ERK directly may overcome these limitations. Recently, it was shown that an ERK1/2-selective inhibitor, SCH772984, was active in Raf- and MEK-resistant *BRAF* mutant melanoma in preclinical models (Morris et al., 2013). SCH772984 binds ERK, preventing MEK phosphorylation and activation of ERK and additionally preventing ATP binding and ERK phosphorylation of its substrates. Additionally, another group described another ERK inhibitor capable of overcoming resistance to MEK inhibitors (Hatzivassiliou et al., 2012). Furthermore, Genetech also produced an ERK inhibitor that is currently being evaluated in pre-clinical models.

ERK inhibition represents a new approach to blocking an old pathway; however, the question remains whether ERK inhibition as a therapy will be successful in combating *RAS* mutant cancers, or succumb to some of the limitations associated with Raf and MEK inhibition. Currently, three ERK inhibitors are under clinical evaluation (MK-8353/SCH 900353 is an orally available analog of SCH772984) (Figure 1.11).

Figure 1.1

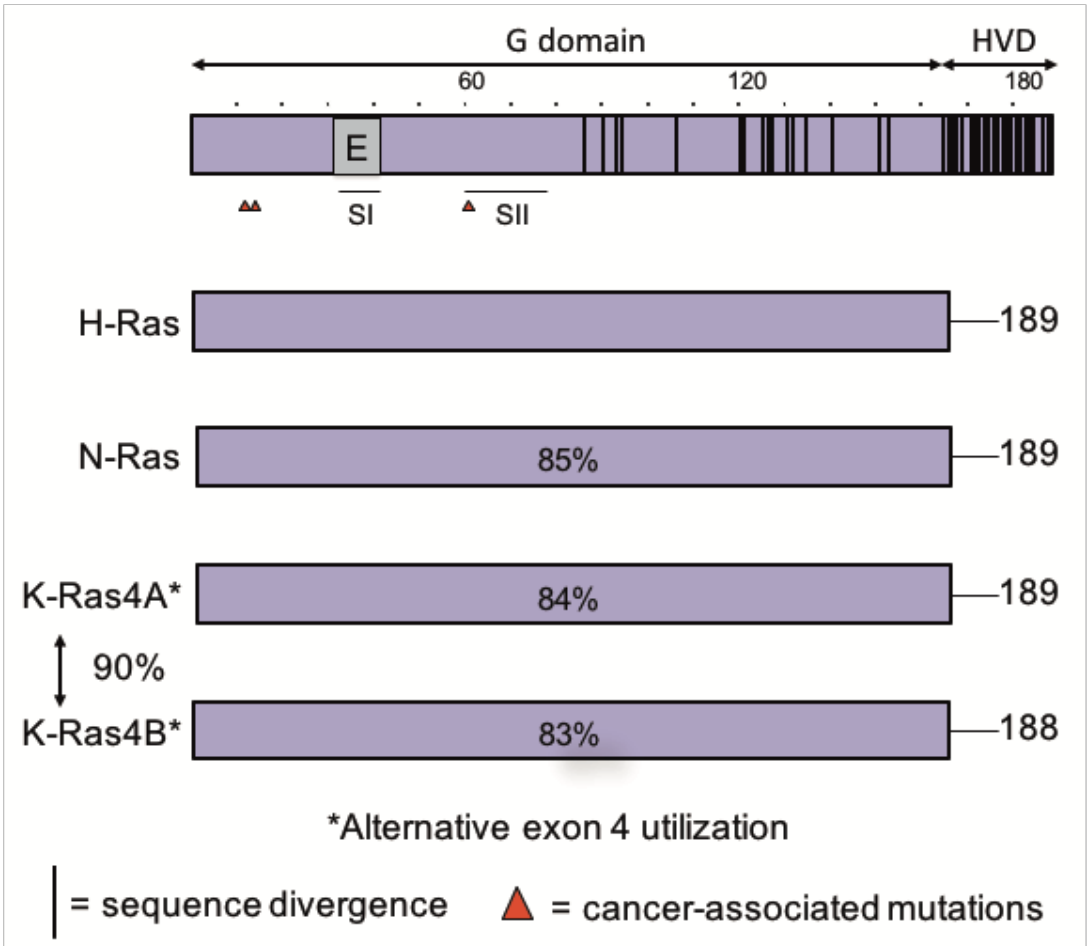

Figure 1.1 Human Ras proteins. The three RAS genes encode four highly related 188/189 amino acid Ras proteins. The two highly related K-Ras 4A and 4B isoforms (90% identical) arise from alternative gene splicing and utilization of alternative fourth exons 4A and 4B. The numbers indicate percent sequence identity with H-Ras (83-85%). Residues 1-164 comprise the G domain that binds and hydrolyses GTP and includes the switch I (SI; aa 30-38) and II (SII; aa 60-76) sequences that change in conformation during GDP-GTP cycling. The core effector domain (E; residues 32-40) is essential for Ras-GTP binding to downstream effectors. The predominant missense mutations (~99%) found in cancer result in single amino acid substitutions at residues 12, 13 or 61. Ras proteins diverge in their C-terminal sequences comprised of the hypervariable domain (HVD).

Figure 1.2.

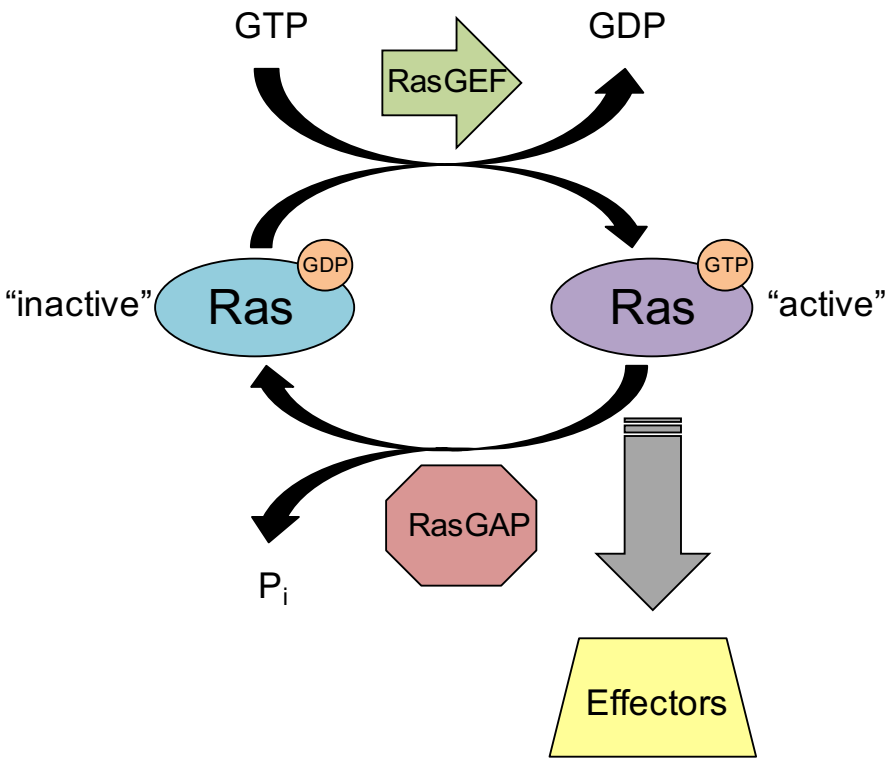

Figure 1.2. Regulation of the Ras GDP-GTP cycle. Ras proteins act as molecular switches alternating between GTP- (active state) and GDP- (inactive state) bound states, where Ras-GTP binds preferentially to downstream effectors (E). There are two classes of regulatory proteins that regulate this cycling process: RasGEFs (guanine exchange factors) and RasGAPs (GTPase activating proteins). In resting cells, normal Ras is predominantly GDP-bound (~95%). Upon growth factor stimulation and activation of RasGEF, rapid and transient GDP-GTP exchange is stimulated. RasGAP stimulation of the intrinsic GTPase activity and GTP hydrolysis restores the inactive Ras-GDP state. Mutant Ras proteins are impaired in their intrinsic and GAP-stimulated GTP hydrolysis activities, resulting in stimulus-independent, persistent Ras-GTP formation (~80%).

Figure 1.3.

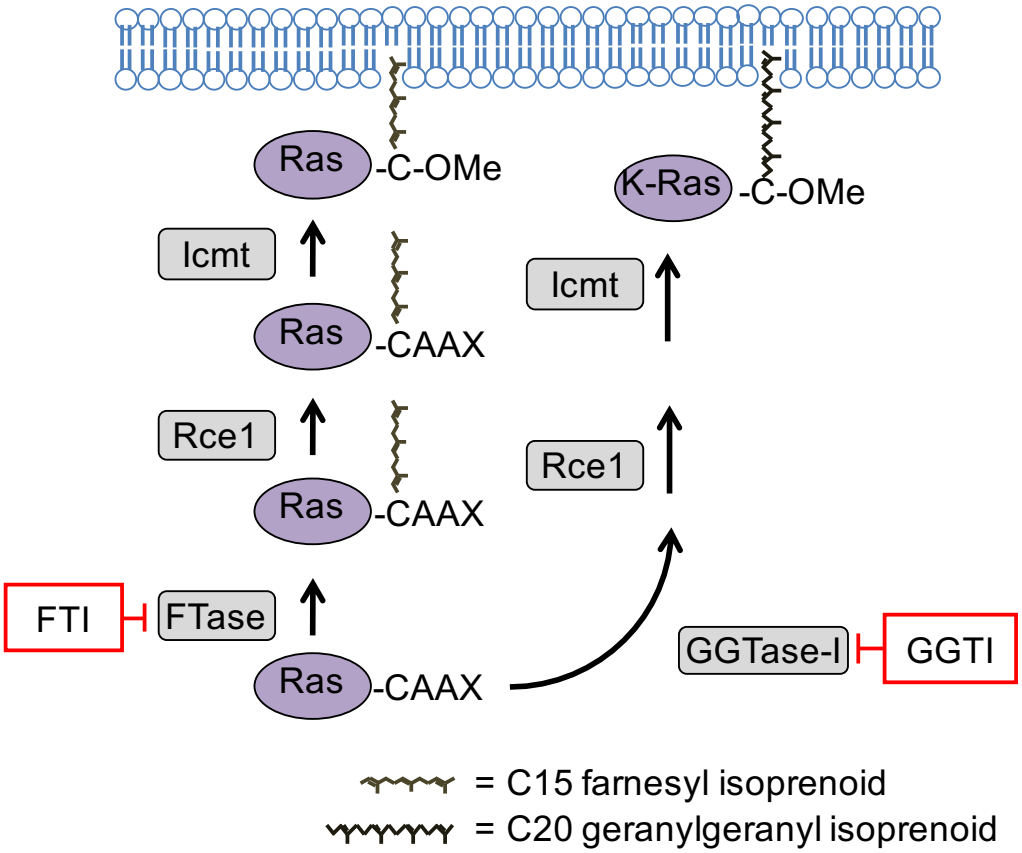

Figure 1.3. Ras proteins and membrane association. Ras proteins are synthesized initially as cytosolic and inactive proteins. Within minutes, they undergo a series of posttranslational modifications signaled by the C-terminal CAAX motif. First, cytosolic farnesyltransferase (FTase) catalyzes covalent, irreversible addition of a C15 isoprenoid lipid to the cysteine residue of the C-terminal CAAX motif. This then allows Rce1-catalyzed proteolytic removal of the AAX residues and Icmt-catalyzed, reversible carboxylmethylation (-OMe) of the now terminal farnesylated cysteine. H-Ras is the only Ras isoform that is solely modified by FTase. Although normally also FTase substrates, when FTase activity is blocked by FTase inhibitor (FTI) treatment, K-Ras and N-Ras, can now be modified by geranylgeranyltransferase-I (GGTase-I)-catalyzed addition of a related C20 geranylgeranyl isoprenoid, resulting in membrane association.

Figure 1.4.

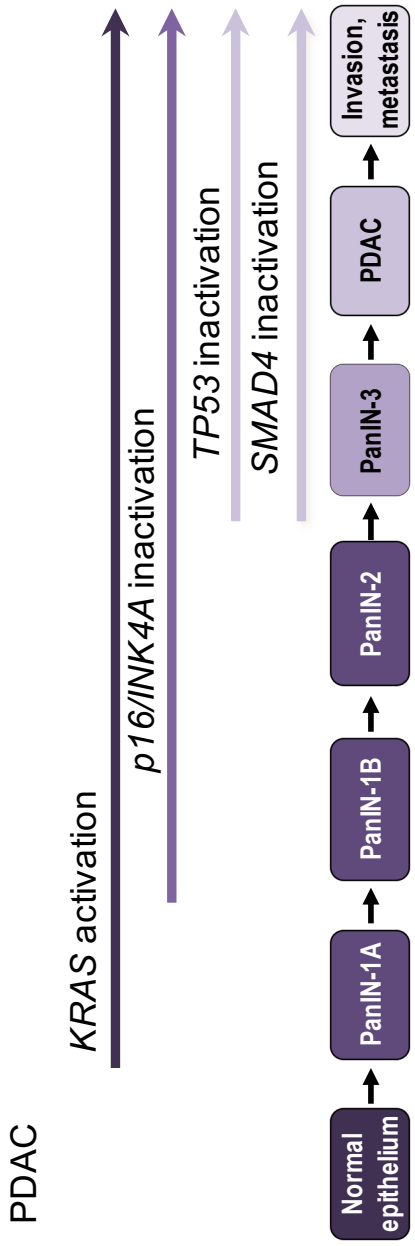

Figure 1.4. PDAC genetic progression model. KRAS mutations occur early in cancer progression followed by loss of important tumor suppressors. KRAS mutation is the initiating step in PDAC development, followed by mutational loss of the CDKN2A, TP53 and SMAD4 tumor suppressors. KRAS is the RAS isoform predominantly mutated in PDAC (98% of all RAS mutations).

Table 1.1.

Table 1.1 Frequency of *RAS* mutations in human cancers[a]

Cancer	% *KRAS*	% *NRAS*	% *HRAS*	% All *RAS*
Pancreatic ductal adenocarcinoma	92	1	0.5	94
Colorectal adenomcarcinoma	45	7	0.0	52
Multiple myeloma	26	25	0.0	51
Lung adenocarcinoma	31	1	<1	32
Skin cutaneous melanoma	1	27	1	29
Uterine corpus endometrioid carcinoma	21	4	<1	25
Thyroid carcinoma	1	9	4	14
Stomach adenocarcinoma	11	1	0.0	12
Acute myeloid leukemia	3	7	2	12
Bladder urothelial carcinoma	3	1	6	10

[a]Compiled from cBioPortal (http://www.cbioportal.org/public-portal/)

Table 1.1. Frequency of *RAS* mutations in human cancers

Figure 1.5.

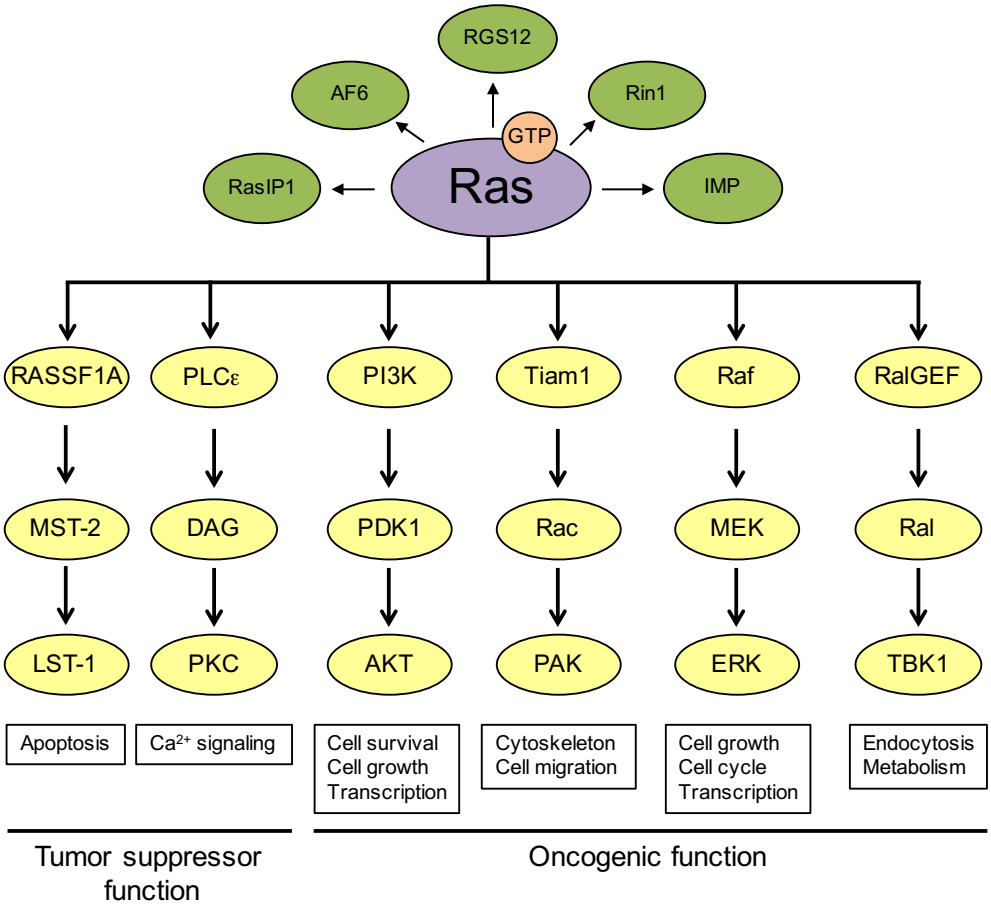

Figure 1.5. Ras effector signaling. Ras-GTP binds preferentially to 11 catalytically-distinct classes of effectors. Cell culture and/or mouse model studies have been implicated six classes in Ras-mediated tumor initiation, progression and/or maintenance. This includes the Raf, p110 catalytic subunits of class I PI3Ks, GEFs for the Ral small GTPases (RalGEFs; RalGDS, Rgl, Rgl2 and Rgl3) and Rac small GTPase (Tiam1) and PLCe whose functions are necessary for tumor growth. In contrast, RASSF1A family members are negative regulators and their expression is lost in cancer.

Figure 1.6.

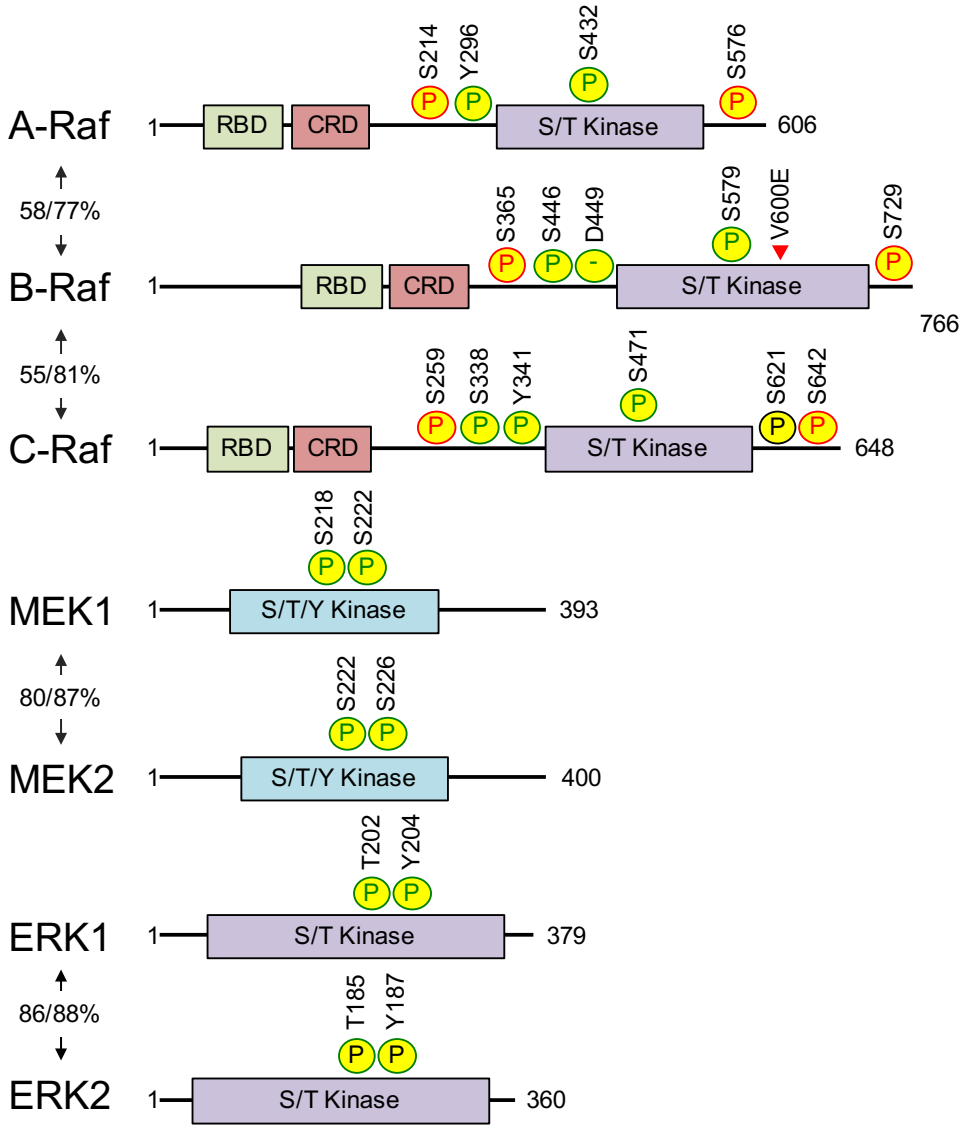

Figure 1.6. Components of the Raf-MEK-ERK protein kinase cascade. Shown are the human proteins, with domain structure determined in SMART. The percentages of overall protein and kinase domain amino acid identities are indicated (%) and were determined by ClustalW multiple sequence alignment analyses. The phosphorylation sites that regulate Raf kinase activity are complex and include both positive (green) and negative (red) phosphorylation events. We have not included all known phosphorylation sites and have included only select key phosphorylation sites. The negative regulatory sites are conserved in all Raf isoforms and serve as recognition sites for 14-3-3 dimer binding and inhibition of Raf. Phosphorylation of S432(A-Raf)/S579(B-Raf)/S471(C-Raf) is important for Raf interaction with MEK. Raf phosphorylation sites in MEK1/2 and MEK1/2 phosphorylation sites in ERK1/2 are indicated. The V600E amino acid substitution comprises ~80% of cancer-associated activating mutations in B-Raf. Abbreviations are: RBD, Ras-binding domain, CRD, cysteine-rich domain; S/T, serine/threonine; S/T/Y, serine/threonine/tyrosine.

Figure 1.7.

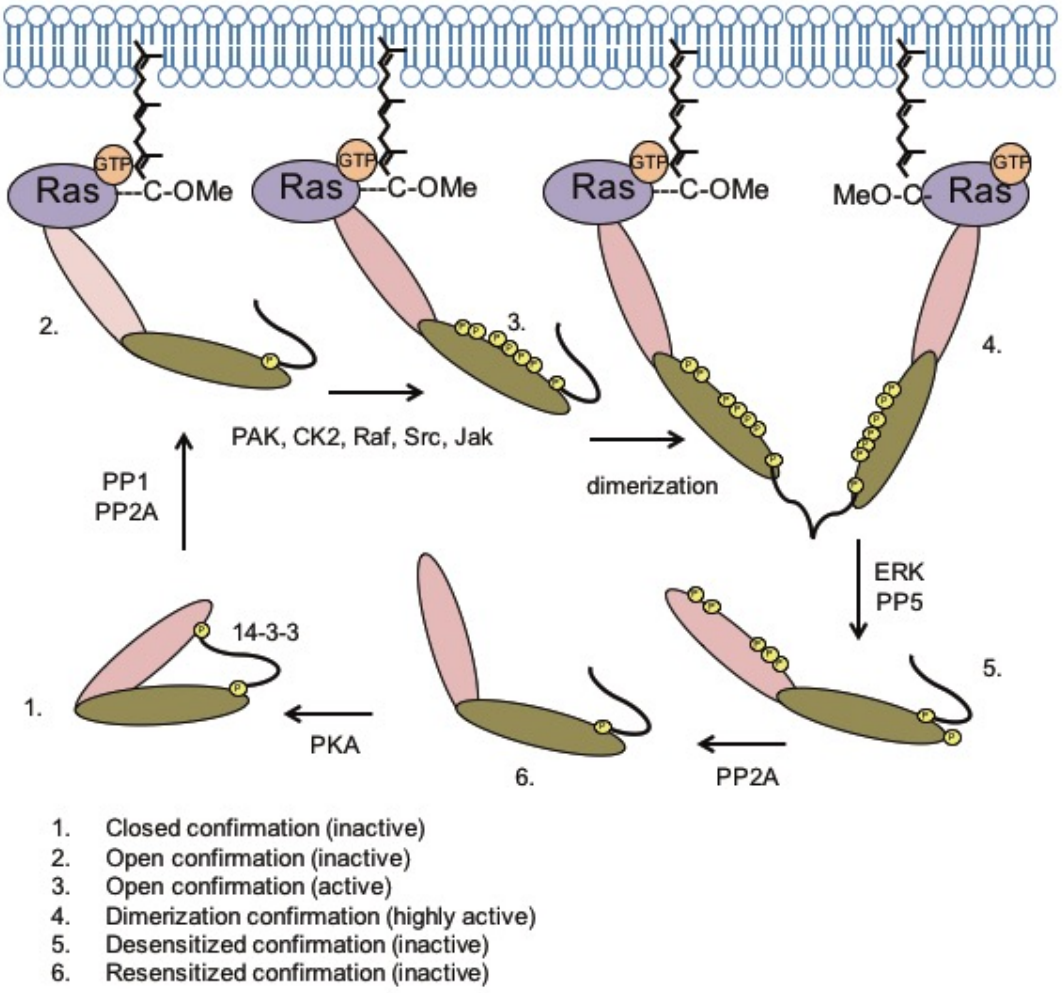

Figure 1.7. Regulation of Raf dimerization and activation. Ras-GTP recruits Raf to the plasma membrane. Here PP1 or PP2A dephosphorylate Raf in its inhibitory domain. This event primes Raf interaction with Ras-GTP and promotes several important phosphorylation events. Once phosphorylated Raf proteins dimerization and are considered active. PP5 and PP2A dephosphorylate each Raf monomer leading to dissociation from the plasma membrane and monomerization. Finally, PKA phosphorylates Raf leading it to adopt a closed, "inactive," confirmation.

Figure 1.8.

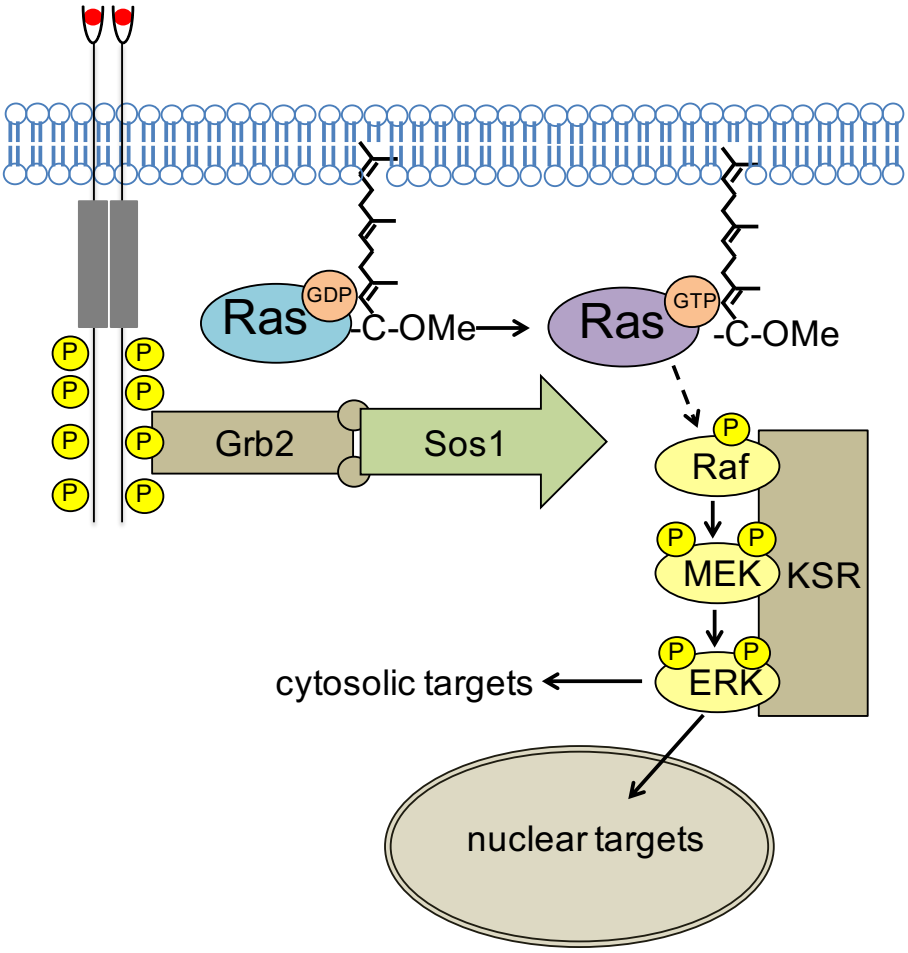

Figure 1.8. Receptor tyrosine kinase-mediated activation of wild type Ras. Wild-type Ras activation occurs when ligands (e.g., epidermal growth factor; EGF) stimulate activation of receptor tyrosine kinases (RTK; e.g., EGF receptor). Once stimulated, RTKs autophosphorylate tyrosine residues in the cytoplasmic domain, creating docking sites for Src homology 2 (SH2) domain-containing proteins (e.g., Grb2). The tandem SH2 domains of Grb2 interact with proline-rich sequences in the Sos1 RasGEF, promoting Sos1 translocation to the plasma membrane, leading to activation of membrane-associated Ras. Sos1-mediated formation of Ras-GTP then promotes Ras association with Raf, leading to activation of the ERK MAPK cascade. Shown here is KSR association with Raf, MEK and ERK. KSR is but one of a number of scaffolding proteins that associate with one or more components of the three-tiered protein kinase cascade. Scaffolds modulate the composition of the pathway and additional influence temporal and spatial activity of ERK signaling. Other ERK scaffolds include IQGAP1, MP1, Sef and b-arrestin.

Figure 1.9.

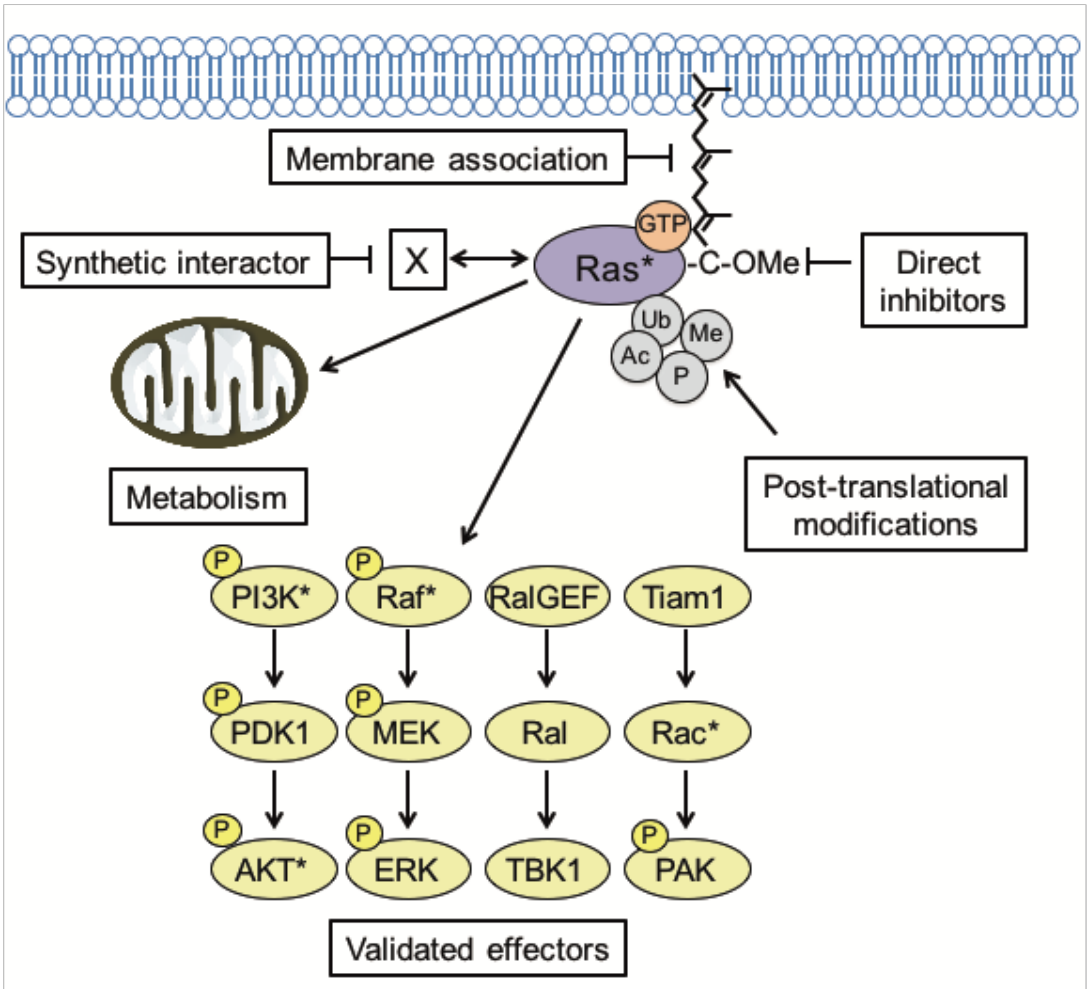

Figure 1.9. Approaches for the development of anti-Ras drugs. Once considered impossible, recent studies have identified direct Ras binding small molecules that alter Ras function. Approaches to inhibit Ras membrane association include the development of farnesyltransferase inhibitors. Inhibitors of Ras effector signaling, in particular the Raf-MEK-ERK protein kinase cascade comprise the most active direction of anti-Ras drug discovery. Unbiased functional siRNA/shRNA library screens have identified genes that when suppressed, cause growth suppression of *RAS* mutant but not *RAS* wild type tumor cells. The identified synthetic lethal interactors (X) typically involve components that have no direct association with Ras signaling. Recently, with evidence that mutant RAS causes altered glucose and glutamine metabolism, approaches to target metabolism have also been considered.

Figure 1.10.

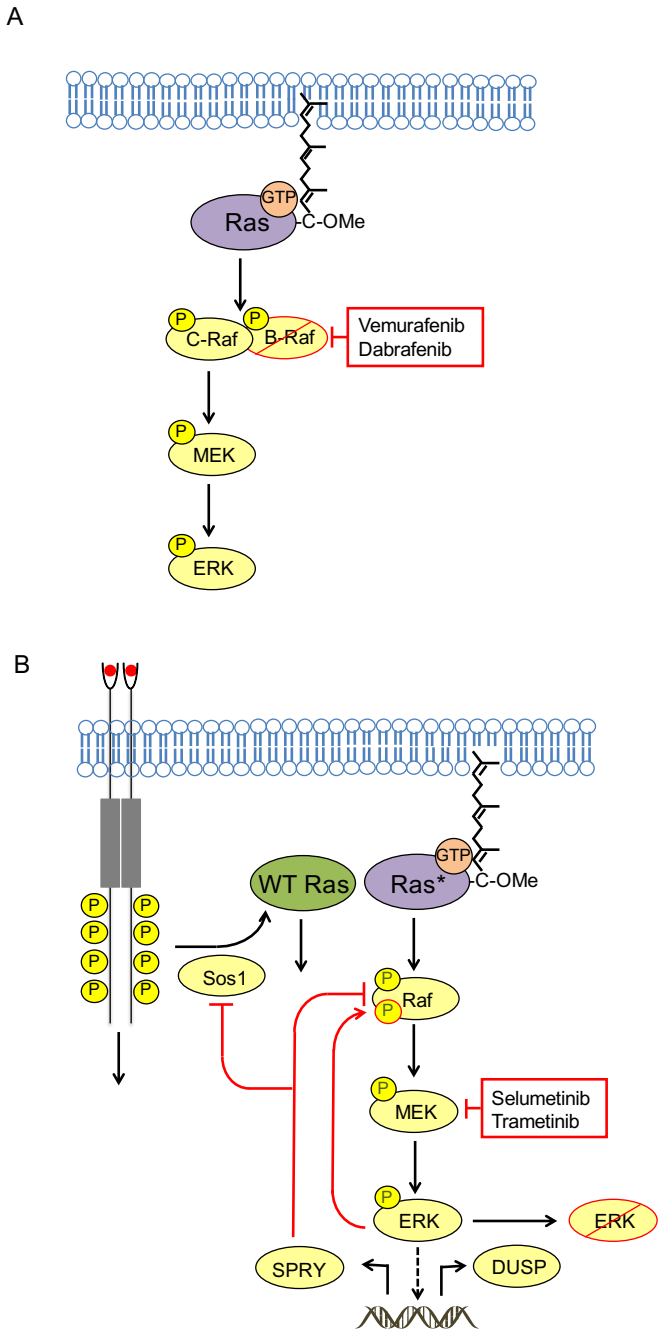

Figure 1.10. Mechanisms of *RAS* mutant cancer cell resistance to Raf or MEK inhibitors. (A). *RAS* mutant cancer cells exhibit paradoxical activation rather than inactivation of ERK signaling. (B) *RAS* mutant cancer cells exhibit multiple mechanisms of resistance to MEK inhibition. The mechanisms that relate to RTK and Sos activation of Ras are not expected to be relevant for mutant (*) Ras activity, since it is already persistently GTP-bound due to GAP insensitivity. However, since there is evidence that wild type (WT) Ras proteins support mutant Ras in cancer growth, these feedback mechanisms are then still important even in *RAS* mutant cancer cells.

Figure 1.11.

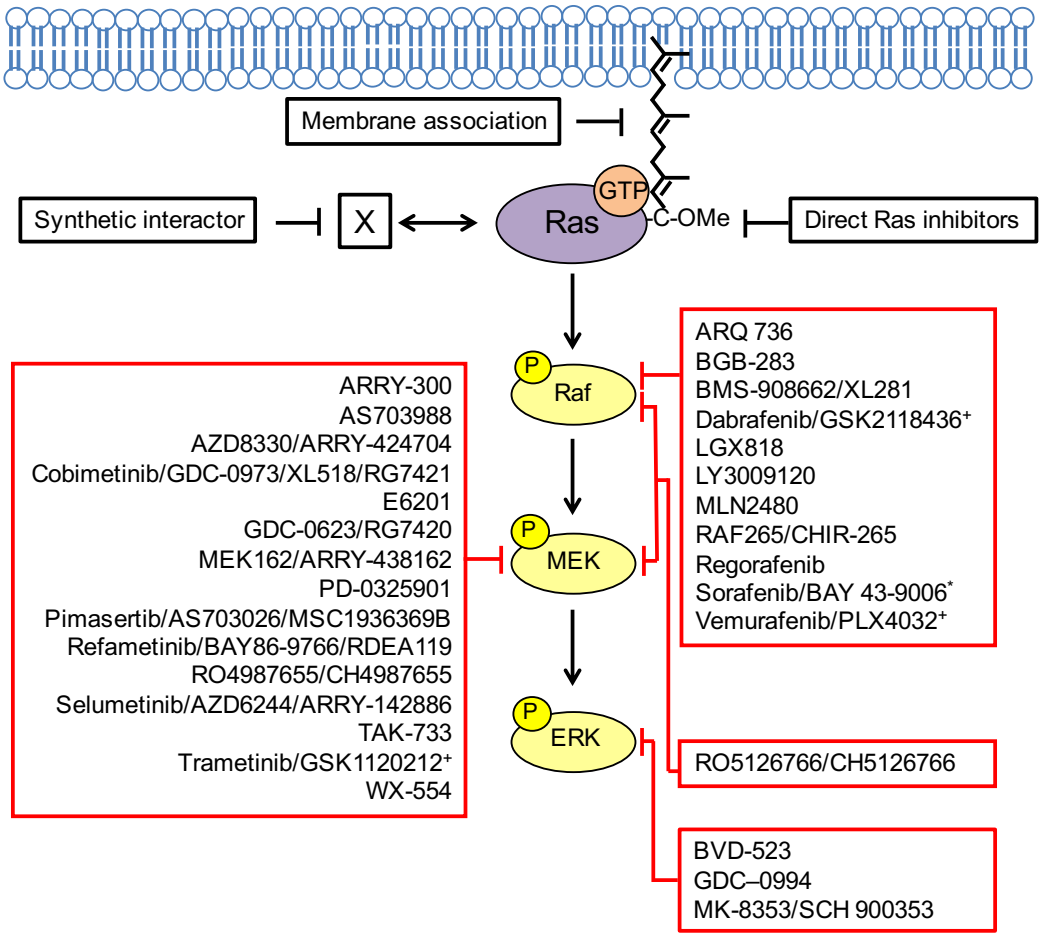

Figure 1.11. Pharmacologic inhibitors of Raf-MEK-ERK under clinical evaluation. Compiled from ClinicalTrials.gov. Past and/or ongoing approaches for targeting Ras include direct Ras binders and inhibitors of Ras function and inhibition of Ras membrane association. Functional si/shRNA library screens have been applied to identify genes (x), that when silenced, impair the growth of *RAS* mutant but not wild type tumor cell lines (aka synthetic lethal interactors of mutant Ras). *FDA-approved for the treatment of renal cell, hepatocellular and thyroid carcinoma; +FDA-approved for the treatment of *BRAF*-mutant melanoma.

REFERENCES

Ahearn, I.M., Haigis, K., Bar-Sagi, D., and Philips, M.R. (2012). Regulating the regulator: post-translational modification of RAS. Nat Rev Mol Cell Biol *13*, 39-51.

Bai, Y., Edamatsu, H., Maeda, S., Saito, H., Suzuki, N., Satoh, T., and Kataoka, T. (2004). Crucial role of phospholipase Cepsilon in chemical carcinogen-induced skin tumor development. Cancer research *64*, 8808-8810.

Bardeesy, N., Aguirre, A.J., Chu, G.C., Cheng, K.H., Lopez, L.V., Hezel, A.F., Feng, B., Brennan, C., Weissleder, R., Mahmood, U., et al. (2006a). Both p16(Ink4a) and the p19(Arf)-p53 pathway constrain progression of pancreatic adenocarcinoma in the mouse. Proc Natl Acad Sci U S A *103*, 5947-5952.

Bardeesy, N., Cheng, K.H., Berger, J.H., Chu, G.C., Pahler, J., Olson, P., Hezel, A.F., Horner, J., Lauwers, G.Y., Hanahan, D., et al. (2006b). Smad4 is dispensable for normal pancreas development yet critical in progression and tumor biology of pancreas cancer. Genes Dev *20*, 3130-3146.

Bass, A.J., Lawrence, M.S., Brace, L.E., Ramos, A.H., Drier, Y., Cibulskis, K., Sougnez, C., Voet, D., Saksena, G., Sivachenko, A., et al. (2011). Genomic sequencing of colorectal adenocarcinomas identifies a recurrent VTI1A-TCF7L2 fusion. Nat Genet *43*, 964-968.

Basso, A.D., Kirschmeier, P., and Bishop, W.R. (2006). Lipid posttranslational modifications. Farnesyl transferase inhibitors. J Lipid Res *47*, 15-31.

Berndt, N., Hamilton, A.D., and Sebti, S.M. (2011). Targeting protein prenylation for cancer therapy. Nature reviews Cancer *11*, 775-791.

Biankin, A.V., Waddell, N., Kassahn, K.S., Gingras, M.C., Muthuswamy, L.B., Johns, A.L., Miller, D.K., Wilson, P.J., Patch, A.M., Wu, J., et al. (2012). Pancreatic cancer genomes reveal aberrations in axon guidance pathway genes. Nature *491*, 399-405.

Blasco, R.B., Francoz, S., Santamaria, D., Canamero, M., Dubus, P., Charron, J., Baccarini, M., and Barbacid, M. (2011). c-Raf, but not B-Raf, is essential for development of K-Ras oncogene-driven non-small cell lung carcinoma. Cancer cell *19*, 652-663.

Brummelkamp, T.R., Bernards, R., and Agami, R. (2002). Stable suppression of tumorigenicity by virus-mediated RNA interference. Cancer Cell *2*, 243-247.

Bryant, K.L., Mancias, J.D., Kimmelman, A.C., and Der, C.J. (2014). KRAS: feeding pancreatic cancer proliferation. Trends Biochem Sci *39*, 91-100.

Burris, H.A., 3rd, Moore, M.J., Andersen, J., Green, M.R., Rothenberg, M.L., Modiano, M.R., Cripps, M.C., Portenoy, R.K., Storniolo, A.M., Tarassoff, P., et al. (1997). Improvements in survival and clinical benefit with gemcitabine as first-line therapy for patients with advanced pancreas cancer: a randomized trial. J Clin Oncol *15*, 2403-2413.

Bustinza-Linares, E., Kurzrock, R., and Tsimberidou, A.M. (2010). Salirasib in the treatment of pancreatic cancer. Future Oncol *6*, 885-891.

Campbell, P.M., Groehler, A.L., Lee, K.M., Ouellette, M.M., Khazak, V., and Der, C.J. (2007). K-Ras promotes growth transformation and invasion of immortalized human pancreatic cells by Raf and phosphatidylinositol 3-kinase signaling. Cancer research *67*, 2098-2106.

Chandra, A., Grecco, H.E., Pisupati, V., Perera, D., Cassidy, L., Skoulidis, F., Ismail, S.A., Hedberg, C., Hanzal-Bayer, M., Venkitaraman, A.R., et al. (2012). The GDI-like solubilizing factor PDEdelta sustains the spatial organization and signalling of Ras family proteins. Nat Cell Biol *14*, 148-158.

Coles, L.C., and Shaw, P.E. (2002). PAK1 primes MEK1 for phosphorylation by Raf-1 kinase during cross-cascade activation of the ERK pathway. Oncogene *21*, 2236-2244.

Collins, M.A., Bednar, F., Zhang, Y., Brisset, J.C., Galban, S., Galban, C.J., Rakshit, S., Flannagan, K.S., Adsay, N.V., and Pasca di Magliano, M. (2012a). Oncogenic Kras is required for both the initiation and maintenance of pancreatic cancer in mice. J Clin Invest *122*, 639-653.

Collins, M.A., Brisset, J.C., Zhang, Y., Bednar, F., Pierre, J., Heist, K.A., Galban, C.J., Galban, S., and di Magliano, M.P. (2012b). Metastatic pancreatic cancer is dependent on oncogenic Kras in mice. PLoS One *7*, e49707.

Collisson, E.A., Trejo, C.L., Silva, J.M., Gu, S., Korkola, J.E., Heiser, L.M., Charles, R.P., Rabinovich, B.A., Hann, B., Dankort, D., et al. (2012). A central role for RAF-->MEK-->ERK signaling in the genesis of pancreatic ductal adenocarcinoma. Cancer Discov *2*, 685-693.

Colvin, E.K., and Scarlett, C.J. (2014). A Historical Perspective of Pancreatic Cancer Mouse Models. Semin Cell Dev Biol.

Conroy, T., Desseigne, F., Ychou, M., Bouche, O., Guimbaud, R., Becouarn, Y., Adenis, A., Raoul, J.L., Gourgou-Bourgade, S., de la Fouchardiere, C., et al. (2011). FOLFIRINOX versus gemcitabine for metastatic pancreatic cancer. N Engl J Med *364*, 1817-1825.

Cowley, S., Paterson, H., Kemp, P., and Marshall, C.J. (1994). Activation of MAP kinase kinase is necessary and sufficient for PC12 differentiation and for transformation of NIH 3T3 cells. Cell *77*, 841-852.

Cox, A.D., and Der, C.J. (2010). Ras history: The saga continues. Small GTPases *1*, 2-27.

Cox, A.D., Fesik, S.W., Kimmelman, A.C., Luo, J., and Der, C.J. (2014). Drugging the undruggable RAS: Mission possible? Nat Rev Drug Discov *13*, 828-851.

Cuadrado, A., Bruder, J.T., Heidaran, M.A., App, H., Rapp, U.R., and Aaronson, S.A. (1993). H-ras and raf-1 cooperate in transformation of NIH3T3 fibroblasts. Oncogene *8*, 2443-2448.

Daouti, S., Higgins, B., Kolinsky, K., Packman, K., Wang, H., Rizzo, C., Moliterni, J., Huby, N., Fotouhi, N., Liu, M., et al. (2010). Preclinical in vivo evaluation of efficacy, pharmacokinetics, and pharmacodynamics of a novel MEK1/2 kinase inhibitor RO5068760 in multiple tumor models. Mol Cancer Ther *9*, 134-144.

Davies, H., Bignell, G.R., Cox, C., Stephens, P., Edkins, S., Clegg, S., Teague, J., Woffendin, H., Garnett, M.J., Bottomley, W., et al. (2002). Mutations of the BRAF gene in human cancer. Nature *417*, 949-954.

Dougherty, M.K., Muller, J., Ritt, D.A., Zhou, M., Zhou, X.Z., Copeland, T.D., Conrads, T.P., Veenstra, T.D., Lu, K.P., and Morrison, D.K. (2005). Regulation of Raf-1 by direct feedback phosphorylation. Molecular cell *17*, 215-224.

Drosten, M., Dhawahir, A., Sum, E.Y., Urosevic, J., Lechuga, C.G., Esteban, L.M., Castellano, E., Guerra, C., Santos, E., and Barbacid, M. (2010). Genetic analysis of Ras signalling pathways in cell proliferation, migration and survival. The EMBO journal *29*, 1091-1104.

Duncan, J.S., Whittle, M.C., Nakamura, K., Abell, A.N., Midland, A.A., Zawistowski, J.S., Johnson, N.L., Granger, D.A., Jordan, N.V., Darr, D.B., et al. (2012). Dynamic reprogramming of the kinome in response to targeted MEK inhibition in triple-negative breast cancer. Cell *149*, 307-321.

Ehrenreiter, K., Kern, F., Velamoor, V., Meissl, K., Galabova-Kovacs, G., Sibilia, M., and Baccarini, M. (2009). Raf-1 addiction in Ras-induced skin carcinogenesis. Cancer cell *16*, 149-160.

Engelman, J.A., Chen, L., Tan, X., Crosby, K., Guimaraes, A.R., Upadhyay, R., Maira, M., McNamara, K., Perera, S.A., Song, Y., et al. (2008). Effective use of PI3K and MEK inhibitors to treat mutant Kras G12D and PIK3CA H1047R murine lung cancers. Nat Med *14*, 1351-1356.

Eser, S., Reiff, N., Messer, M., Seidler, B., Gottschalk, K., Dobler, M., Hieber, M., Arbeiter, A., Klein, S., Kong, B., et al. (2013). Selective requirement of PI3K/PDK1 signaling for Kras oncogene-driven pancreatic cell plasticity and cancer. Cancer cell *23*, 406-420.

Farrell, A.S., and Sears, R.C. (2014). MYC Degradation. Cold Spring Harb Perspect Med *4*.

Feig, L.A., and Cooper, G.M. (1988). Inhibition of NIH 3T3 cell proliferation by a mutant ras protein with preferential affinity for GDP. Mol Cell Biol *8*, 3235-3243.

Fischmann, T.O., Smith, C.K., Mayhood, T.W., Myers, J.E., Reichert, P., Mannarino, A., Carr, D., Zhu, H., Wong, J., Yang, R.S., et al. (2009). Crystal structures of MEK1 binary and ternary complexes with nucleotides and inhibitors. Biochemistry *48*, 2661-2674.

Flaherty, K.T., Puzanov, I., Kim, K.B., Ribas, A., McArthur, G.A., Sosman, J.A., O'Dwyer, P.J., Lee, R.J., Grippo, J.F., Nolop, K., et al. (2010). Inhibition of mutated, activated BRAF in metastatic melanoma. N Engl J Med *363*, 809-819.

Fritsch, R., de Krijger, I., Fritsch, K., George, R., Reason, B., Kumar, M.S., Diefenbacher, M., Stamp, G., and Downward, J. (2013). RAS and RHO families of GTPases directly regulate distinct phosphoinositide 3-kinase isoforms. Cell *153*, 1050-1063.

Gupta, S., Ramjaun, A.R., Haiko, P., Wang, Y., Warne, P.H., Nicke, B., Nye, E., Stamp, G., Alitalo, K., and Downward, J. (2007). Binding of ras to phosphoinositide 3-kinase p110alpha is required for ras-driven tumorigenesis in mice. Cell *129*, 957-968.

Hatano, N., Mori, Y., Oh-hora, M., Kosugi, A., Fujikawa, T., Nakai, N., Niwa, H., Miyazaki, J., Hamaoka, T., and Ogata, M. (2003). Essential role for ERK2 mitogen-activated protein kinase in placental development. Genes Cells *8*, 847-856.

Hatzivassiliou, G., Liu, B., O'Brien, C., Spoerke, J.M., Hoeflich, K.P., Haverty, P.M., Soriano, R., Forrest, W.F., Heldens, S., Chen, H., et al. (2012). ERK inhibition overcomes acquired resistance to MEK inhibitors. Mol Cancer Ther *11*, 1143-1154.

Hauge, C., and Frodin, M. (2006). RSK and MSK in MAP kinase signalling. J Cell Sci *119*, 3021-3023.

Heidorn, S.J., Milagre, C., Whittaker, S., Nourry, A., Niculescu-Duvas, I., Dhomen, N., Hussain, J., Reis-Filho, J.S., Springer, C.J., Pritchard, C., et al. (2010). Kinase-dead BRAF and oncogenic RAS cooperate to drive tumor progression through CRAF. Cell *140*, 209-221.

Hingorani, S.R., Jacobetz, M.A., Robertson, G.P., Herlyn, M., and Tuveson, D.A. (2003a). Suppression of BRAF(V599E) in human melanoma abrogates transformation. Cancer Res *63*, 5198-5202.

Hingorani, S.R., Petricoin, E.F., Maitra, A., Rajapakse, V., King, C., Jacobetz, M.A., Ross, S., Conrads, T.P., Veenstra, T.D., Hitt, B.A., et al. (2003b). Preinvasive and invasive ductal pancreatic cancer and its early detection in the mouse. Cancer Cell *4*, 437-450.

Hingorani, S.R., Wang, L., Multani, A.S., Combs, C., Deramaudt, T.B., Hruban, R.H., Rustgi, A.K., Chang, S., and Tuveson, D.A. (2005). Trp53R172H and KrasG12D cooperate to promote chromosomal instability and widely metastatic pancreatic ductal adenocarcinoma in mice. Cancer Cell *7*, 469-483.

Hoeflich, K.P., Gray, D.C., Eby, M.T., Tien, J.Y., Wong, L., Bower, J., Gogineni, A., Zha, J., Cole, M.J., Stern, H.M., et al. (2006). Oncogenic BRAF is required for tumor growth and maintenance in melanoma models. Cancer research *66*, 999-1006.

Hou, J., Lam, F., Proud, C., and Wang, S. (2012). Targeting Mnks for cancer therapy. Oncotarget *3*, 118-131.

Huguet, F., Andre, T., Hammel, P., Artru, P., Balosso, J., Selle, F., Deniaud-Alexandre, E., Ruszniewski, P., Touboul, E., Labianca, R., et al. (2007). Impact of chemoradiotherapy after disease control with chemotherapy in locally advanced pancreatic adenocarcinoma in GERCOR phase II and III studies. J Clin Oncol *25*, 326-331.

Jones, S., Zhang, X., Parsons, D.W., Lin, J.C., Leary, R.J., Angenendt, P., Mankoo, P., Carter, H., Kamiyama, H., Jimeno, A., et al. (2008). Core signaling pathways in human pancreatic cancers revealed by global genomic analyses. Science *321*, 1801-1806.

Karakas, B., Bachman, K.E., and Park, B.H. (2006). Mutation of the PIK3CA oncogene in human cancers. Br J Cancer *94*, 455-459.

Karasarides, M., Chiloeches, A., Hayward, R., Niculescu-Duvaz, D., Scanlon, I., Friedlos, F., Ogilvie, L., Hedley, D., Martin, J., Marshall, C.J., et al. (2004). B-RAF is a therapeutic target in melanoma. Oncogene *23*, 6292-6298.

Karreth, F.A., Frese, K.K., DeNicola, G.M., Baccarini, M., and Tuveson, D.A. (2011). C-Raf is required for the initiation of lung cancer by K-Ras(G12D). Cancer Discov *1*, 128-136.

Khosravi-Far, R., Solski, P.A., Clark, G.J., Kinch, M.S., and Der, C.J. (1995). Activation of Rac1, RhoA, and mitogen-activated protein kinases is required for Ras transformation. Mol Cell Biol *15*, 6443-6453.

Khosravi-Far, R., White, M.A., Westwick, J.K., Solski, P.A., Chrzanowska-Wodnicka, M., Van Aelst, L., Wigler, M.H., and Der, C.J. (1996). Oncogenic Ras activation of Raf/mitogen-activated protein kinase-independent pathways is sufficient to cause tumorigenic transformation. Mol Cell Biol *16*, 3923-3933.

Kolch, W., Heidecker, G., Lloyd, P., and Rapp, U.R. (1991). Raf-1 protein kinase is required for growth of induced NIH/3T3 cells. Nature *349*, 426-428.

Lefloch, R., Pouyssegur, J., and Lenormand, P. (2009). Total ERK1/2 activity regulates cell proliferation. Cell Cycle *8*, 705-711.

Li, Y., Takahashi, M., and Stork, P.J. (2013). Ras-mutant cancer cells display B-Raf binding to Ras that activates extracellular signal-regulated kinase and is inhibited by protein kinase A phosphorylation. The Journal of biological chemistry *288*, 27646-27657.

Lim, K.H., and Counter, C.M. (2005). Reduction in the requirement of oncogenic Ras signaling to activation of PI3K/AKT pathway during tumor maintenance. Cancer Cell *8*, 381-392.

Little, A.S., Balmanno, K., Sale, M.J., Newman, S., Dry, J.R., Hampson, M., Edwards, P.A., Smith, P.D., and Cook, S.J. (2011). Amplification of the driving oncogene, KRAS or BRAF, underpins acquired resistance to MEK1/2 inhibitors in colorectal cancer cells. Sci Signal *4*, ra17.

Luo, T., Masson, K., Jaffe, J.D., Silkworth, W., Ross, N.T., Scherer, C.A., Scholl, C., Frohling, S., Carr, S.A., Stern, A.M., et al. (2012). STK33 kinase inhibitor BRD-8899 has no effect on KRAS-dependent cancer cell viability. Proceedings of the National Academy of Sciences of the United States of America *109*, 2860-2865.

Malliri, A., van der Kammen, R.A., Clark, K., van der Valk, M., Michiels, F., and Collard, J.G. (2002). Mice deficient in the Rac activator Tiam1 are resistant to Ras-induced skin tumours. Nature *417*, 867-871.

Matallanas, D., Birtwistle, M., Romano, D., Zebisch, A., Rauch, J., von Kriegsheim, A., and Kolch, W. (2011). Raf family kinases: old dogs have learned new tricks. Genes Cancer *2*, 232-260.

Maurer, T., Garrenton, L.S., Oh, A., Pitts, K., Anderson, D.J., Skelton, N.J., Fauber, B.P., Pan, B., Malek, S., Stokoe, D., et al. (2012). Small-molecule ligands bind to a distinct pocket in Ras and inhibit SOS-mediated nucleotide exchange activity. Proceedings of the National Academy of Sciences of the United States of America.

Mitin, N., Rossman, K.L., and Der, C.J. (2005). Signaling interplay in Ras superfamily function. Curr Biol *15*, R563-574.

Moloney, J.B. (1966). A virus-induced rhabdomyosarcoma of mice. Natl Cancer Inst Monogr *22*, 139-142.

Moore, M.J., Goldstein, D., Hamm, J., Figer, A., Hecht, J.R., Gallinger, S., Au, H.J., Murawa, P., Walde, D., Wolff, R.A., et al. (2007). Erlotinib plus gemcitabine compared with gemcitabine alone in patients with advanced pancreatic cancer: a phase III trial of the National Cancer Institute of Canada Clinical Trials Group. J Clin Oncol *25*, 1960-1966.

Morris, E.J., Jha, S., Restaino, C.R., Dayananth, P., Zhu, H., Cooper, A., Carr, D., Deng, Y., Jin, W., Black, S., et al. (2013). Discovery of a novel ERK inhibitor with activity in models of acquired resistance to BRAF and MEK inhibitors. Cancer Discov *3*, 742-750.

Nazarian, R., Shi, H., Wang, Q., Kong, X., Koya, R.C., Lee, H., Chen, Z., Lee, M.K., Attar, N., Sazegar, H., et al. (2010). Melanomas acquire resistance to B-RAF(V600E) inhibition by RTK or N-RAS upregulation. Nature *468*, 973-977.

Neoptolemos, J.P., Stocken, D.D., Bassi, C., Ghaneh, P., Cunningham, D., Goldstein, D., Padbury, R., Moore, M.J., Gallinger, S., Mariette, C., et al. (2010). Adjuvant chemotherapy with fluorouracil plus folinic acid vs gemcitabine following pancreatic cancer resection: a randomized controlled trial. JAMA *304*, 1073-1081.

Nissan, M.H., Rosen, N., and Solit, D.B. (2013). ERK pathway inhibitors: how low should we go? Cancer Discov *3*, 719-721.

Oettle, H., Post, S., Neuhaus, P., Gellert, K., Langrehr, J., Ridwelski, K., Schramm, H., Fahlke, J., Zuelke, C., Burkart, C., et al. (2007). Adjuvant chemotherapy with gemcitabine vs observation in patients undergoing curative-intent resection of pancreatic cancer: a randomized controlled trial. JAMA *297*, 267-277.

Ostrem, J.M., Peters, U., Sos, M.L., Wells, J.A., and Shokat, K.M. (2013). K-Ras(G12C) inhibitors allosterically control GTP affinity and effector interactions. Nature *503*, 548-551.

Pages, G., Guerin, S., Grall, D., Bonino, F., Smith, A., Anjuere, F., Auberger, P., and Pouyssegur, J. (1999). Defective thymocyte maturation in p44 MAP kinase (Erk 1) knockout mice. Science *286*, 1374-1377.

Pratilas, C.A., Taylor, B.S., Ye, Q., Viale, A., Sander, C., Solit, D.B., and Rosen, N. (2009). (V600E)BRAF is associated with disabled feedback inhibition of RAF-MEK signaling and elevated transcriptional output of the pathway. Proceedings of the National Academy of Sciences of the United States of America *106*, 4519-4524.

Prior, I.A., Lewis, P.D., and Mattos, C. (2012). A comprehensive survey of Ras mutations in cancer. Cancer Res *72*, 2457-2467.

Qin, J., Xin, H., and Nickoloff, B.J. (2012). Specifically targeting ERK1 or ERK2 kills melanoma cells. J Transl Med *10*, 15.

Rajagopalan, H., Bardelli, A., Lengauer, C., Kinzler, K.W., Vogelstein, B., and Velculescu, V.E. (2002). Tumorigenesis: RAF/RAS oncogenes and mismatch-repair status. Nature *418*, 934.

Rauen, K.A. (2013). The RASopathies. Annu Rev Genomics Hum Genet *14*, 355-369.

Rodriguez-Viciana, P., Sabatier, C., and McCormick, F. (2004). Signaling specificity by Ras family GTPases is determined by the full spectrum of effectors they regulate. Mol Cell Biol *24*, 4943-4954.

Romeo, Y., Zhang, X., and Roux, P.P. (2012). Regulation and function of the RSK family of protein kinases. Biochem J *441*, 553-569.

Roskoski, R., Jr. (2010). RAF protein-serine/threonine kinases: structure and regulation. Biochem Biophys Res Commun *399*, 313-317.

Roskoski, R., Jr. (2012a). ERK1/2 MAP kinases: structure, function, and regulation. Pharmacol Res *66*, 105-143.

Roskoski, R., Jr. (2012b). MEK1/2 dual-specificity protein kinases: structure and regulation. Biochem Biophys Res Commun *417*, 5-10.

Saba-El-Leil, M.K., Vella, F.D., Vernay, B., Voisin, L., Chen, L., Labrecque, N., Ang, S.L., and Meloche, S. (2003). An essential function of the mitogen-activated protein kinase Erk2 in mouse trophoblast development. EMBO Rep *4*, 964-968.

Salmeron, A., Ahmad, T.B., Carlile, G.W., Pappin, D., Narsimhan, R.P., and Ley, S.C. (1996). Activation of MEK-1 and SEK-1 by Tpl-2 proto-oncoprotein, a novel MAP kinase kinase kinase. EMBO J *15*, 817-826.

Schaap, D., van der Wal, J., Howe, L.R., Marshall, C.J., and van Blitterswijk, W.J. (1993). A dominant-negative mutant of raf blocks mitogen-activated protein kinase activation by growth factors and oncogenic p21ras. The Journal of biological chemistry *268*, 20232-20236.

Scheffzek, K., Ahmadian, M.R., Kabsch, W., Wiesmuller, L., Lautwein, A., Schmitz, F., and Wittinghofer, A. (1997). The Ras-RasGAP complex: structural basis for GTPase activation and its loss in oncogenic Ras mutants. Science *277*, 333-338.

Scheidig, A.J., Burmester, C., and Goody, R.S. (1999). The pre-hydrolysis state of p21(ras) in complex with GTP: new insights into the role of water molecules in the GTP hydrolysis reaction of ras-like proteins. Structure *7*, 1311-1324.

Seshagiri, S., Stawiski, E.W., Durinck, S., Modrusan, Z., Storm, E.E., Conboy, C.B., Chaudhuri, S., Guan, Y., Janakiraman, V., Jaiswal, B.S., et al. (2012). Recurrent R-spondin fusions in colon cancer. Nature *488*, 660-664.

Sharma, A., Trivedi, N.R., Zimmerman, M.A., Tuveson, D.A., Smith, C.D., and Robertson, G.P. (2005). Mutant V599EB-Raf regulates growth and vascular development of malignant melanoma tumors. Cancer research *65*, 2412-2421.

Shin, S., Dimitri, C.A., Yoon, S.O., Dowdle, W., and Blenis, J. (2010). ERK2 but not ERK1 induces epithelial-to-mesenchymal transformation via DEF motif-dependent signaling events. Molecular cell *38*, 114-127.

Sieben, N.L., Macropoulos, P., Roemen, G.M., Kolkman-Uljee, S.M., Jan Fleuren, G., Houmadi, R., Diss, T., Warren, B., Al Adnani, M., De Goeij, A.P., et al. (2004). In ovarian neoplasms,

BRAF, but not KRAS, mutations are restricted to low-grade serous tumours. J Pathol *202*, 336-340.

Siegel, R., Ma, J., Zou, Z., and Jemal, A. (2014). Cancer statistics, 2014. CA Cancer J Clin *64*, 9-29.

Singer, G., Oldt, R., 3rd, Cohen, Y., Wang, B.G., Sidransky, D., Kurman, R.J., and Shih Ie, M. (2003). Mutations in BRAF and KRAS characterize the development of low-grade ovarian serous carcinoma. J Natl Cancer Inst *95*, 484-486.

Singh, A., Greninger, P., Rhodes, D., Koopman, L., Violette, S., Bardeesy, N., and Settleman, J. (2009). A gene expression signature associated with "K-Ras addiction" reveals regulators of EMT and tumor cell survival. Cancer Cell *15*, 489-500.

Slack-Davis, J.K., Eblen, S.T., Zecevic, M., Boerner, S.A., Tarcsafalvi, A., Diaz, H.B., Marshall, M.S., Weber, M.J., Parsons, J.T., and Catling, A.D. (2003). PAK1 phosphorylation of MEK1 regulates fibronectin-stimulated MAPK activation. J Cell Biol *162*, 281-291.

Solit, D.B., Garraway, L.A., Pratilas, C.A., Sawai, A., Getz, G., Basso, A., Ye, Q., Lobo, J.M., She, Y., Osman, I., et al. (2006). BRAF mutation predicts sensitivity to MEK inhibition. Nature *439*, 358-362.

Stephen, A.G., Esposito, D., Bagni, R.K., and McCormick, F. (2014). Dragging Ras Back in the Ring. Cancer cell *25*, 272-281.

Subramanian, R.R., and Yamakawa, A. (2012). Combination therapy targeting Raf-1 and MEK causes apoptosis of HCT116 colon cancer cells. Int J Oncol *41*, 1855-1862.

Sumimoto, H., Hirata, K., Yamagata, S., Miyoshi, H., Miyagishi, M., Taira, K., and Kawakami, Y. (2006). Effective inhibition of cell growth and invasion of melanoma by combined suppression of BRAF (V599E) and Skp2 with lentiviral RNAi. Int J Cancer *118*, 472-476.

Sun, Q., Burke, J.P., Phan, J., Burns, M.C., Olejniczak, E.T., Waterson, A.G., Lee, T., Rossanese, O.W., and Fesik, S.W. (2012). Discovery of Small Molecules that Bind to K-Ras and Inhibit Sos-Mediated Activation. Angew Chem Int Ed Engl.

Vigil, D., Cherfils, J., Rossman, K.L., and Der, C.J. (2010). Ras superfamily GEFs and GAPs: validated and tractable targets for cancer therapy? Nat Rev Cancer *10*, 842-857.

Von Hoff, D.D., Ervin, T., Arena, F.P., Chiorean, E.G., Infante, J., Moore, M., Seay, T., Tjulandin, S.A., Ma, W.W., Saleh, M.N., et al. (2013). Increased survival in pancreatic cancer with nab-paclitaxel plus gemcitabine. N Engl J Med *369*, 1691-1703.

Waddell, N., Pajic, M., Patch, A.M., Chang, D.K., Kassahn, K.S., Bailey, P., Johns, A.L., Miller, D., Nones, K., Quek, K., et al. (2015). Whole genomes redefine the mutational landscape of pancreatic cancer. Nature *518*, 495-501.

Wagle, N., Van Allen, E.M., Treacy, D.J., Frederick, D.T., Cooper, Z.A., Taylor-Weiner, A., Rosenberg, M., Goetz, E.M., Sullivan, R.J., Farlow, D.N., et al. (2014). MAP Kinase Pathway Alterations in BRAF-Mutant Melanoma Patients with Acquired Resistance to Combined RAF/MEK Inhibition. Cancer Discov *4*, 61-68.

Weiwer, M., Spoonamore, J., Wei, J., Guichard, B., Ross, N.T., Masson, K., Silkworth, W., Dandapani, S., Palmer, M., Scherer, C.A., et al. (2012). A Potent and Selective Quinoxalinone-Based STK33 Inhibitor Does Not Show Synthetic Lethality in KRAS-Dependent Cells. ACS Med Chem Lett *3*, 1034-1038.

White, M.A., Nicolette, C., Minden, A., Polverino, A., Van Aelst, L., Karin, M., and Wigler, M.H. (1995). Multiple Ras functions can contribute to mammalian cell transformation. Cell *80*, 533-541.

Wood, L.D., Parsons, D.W., Jones, S., Lin, J., Sjoblom, T., Leary, R.J., Shen, D., Boca, S.M., Barber, T., Ptak, J., et al. (2007). The genomic landscapes of human breast and colorectal cancers. Science *318*, 1108-1113.

Yao, Y., Li, W., Wu, J., Germann, U.A., Su, M.S., Kuida, K., and Boucher, D.M. (2003). Extracellular signal-regulated kinase 2 is necessary for mesoderm differentiation. Proceedings of the National Academy of Sciences of the United States of America *100*, 12759-12764.

Ying, H., Kimmelman, A.C., Lyssiotis, C.A., Hua, S., Chu, G.C., Fletcher-Sananikone, E., Locasale, J.W., Son, J., Zhang, H., Coloff, J.L., et al. (2012). Oncogenic Kras maintains pancreatic tumors through regulation of anabolic glucose metabolism. Cell *149*, 656-670.

Yoon, S., and Seger, R. (2006). The extracellular signal-regulated kinase: multiple substrates regulate diverse cellular functions. Growth Factors *24*, 21-44.

Zimmermann, G., Papke, B., Ismail, S., Vartak, N., Chandra, A., Hoffmann, M., Hahn, S.A., Triola, G., Wittinghofer, A., Bastiaens, P.I., et al. (2013). Small molecule inhibition of the KRAS-PDEdelta interaction impairs oncogenic KRAS signalling. Nature *497*, 638-642.

CHAPTER 2: PROLONGED ERK INHIBITION IN *KRAS*-MUTANT PANCREATIC CANCER IS ASSOCIATED WITH MYC DEGRADATION AND SENESCENCE-LIKE GROWTH SUSPRESSON[1]

INTRODUCTION

Mutational activation of *KRAS* is found in >95% of pancreatic ductal adenocarcinomas (PDAC) (Bryant et al., 2014). With strong and compelling evidence that the continued function of mutant *KRAS* is essential for PDAC maintenance, there has been intense effort in developing pharmacologic approaches to block mutationally activated KRAS for cancer treatment (Cox et al., 2014; Stephen et al., 2014). Currently the most promising strategy involves inhibitors of RAS effector signaling, in particular the RAF serine/threonine kinases (Cox et al., 2014; Stephen et al., 2014). Activated RAS binds to RAF and promotes its activation. RAF then phosphorylates and activates the MEK1 and MEK2 dual specificity protein kinases, which in turn phosphorylate the related ERK1 and ERK2 MAPKs. Activated ERK1/2 then phosphorylate more than 200 substrates (Yoon and Seger, 2006).

The limited substrates of RAF and MEK prompted earlier assumptions that pharmacologic inhibitors of either kinase would be equivalent and equally effective in blocking ERK activation. This led to the development and evaluation of small molecule inhibitors of RAF or MEK, with at least 27 under clinical evaluation (ClinicalTrials.gov). However, RAF kinase inhibitors have been ineffective in *RAS*-mutant cancers as a consequence of paradoxical induction of Ras-dependent RAF dimerization and activation, with subsequent enhanced ERK activation (Lito et al., 2013).

MEK inhibitors have shown limited to no activity in *RAS*-mutant cancers, most commonly attributed to loss of ERK feedback inhibition and compensatory mechanisms that cause reactivation of ERK (Samatar and Poulikakos, 2014). [1]

Since reactivation of ERK is a major mechanism overcoming RAF or MEK inhibitor efficacy, we hypothesized that direct inhibition of ERK may overcome these limitations. In support of this, we recently described the development of a ERK1/2-selective pharmacologic inhibitor (SCH772984) and showed that *BRAF*-mutant melanomas with acquired resistance to RAF and/or to MEK inhibitors were still sensitive to ERK1/2-selective pharmacologic inhibitors (Hatzivassiliou et al., 2012; Morris et al., 2013). ERK inhibition suppressed the growth of ~50% of *RAS*-mutant human tumor cell lines in vitro. However, the mechanisms behind ERK inhibitor susceptibility versus resistance of subsets of *RAS*-mutant cancers remain unresolved (Hatzivassiliou et al., 2012). In the present study we assessed the mechanistic basis of ERK inhibitor sensitivity in *KRAS*-mutant PDAC, and applied unbiased chemical and genetic library screens to identify combination approaches to enhance anti-ERK therapies.

RESULTS

MEK Inhibitor-Resistant PDAC Cell Lines Are Sensitive to ERK Inhibitor

Our recent analyses showed that the ERK1/2-selective inhibitor SCH772984 potently suppressed the growth of ~50% of *RAS*-mutant human tumor cell lines in vitro (Morris et al., 2013). However, the mechanistic bases for ERK inhibitor sensitivity and de novo resistance were not addressed. Since PDAC is the most *KRAS*-addicted cancer, we first focused on evaluating SCH772984 in a panel of 11 *KRAS*-mutant PDAC cell lines (Table 2.1). Anchorage-dependent proliferation was monitored for 72 hr (Figure 2.1A). We found that five cell lines were sensitive to SCH772984 (GI_{50} <4 μM), whereas six exhibited de novo resistance (GI_{50} >4 μM). Surprisingly, three out of four SCH772984-sensitive cell lines were resistant to the MEK inhibitor selumetinib

[1] Hayes et al. Cancer Cell, in press

(Figure 2.1B), independent of the degree of suppression of ERK phosphorylation (Figure 2.2C). Thus, inhibition of the pathway at the level of ERK has distinct consequences from inhibition at the level of MEK.

We next expanded our panel of *KRAS*-mutant pancreatic cancer cell lines to include those derived from PDAC patient-derived xenografts (Table 2.2). Interestingly, we found a similar pattern of sensitivity to SCH772984, where some cell lines were sensitive and others were resistant (Figure 2.2A). We observed that treatment with a chemically and mechanistically distinct ERK inhibitor, BVD-523 (ulixertinib), a current clinical candidate (NCT01781429) (Germann, 2015), resulted in a similar pattern of sensitivity in both established and PDX cell lines (Figure 2.2A and 2.2B).

ERK Inhibitor Sensitivity Is Not Associated with KRAS Dependency or with K-Ras-dependent Effector Signaling

Previous studies showed that only a subset of *KRAS*-mutant PDAC cell lines exhibited *KRAS* dependency (Singh et al., 2009). To determine if *KRAS* dependency correlates with sensitivity to SCH772984, we evaluated the consequence of transient siRNA-mediated suppression of *KRAS* expression in our cell lines (Figure 2.1C). *KRAS* knockdown resulted in ~50% reduction in anchorage-dependent viability (Figures 2.1D and 2.2D) and 50% or greater reduction in clonogenic growth (Figures 2.1E and 2.2E). Using the same shRNA *KRAS* vectors used in the previous study (Singh et al., 2009), we established mass populations of stably infected cells displaying >80% reduction in K-Ras4B protein (Figure 2.2F). We found >50% reduction in both anchorage-dependent and anchorage-independent growth in all cell lines (Figures 2.2G and 2.2H). We conclude that *KRAS*-dependent growth is not a predictor of ERK inhibitor sensitivity.

We next determined whether ERK inhibitor sensitivity correlates with K-Ras-dependent ERK activation. Neither transient nor sustained *KRAS* suppression reproducibly suppressed pERK in any cell line (Figures 2.1C and 2.2F). Transient *KRAS* suppression significantly reduced

pAKT in 3 of 9 cell lines, whereas stable suppression did not. Thus, SCH772984 sensitivity was not associated with K-Ras-dependent ERK or AKT activation.

Short-term Treatment with SCH772984 Enhances Apoptosis and Alters Cell Cycle Regulation

Next, we investigated the mechanism of SCH772984-induced growth suppression. After 72 hr treatment, we observed a significant fraction of non-adherent cells in the sensitive cell lines. Enhanced caspase-3 cleavage was detected in both non-adherent (Figure 2.3A) and adherent (Figure 2.4A) cell populations.

We then determined if ERK inhibition perturbed cell cycle progression. Using flow cytometry, we observed that three of four sensitive cell lines showed a significant treatment-induced increase in cells in G_0/G_1 and a concomitant decrease in cells in S and G_2/M (Figure 2.3B). Treated cell lines also exhibited reduced levels of cyclin D1 and B1, regulators of progression through G_1 and M, respectively, as well as hypophosphorylation and activation of RB, and reduced p21 protein levels (Figure 2.3C). Additionally, we found that sensitive cell lines exhibited increased sensitivity to SCH772984 over time as measured by changes in GI_{50} values (Figure 2.4B). We conclude that short-term treatment with SCH772984 suppresses PDAC tumor cell growth by enhancing apoptosis and/or by impairing progression through G_1 and mitosis.

ERK Inhibitor Induction of AKT Activation Is a Marker of Sensitivity

Rapid ERK inhibitor-induced kinome reprogramming may cause dynamic changes in the activities of signaling components that distinguish sensitive from resistant cell lines (Duncan et al., 2012). Therefore, we evaluated signaling changes caused by SCH772984 treatment at 4, 24 and 72 hr. We monitored the consequences of both mechanisms of SCH772984 inhibition of ERK (Morris et al., 2013): inhibition of MEK1/2 binding and phosphorylation of ERK1/2, and inhibition of ATP binding and ERK1/2 phosphorylation of their cytoplasmic substrate, p90 RSK. After 4 hr, pERK and pRSK levels were reduced in both sensitive and resistant cell lines (Figure 2.5A). After 24 hr, pERK but not pRSK levels rebounded over vehicle control levels in both

sensitive and resistant cell lines. However, by 72 hr, pERK increased further in a dose-dependent manner, whereas pRSK levels remained reduced even at 72 hr (Figures 2.6A and 2.6C). Thus, kinome reprogramming overcomes SCH772984 inhibition of ERK phosphorylation by MEK, but not ERK signaling, in both sensitive and resistant cell lines.

We next determined a basis for the transient and reversible suppression of ERK1/2 phosphorylation by SCH772984. Treatment with SCH772984 for 72 hr caused suppression of the ERK phosphatase DUSP4 in 5 of 6 cell lines, which could contribute to pERK restoration (Figures 2.5B and 2.6E). However, an alternative mechanism was suggested by the increased levels of pMEK1/2 observed at 4 and 24 hr (Figure 2.5A and 2.6B), indicating potential loss of ERK-mediated negative feedback inhibition of KRAS-RAF-MEK signaling (Dougherty et al., 2005). Consistent with this possibility, concurrent treatment with the MEK inhibitor selumetinib prevented the increase in pERK1/2 (Figure 2.5C). Furthermore, SCH772984 both reduced ERK-mediated phosphorylation of CRAF at S289/296/301 and increased phosphorylation at S338, a marker of CRAF activation (Figures 2.5D and 2.6D). Thus, SCH772984-initiated loss of ERK-dependent negative feedback leads to increased CRAF and MEK activation in both sensitive and resistant cell lines without inducing the restoration of active ERK signaling as measured by pRSK.

MEK inhibitor treatment has been linked to activation of phosphatidylinositol-3 kinase (PI3K)-AKT serine/threonine kinase signaling to re-sensitize *BRAF* inhibitor-resistant melanoma cell lines (Villanueva et al., 2010). Therefore, we determined whether phosphorylation of the PI3K substrate AKT was also elevated as a consequence of SCH772984 treatment in our sensitive cell lines. Consistent with that previous study (Villanueva et al., 2010), we observed a dose-dependent increase in pAKT at 72 hr in all sensitive but not resistant cell lines (Figure 2.6B and 2.6D). Next, we expanded our analysis to the PDX cell lines. We found that 66% of sensitive cell lines exhibited increased levels of pAKT (Figure 2.6G). Thus, treatment-induced pAKT elevation provided a biomarker for ERK inhibitor sensitivity.

To assess whether increased AKT activation is a compensatory protective response to overcome ERK inhibition-induced growth suppression, we co-treated cells with both SCH772984 and the PI3K inhibitor AZD8186 (Hancox et al., 2015) to block the ERK inhibitor-associated increases in pAKT (Figures 2.5F and 2.6F). Concurrent PI3K inhibition increased growth inhibition in sensitive cell lines, associated with caspase-3 cleavage, but surprisingly not in resistant cell lines (Figure 2.5E). SCH772984-sensitive PDX cell lines also exhibited synergy when exposed to the combination of SCH772984 and AZD8186 (Figure 2.6H). Similarly, in sensitive cell lines we also observed synergy with BVD-523 in combination with PI3K inhibition (Figure 2.6I-J). Together, our data suggest ERK and PI3K inhibitors as a potential clinically relevant combination therapy in *KRAS*-mutant PDAC.

Mechanistically Diverse Inhibitor Combinations Synergistically Enhance the Growth Inhibitory Activity of ERK Inhibitor versus MEK Inhibitor

Since we determined that concurrent inhibition of PI3K synergistically enhanced ERK inhibitor-induced anti-proliferative activity, we next performed an unbiased chemical library screen to identify additional combinations for SCH772984-based therapy. We applied a chemical library, comprised of 304 approved cytotoxic chemotherapeutic drugs and clinically available molecularly targeted drugs (Pemovska et al., 2013), to two SCH772984-sensitive cell lines, and we additionally screened for combinations with selumetinib. Synergistic and antagonistic interactions were assessed by comparing the response to each drug in the drug collection in the presence or absence of SCH772984 or selumetinib (deltaDSS score). DeltaDSS scores greater than 5 or less than -5 were cutoffs for likely synergistic or antagonistic interactions, respectively. Complementing our findings with the PI3K inhibitor AZD8186, additional inhibitors of PI3K signaling (mTOR, AKT and S6 kinase inhibitors) also enhanced SCH772984 activity in both cell lines (Figure 2.7). Interestingly, the drug interactions of SCH772984 and selumetinib were strikingly different. For example, in HPAC cells, SCH772984, but not selumetinib, was synergistic with mTOR and AKT inhibitors, as well as with a bromodomain inhibitor (Figure 4, upper right

panels). The latter results indicate distinct mechanisms of resistance to inhibitors of these two nodes of the ERK-MAPK cascade.

Long-term ERK Inhibition Causes a Senescence-like Phenotype

Since acquired resistance is a limitation of essentially all protein kinase inhibitor-based therapies, we expect that ERK inhibitor treatment will be similarly limited. To investigate likely mechanisms of acquired resistance, we first attempted to select resistant subpopulations by long-term high-dose inhibitor treatment of sensitive cells, an approach used widely with inhibitors of RAF and MEK (Samatar and Poulikakos, 2014). However, even after 2-3 months of SCH772984 treatment, we did not observe outgrowth of ERK inhibitor-resistant cells. Instead, treated cells remained quiescent and displayed a flattened cellular morphology characteristic of senescent cells (Campisi, 2013) (Figure 2.8A). To investigate whether they were indeed senescent, we determined if the treated cells exhibited elevated β-galactosidase activity, the only reliable marker of oncogene-induced senescence in pancreatic cancer (Caldwell et al., 2012). We found that treatment of sensitive cell lines with SCH772984 at 1x or 2x GI_{50} induced increased β-galactosidase activity in ~60% of cells after 7 to 14 days (Figures 2.8A, 2.8B and 2.9E) or even 72 hr (e.g., HPAF-II cells, Figure 2.9A and 2.9B).

Mutant *RAS*-induced senescence can be prevented through loss of one of two tumor suppressor pathways: p53 and its target p21, or p16-mediated dephosphorylation and activation of RB (Campisi, 2013). We found that the p53-p21 pathway was not induced in either sensitive or resistant cell lines after 7 or 14 days of continuous exposure to SCH772984 (Figure 2.9C, 2.9F, 2.9H, and 2.9K). However, sensitive cell lines displayed both induction of p16 and loss of phospho-RB (Figures 2.8C, 2.9C, and 2.9G). Furthermore, we observed onset of senescence in the SCH772984-sensitive PDX cell lines (Figure 2.9M and 2.9N). Thus, consistent with previous studies where loss of p16 was required to prevent *KRAS*-induced senescence in pancreatic cancer (Bardeesy et al., 2006; Eser et al., 2013), we suggest that restoration of p16 function upon

ERK inhibitor treatment in turn unmasked *KRAS*-induced senescence activity in sensitive PDAC cell lines.

Senescence is conventionally an irreversible process. We found that removal of SCH772984 for as long as 14 days reversed neither the sustained β-galactosidase activity nor the reduced cell growth induced by 28 days of treatment (Figure 2.9O-R). Additionally, p16 protein expression remained high whereas Myc and pRB protein expression remained low after SCH772984 removal (Figure 2.9S and 2.9T). Thus, ERK inhibition induced an irreversible senescence-like phenotype.

ERK inhibition-induced Degradation of MYC Is Necessary and Sufficient for Induction of Senescence

Next, we determined the signaling mechanism whereby ERK inhibition induced this phenotype. Recently, one study showed that Ras activation-induced senescence was characterized by both high ERK activity and increased degradation of selected proteins (Deschenes-Simard et al., 2013). In contrast, we found that long-term ERK inhibitor treatment (7 or 14 days) increased widespread protein ubiquitination in sensitive cell lines (Figures 2.8D, 2.8E, 2.9D, 2.9I, 2.9J, and 2.9L). Thus, ERK inhibition may cause the degradation and loss of one or more specific ERK substrate(s) to induce senescence-like growth suppression.

We next determined if long-term SCH772984 treatment caused loss of specific ERK substrates or gene targets with known roles in senescence. The MYC transcription factor is an ERK substrate, and loss of MYC induced tumor cell senescence by an RB- or p16-dependent mechanism (Ohtani et al., 2001; Wu et al., 2007). Altered expression of ERK-regulated ETS family transcription factors (Ets-1 and Ets-2) stimulated *CDKN2A* (encoding p16) gene expression in senescent fibroblasts (Ohtani et al., 2001; Wu et al., 2007). In *BRAF*-mutant melanoma, ERK stimulated *AURKB* gene transcription, and suppression of *AURKB* expression induced senescence (Bonet et al., 2012). We therefore determined if long-term treatment with SCH772984

altered the levels of ETS1, ETS2, MYC or Aurora B proteins. We found that 7-day treatment resulted in decreased their levels in sensitive cell lines (Figure 2.10A).

Next, we investigated the mechanisms whereby SCH772984 modulates Aurora B, MYC, ETS1, and ETS2 protein levels. First, RT-PCR analyses revealed no reduction in mRNA levels of any of the four proteins after 7 days of treatment, suggesting posttranscriptional mechanisms (Figure 2.11A). ERK phosphorylation of MYC is known to prevent its degradation (Farrell and Sears, 2014), implying that ERK inhibition would enhance its degradation. Consistent with this possibility, the proteasome inhibitor MG132 restored the protein levels of ETS1, ETS2, and MYC in SCH772984-treated cells (Figures 2.10B, 2.10C and 2.11B).

MYC protein stability can be controlled in a multi-step process by RAS effector signaling (Farrell and Sears, 2014). ERK phosphorylation of MYC at residue S62 facilitates its subsequent phosphorylation at T58 by GSK3β, leading to proteasomal degradation. We found that SCH772984 induced loss of the majority of MYC protein. Consistent with the current model, each sensitive cell line displayed hypophosphorylation at T58 in the remaining MYC protein (Figures 2.10D, 2.10E and 2.11E). Furthermore, MYC ubiquitination was increased in sensitive cells after SCH772984 treatment (Figures 2.10F, 2.11C and 2.11D). Interestingly, the remaining low level of MYC was hyperphosphorylated at S62 in HPAF-II cells, suggesting ERK-independent phosphorylation at S62 in these cells.

We then determined whether loss of MYC is a driver of the SCH772984-induced senescence-like phenotype, using a well-characterized MYC variant in which the T58 phosphorylation site is substituted with an alanine residue (T58A) to prevent degradation by the proteasome (Yeh et al., 2004). We found that Panc10.05 and HPAC cells ectopically expressing MYC T58A partially retained MYC expression upon SCH772984 treatment (Figure 2.10G), and that induction of β-galactosidase activity was significantly inhibited (Figure 2.10H and 2.10I). Conversely, depletion of *MYC* with siRNA in both sensitive and resistant cell lines was associated

with increased β-galactosidase activity (Figure 2.11F-I). Thus, loss of MYC is necessary and sufficient to cause senescence-associated increased β-galactosidase activity.

Since we noted that MYC T58A protein stability unexpectedly decreased upon ERK inhibition, we assessed the requirements for phosphorylation at S62 and T58 to modulate SCH772984-mediated loss of MYC protein. Our analyses indicated that the regulation of MYC protein stability by ERK signaling is more complex than currently understood and must involve additional phosphorylation events and sites (Figure 2.11J-W).

SCH772984 Treatment Reduces Tumor Xenograft Growth and MYC Protein Levels in vivo

We next determined if loss of MYC also correlated with sensitivity to SCH772984 in vivo. We first determined the ability of SCH772984 to inhibit tumor xenograft growth of two PDAC cell lines that were sensitive to SCH772984 in vitro. We found that SCH772984 treatment of established tumors caused tumor regression (HPAC) or impaired progression (HPAF-II) (Figure 2.12A). No weight loss was seen, indicating that the treatment was well tolerated (Figure S6A). These anti-tumor activities were associated with reductions in pRSK in the tumor tissues (Figure 2.13B, 2.13E and 2.13F), consistent with ERK inhibition at the tumor sites, and with reduced total protein levels of MYC and Aurora B (Figure 2.12B). We did not observe depleted levels of *MYC* mRNA, supporting a mechanism whereby loss of MYC in vivo was due to protein degradation (Figure 2.12C). Furthermore, two in vitro-resistant cell lines were similarly not sensitive to SCH772984 in vivo (Figure 2.13C and 2.13D).

Since PDAC PDX mouse models may more accurately model drug response in cancer patients (Hidalgo et al., 2014), we next evaluated SCH772984 sensitivity in four different serially passaged *KRAS*-mutant PDX tumors surgically implanted into the flanks of nude mice. SCH772984 significantly reduced (70-90%) tumor growth in all four PDX models (Figure 2.12D), and this was associated with decreases in protein but not RNA levels of MYC and Aurora B (Figures 2.12E, 2.12F, 2.13G, and data not shown). We also observed loss of cyclin B1, cyclin

D1, and pRB, but no induction of cleaved caspase-3, suggesting halted cell growth rather than induction of apoptosis (Figures 2.12E and 2.13G). Together with our in vitro observations, these results in both cell line- and patient-derived tumor xenografts indicate that loss of MYC and Aurora B proteins may be accurate in vivo markers of SCH772984 sensitivity.

We next expanded our analysis to include an orthotopic xenograft mouse model of PDAC, as stromal cells are known barriers to drug delivery/efficacy in the pancreas. We observed that SCH772984 decreased pERK, pRSK, and MYC levels and reduced tumor size (Figures 2.12G, 2.12H, 2.12I, and 2.13H). Since we showed previously that Ral inhibition suppressed pancreatic tumor growth (Lim et al., 2006), we also tested the combination of SCH772984 with dinaciclib, a CDK inhibitor that blocks pancreatic tumor growth by suppressing KRAS-Ral signaling (Feldmann et al., 2011; Feldmann et al., 2010). This combination resulted in a more significant reduction in tumor growth than either treatment alone.

Finally, because we had observed that the clinical candidate ERK inhibitor BVD-523 also synergized with the PI3K inhibitor AZD8186 *in vitro*, we sought to determine its efficacy *in vivo*. We observed markedly reduced tumor growth with this combination (Figure 2.13I). Importantly, western blot analysis and tumor staining revealed ERK target inhibition, as measured by decreases in pERK, pRSK, pS6, and p4E-BP1 levels (Figure 2.13J and 2.13K). Together, our data suggest that ERK inhibition alone or in combination with other targeted agents may be beneficial for treatment of PDAC patients.

Identification of Resistance Mechanisms to Short-term SCH772984 Treatment

To assess the mechanistic basis of de novo resistance (Figure 2.1A), we used two strategies. First, we applied reverse-phase protein array (RPPA)-based pathway activation mapping analysis (Liotta et al., 2003) to a panel of sensitive and de novo resistant cell lines to measure the basal activation/phosphorylation state of 135 key signaling proteins involved in cell proliferation, autophagy, apoptosis, survival, migration and adhesion. We identified a distinct

signature that distinguished sensitive versus resistant cell lines (Figure 2.14A). Within this signature, there was a significant ($p<0.05$) activation of the PI3K-AKT-mTOR signaling network, with increased phosphorylation/activation of AKT and of multiple AKT substrates (e.g., p27, NF-κB, as well as mTOR substrates such as 4E-BP1, EIF4G, S6 ribosomal protein) (Figure 2.14A). In agreement with our observation that inhibitors of PI3K signaling synergistically enhanced SCH772984 inhibitory activity in sensitive cell lines, RPPA pathway mapping analyses identified PI3K-AKT-mTOR signaling as a key driver of ERK inhibitor resistance.

Second, we applied a kinome siRNA library screen to identify genes displaying synthetic lethality with SCH772984. Using two SCH772984-resistant PDAC cell lines (CFPAC-1 and SW1990), we performed two independent kinome-wide siRNA screens (711 genes) in the absence or presence of SCH772984. Subsequent validation analyses in three PDAC cell lines (CFPAC-1, SW1990 and DAN-G) verified 24 genes whose targeting by at least two different siRNAs enabled SCH772984 to suppress anchorage-dependent growth in otherwise resistant cell lines (Figure 2.14B and 2.14C). Further validation showed that siRNA suppression along with SCH772984 treatment decreased cell growth by greater than 70% (Figure 2.14D-G). We identified new genes as well as known modulators of MAPK-inhibitor resistance (Johannessen et al., 2010). These analyses reveal the striking heterogeneity in the signaling mechanisms that can drive de novo resistance to ERK inhibition.

Since the majority of kinases identified in our screen have not been associated previously with resistance to RAF or MEK inhibitors, we performed Ingenuity Pathway Analysis on our hits to determine their possible relevance to ERK signaling. This analysis identified recognized associations with ERK signaling in 13 of the 24 kinases (Figure 2.15). These results indicate that multiple and diverse mechanisms will likely drive *de novo* and/or acquired resistance to ERK inhibition.

To investigate mechanisms of acquired resistance to ERK inhibition, we applied an innovative gain-of-function screen (aka Cancer Toolkit, CTK (Martz et al., 2014)) to identify

activated signaling components that can cause acquired resistance. The CTK is a library of barcoded expression constructs consisting of key genes in 20 of the oncogenic pathways most commonly activated in cancer. We examined potential mechanisms of acquired resistance to both SCH772984 and the clinical candidate BVD-523. Interestingly, we found that CTK-induced acquired resistance to SCH772984 and BVD-523 yielded many overlapping hits, which included PI3K, Notch, and p38 signaling cascades (Figure 2.14H-J). With inhibitors of Notch and p38 under clinical evaluation, their application together with ERK inhibitors may be tested rapidly to determine if these combinations delay onset of acquired resistance.

DISCUSSION

Clinical experiences with RAF and MEK inhibitors in *BRAF*-mutant melanomas emphasize that the RAF-MEK-ERK cascade is not a simple linear signaling pathway (Samatar and Poulikakos, 2014). Clearly, each level of the cascade is subject to distinct regulatory mechanisms, with inhibition at each level leading to distinct compensatory mechanisms and drivers of inhibitor resistance. Furthermore, Raf and MEK inhibitors that induce loss of ERK-mediated negative feedback mechanisms, leading to increased pathway flux and ERK reactivation (Nissan et al., 2013) have been largely ineffective in *RAS*-mutant cancers. Our recent finding that ~50% of *RAS*-mutant human cancer cells are responsive to the ERK-selective inhibitors SCH772984 and BVD-523 (clinical candidate), despite their resistance to MEK inhibitors (Morris et al., 2013), suggests that inhibition of the pathway at the level of ERK may be advantageous (Hatzivassiliou et al., 2012).

An unexpected finding from our studies was the different mechanisms of growth suppression seen upon short-term (24-72 hr) versus long-term (1-2 weeks) ERK inhibitor treatment. Conventionally, mechanisms of growth suppression by signaling inhibitors are characterized by short-term analyses, yet clinical application of such inhibitors involves persistent long-term treatment. As with MEK inhibitors (Alagesan et al., 2015), short-term treatment (24-72 hr) with this ERK inhibitor induced growth suppression that was associated with perturbation of

progression through G1 and induction of apoptosis. In contrast, we found that long-term treatment (weeks) instead caused a senescence-like growth suppressive phenotype, which was dependent on the proteasomal degradation of MYC. Since clinical use of ERK inhibitors will certainly require long-term treatment, the induction of this phenotype may be the more clinically relevant mechanism of action. There is emerging appreciation that drug-induced senescence may be part of an important and effective approach for cancer treatment (Nardella et al., 2011) by rendering cancer cells sensitive to cytotoxic drugs.

Our application of unbiased chemical library screening and phosphoprotein profiling independently identified the PI3K-AKT-mTOR pathway as a key mediator of ERK inhibitor sensitivity. However, while concurrent treatment with MEK and PI3K inhibitors has recently been explored in mouse models of pancreatic cancer, only modest anti-tumor activity was observed (Alagesan et al., 2015; Junttila et al., 2015). Furthermore, clinical trial evaluations of MEK and PI3K inhibitor combinations also suggest that normal tissue toxicity may limit this combination (Shimizu et al., 2012; Tolcher et al., 2015). Clinical evaluation of PI3K and ERK inhibitor combinations will be needed to determine whether targeting ERK rather than MEK will overcome these limitations.

We found that a significant subset of *KRAS*-dependent pancreatic cancer cell lines exhibited de novo resistance to this ERK inhibitor. Our RPPA phosphoprotein profiling analyses identified a PI3K-AKT-mTOR activation signature that distinguished sensitive versus resistant cell lines. Mutations activating the PI3K-PTEN-AKT signaling cascade have been associated with de novo resistance to MEK inhibition in *RAS*-mutant cancers (Wee et al., 2009). However, most of our ERK inhibitor-resistant cell lines did not contain such mutations. Furthermore, concurrent PI3K inhibition, which conferred increased growth inhibition in ERK inhibitor-sensitive cells, could not overcome ERK inhibitor resistance in the de novo resistant cells. Thus, increased PI3K signaling together with additional mechanisms must drive de novo resistance.

In support of such additional mechanisms, our kinome siRNA library screen identified a striking diversity of protein kinases that, when inactivated, overcame ERK inhibitor resistance. Although there was but one overlap in the hits from two full kinome siRNA library screens, validation of the combined hits showed that the majority drove resistance in a third cell line. This striking heterogeneity is not unexpected in light of the fact that there are numerous alterations in non-*KRAS* genes that are not widely shared among PDAC tumors (Waddell et al., 2015). This may be why both ERK-dependent and -independent pathways can overcome *KRAS* addiction. Recent studies identified the transcription factor YAP1 as one mechanism that can overcome loss of mutant K-Ras in *KRAS*-mutant PDAC (Kapoor et al., 2014; Shao et al., 2014). While these studies provided compelling evidence in support of YAP1, additional modulators are likely to be revealed. Future studies will be needed to expand on these observations.

Importantly, we employed a genetic gain-of-function screen to identify mechanisms of acquired resistance to ERK inhibition. SCH772984 and BVD-523 shared several hits from the screen, namely, PI3K, Notch and p38. None of these has previously been identified as a modulator of ERK resistance (Goetz et al., 2014; Vogel et al., 2015). Together, our results stress that many distinct ERK inhibitor-based combinations will be needed for efficacy across different *KRAS*-mutant PDAC populations. Elucidation of the molecular determinants of ERK inhibitor response will be critically needed to accomplish our goal of achieving effective personalized medicine for KRAS-mutant PDAC patients.

MATERIALS AND METHODS

Cell Lines

PDAC cell lines were obtained from ATCC and were maintained in Dulbecco's Modified Eagle Medium supplemented with 10% fetal calf serum (FCS) (HPAC, PANC-1, and MIA PaCa-2), in RPMI 1640 supplemented with 10% FCS (AsPC-1, CFPAC-1, HPAF-II, HuPT3, Panc10.05, and SW-1990) or with 15% FCS (Capan-1 and Capan-2).

Western Blot Reagents

Cells were lysed in 10% NP-40 Buffer (1 M Tris pH 7.5, 1 M $MgCl_2$, 5 M NaCl, 10% NP-40, 10% glycerol, 0.25% sodium deoxycholate; phosphatase and protease inhibitors) and resolved by SDS-PAGE. To determine the levels of activated proteins, blot analyses were done with phospho-specific antibodies to AKT(S473), MEK1/2(S217/S221), RSK(T359/S363), and ERK1/2(T202/Y204), with antibodies recognizing total AKT, MEK1/2, RSK, and ERK1/2 to control for total protein expression (Cell Signaling Technologies). Antibodies to MYC, Aurora B, ubiquitin, ETS1, DUSP4, p21/CIP1, and p53 (Cell Signaling Technologies), and to ETS2 and DUSP6 (Abcam), and to DUSP1 and p16 (Millipore) were used to monitor total protein expression. To assess the mechanism of MYC degradation, phospho-specific MYC (T58 or S62) antibodies (Abcam) were used. Antibody to KRAS4B was obtained from Calbiochem. Antibodies for cleaved caspase-3 (Cell Signaling Technologies) were used to monitor apoptosis. Antibody for β-actin (Sigma AC15) was used to verify equivalent loading of total cellular protein.

Small Molecule Inhibitors

The ERK1/2-selective inhibitor SCH772984 was synthesized at Merck. The MEK1/2-selective inhibitor selumetinib/AZD6244 was provided by G. Johnson (UNC-CH). The PI3K inhibitor AZD8186 was provided by AstraZeneca. Inhibitors for in vitro studies were dissolved in dimethyl sulfoxide (DMSO) to a yield of 10 or 20 μM stock concentrations stored at -20 or -80°C, respectively.

siRNA Transfections

siRNA silencer select oligonucleotides against scrambled and *KRAS* sequences were obtained from Invitrogen and transfected into cells by using Lipofectamine RNAiMAX, according to the manufacturer's instructions.

Retroviral Expression Vector Infections

The pMSCVpuro retrovirus vector and pMSCVpuro encoding Flag epitope-tagged MYC (T58A) were provided by Juan Belmonte (Addgene plasmid 20076) (Aasen et al., 2008), and were transiently transfected into 293T cells with a pCL-10A1 packaging system using a calcium chloride transfection reagent. Viral particles were collected and infected as described above for lentiviruses. Infection of PDAC cell lines was done in growth media supplemented with 8 g/ml polybrene.

Anchorage-Dependent Growth Assays

To monitor proliferation, cells were plated into 96-well plates at a density of 1 x 10^3 (MIA PaCa-2, PANC-1, HPAC), 2 x 10^3 (CFPAC-1, SW-1990, HPAF-II, Panc10.05, AsPC-1), or 3 x 10^3 (Capan-1) cells per well. To quantitate cell number, after 4 or 7 days, cells were stained with 3-(4,5-dimethylthiazol-2-yl)-2,5-diphenyltetrazolium bromide (MTT) and absorbance was measured at 550 nm. We also performed a second proliferation assay to monitor clonogenic growth. Cells were plated at the same number of cells per well as for the MTT assay, but in 6-well plates. After 7 to 10 days, paraformaldehyde-fixed cells were stained with crystal violet to visualize and quantitate colony growth.

Determination of GI_{50}

To determine the 50% growth inhibitory concentration (GI_{50}), 1-2 x 10^3 cells were seeded in 96-well plates and treated with concentrations of SCH772984 or selumetinib from 3.9 nM to 4 μM). After 72 hr of treatment, cell proliferation was analyzed with MTT and read at an absorbance of 550 nm. GI_{50} values were calculated with CalcuSyn or CompuSyn software.

Cell Cycle Assay

Cell cycle progression was quantified by flow cytometry as described (Nusse et al., 1990). Cells were treated at GI_{50} for 72 hr and then washed with phosphate-buffered saline (PBS), fixed in cold 70% ethanol, and then stained with propidium iodide (PI). Modfit software was used for analyses.

Drug Sensitivity and Resistance Testing (DSRT) Chemical Library Screen

DSRT was performed on pancreatic cancer cell lines. The compounds were dissolved in 100% dimethyl sulfoxide (DMSO) and dispensed on tissue culture–treated 384-well plates (Corning) using an acoustic liquid handling device, Echo 550 (Labcyte Inc.). The compounds were plated in five different concentrations in 10-fold dilutions covering a 10,000-fold concentration range relevant for each drug (e.g., 1–10,000 nmol/L). The predrugged plates were kept in pressurized StoragePods (Roylan Developments Ltd.) under inert nitrogen gas until needed. The compounds were dissolved with 5 µL of culture medium while shaking for 30 min. Twenty µL of single-cell suspension (1,000 cells) was transferred to each well using a MultiDrop Combi (Thermo Scientific) peristaltic dispenser. The plates were incubated in a humidified environment at 37°C and 5% CO_2, and after 72 hr cell viability was measured using CellTiter-Glo luminescent assay (Promega) with a Molecular Devices Paradigm plate reader according to the manufacturer's instructions. The data were normalized to negative control (DMSO only) and positive control wells (containing 100 µmol/L benzethonium chloride, effectively killing all cells). Curve fitting and calculations of drug sensitivity scores were performed as previously described (Yadav et al., 2014).

Senescence-Associated β-Galactosidase Assay

Cell lines were treated with SCH772984 at GI_{50} or 2 x GI_{50} for 7, 10, or 14 days on plastic. Cells were then plated in 12-well plates at a density of 1-5 x 10^3 cells per well and stained using the Senescence β-galactosidase Staining Kit from Cell Signaling Technologies. Positive cells were quantitated after 24 hr staining

PDAC Cell Line Xenografts

Female athymic nude mice (nu/nu, 6 to 8 weeks of age, Charles River Laboratories, Wilmington, MA) were maintained under pathogen-free conditions in microisolator cages. Animal procedures were performed in accordance with the rules set forth in the NIH Guide For The Care And Use of Laboratory Animals and were approved by the Institutional Animal Care and Use Committee at Merck. All animals received food and water *ad libitum*.

HPAC, HPAF-II, CFPAC-1 and PANC-1 cells (3.5 × 10^6 in PBS:Matrigel (1:1)) were injected s.c. into the right flank region of the mice. Tumors were allowed to reach 300 to 450 mm^3 before randomization to treatment groups. For continuous dosing studies, SCH772984 was administered intraperitoneally (i.p.) at 75 mg or 90 mg per kilogram body weight (mpk) once daily (qd) for 14 to 21 days. Mice in vehicle-control arms received 20% (2-hydroxypropyl)-β-cyclodextrin (HPBCD) on the same schedules that SCH772984 was administered. Ten mice were in each treatment group. Tumor volumes were measured twice weekly using calipers and calculated by the formula (length x width x width x 0.5). Animal body weights were measured on the same days twice weekly. Statistically significant differences between the treatment groups were determined by the Student's *t*-test and 2-way ANOVA using GraphPad Prism. Six hr after their last dose, mice were euthanized by carbon dioxide inhalation. The tumors were then removed and cut into two pieces. One piece was frozen in liquid nitrogen while the second piece was fixed in 10% formalin for future analysis.

Patient-derived Subcutaneous Xenograft Studies

All animal experiments conformed to the guidelines of the Animal Care and Use Committee of Johns Hopkins University and animals were maintained in accordance to guidelines of the American Association of Laboratory Animal Care. Subcutaneous murine xenografts were generated from low-passage patient-derived human pancreatic cancer xenograft (PDX) models Panc185 and Panc215, as previously described (Rubio-Viqueira et al., 2006). Xenografts were serially transplanted into both flanks of ten male CD1 nu/nu athymic mice each (n = 20 xenograft tumors per case). Mice for each model were randomized into two groups of five mice with similar average xenograft tumor volumes and assigned to receive treatment with SCH772984 (50 mg/kg in 10% (2-hydroxypropyl)-β-cyclodextrin, b.i.d.) or vehicle only (n = 10 xenografts per arm). Treatment was initiated when xenografts were 150-250 mm^3. After treatment (Panc354, Panc215, Panc185, and Panc374) all mice were euthanized and tumor tissues harvested, within 3 hr after final drug treatment. Tumors were measured, and half of the tumor tissues were fixed with 10% formalin and half of them were frozen for future analysis.

Patient-derived Orthotopic Xenografts

All animal experiments conformed to the guidelines of the Animal Care and Use Committee of Johns Hopkins University and animals were maintained in accordance to guidelines of the American Association of Laboratory Animal Care. For orthotopic models, PDX tumors were surgically implanted in the pancreata of 40 male CD1 nu/nu athymic mice each. Tumor growth was monitored by ultrasound (Vevo 770); treatment was initiated when orthotopic tumors were 150-250 mm^3. Mice for each model were randomized into 4 treatment groups with similar average xenograft tumor volumes and assigned to receive treatment with SCH772984 (25 mg/kg in 10% (2-hydroxypropyl)-β-cyclodextrin (HPBCD), i.p. three times per week), dinaciclib (20 mg/kg in 10% HPBCD, i.p. twice weekly), a combination of SCH772984 and dinaciclib, or vehicle only (n = 10 xenografts per arm). After treatment, all mice were euthanized and tumor tissues harvested, within

3 hr after final drug treatment. Tumors were measured, and half of the tumor tissues were fixed with 10% formalin and half of them were frozen for future analysis.

Reverse-Phase Protein Array (RPPA)

Cell lysates were prepared in SDS sample buffer and printed in triplicate onto nitrocellulose coated slides (Grace Bio-labs, Bend, OR) using an Aushon 2470 arrayer (Aushon BioSystems, Billerica, MA). Each array was probed with one primary antibody, subjected to extensive pre-validation by single band western blotting and ligand induced activation (for phosphoproteins) on an automatic Autostainer (Dako Cytomation, Carpinteria, CA) using the Catalyzed Signal Amplification System kit (CSA; Dako Cytomation). Fluorescent detection was achieved using the streptavidin-conjugated IRDye680 (LI-COR Biosciences, Lincoln, NE) according to the manufacturer's instructions. The total amount of protein contained in each sample was measured by Sypro Ruby Protein Blot Stain (Molecular Probes, Eugene, OR). Images were acquired using the PowerScanner (TECAN, Mönnedorf, Switzerland) and spot intensity values were quantified using MicroVigene software Version 5.1.0.0 (Vigenetech, Carlisle, MA) as previously described (Pin 2014). The quantitative values obtained for each analyte were checked for data normalcy, and parametric two-tailed *t*-test (normally distributed data) or non-parametric Wilcoxon rank sum test (non-normally distributed data) was performed to identify statistically significant ($p<0.05$) differences in the basal signaling activation between ERK resistant and ERK sensitive cell lines. Because of data dependency of the kinase-based phosphoprotein data, no false discovery rate filtering was applied. Analysis was performed using R v2.13.2. GraphPad Prism v5.02 (GraphPad Software) was used to generate data plots.

siRNA Library Screening

Four siRNA sequences for each gene from the Human Validated Kinase V4 siRNA Library (Qiagen) were selected for screening and utilized to create nine 384-well assay plates. In addition, all assay plates included negative control siRNAs (Non-Silencing, All-Star Non-Silencing, and GFP), and two positive control siRNAs for transfection (UBBs1 and All-Star Cell Death Control), all of which were purchased from Qiagen. The siRNAs were printed individually into white solid 384-well plates (1 µl of 0.667 µM siRNA per well for a total of 9 ng siRNA) using a Biomek FX (Beckman Coulter). Lipofectamine RNAiMax (Invitrogen) was diluted in serum-free RPMI media and 20 µl was transferred into each well of the 384-well plate containing siRNAs using a BIO-TEK µFill Microplate Dispenser (final concentration is 40 nl of lipid per well). After an incubation period of 30 min at room temperature to allow the siRNA and lipid to form complexes, 750 cells in 20 µl volume of cells were added into each well using a µFill. Transfected cells were incubated at 37°C for 24 hr prior to the addition of 10 µl per well of varying concentrations of SCH772984 or vehicle control (DMSO) for a total assay volume of 50 µl. Cells were then incubated at 37°C for 96 hr post drug treatment. Cell viability was measured using the CellTiter-Glo assay (Promega) and an Analyst GT Multimode reader (Molecular Devices).

siRNA Library Screening Data Analysis

The raw luminescence values generated in the primary high-throughput RNAi screen were aligned and annotated with their respective gene names. The data were initially subjected to quality control evaluation. The overall transfection efficiency of >98%, coefficient of variation (CV) <10%, and assay quality measure, Z-Factor >0.9 were achieved, indicating a high-quality screen. A nonlinear four-parameter curve was fitted through the 6 doses corresponding to each siRNA per gene, using Prism 5.0 (GraphPad). GFP negative control was selected as the reference control because it has the most robust, non-toxic consistent fit when compared to the other

negative siRNA controls. The curve fitting resulted in a four-parameter output for each fit, namely top, slope, IC_{50} and bottom. The top of each siRNA curve fit was compared to the corresponding GFP top parameter. A ratio was generated, and any siRNA which indicated >20% toxicity was flagged and removed from further analysis as being "toxic". For hit selection, a fold change was calculated between the IC_{50} of each siRNA curve and the corresponding IC_{50} of the GFP control curve. A five-fold cutoff was applied in order to select strong hits. To minimize the off-target effect, we set a stringent criteria of at least 2 corresponding siRNAs targeting the same gene to have a IC_{50} fold change of ≥5. Based on this criterion, a final primary screen hit list of 23 genes was generated.

Cancer Toolkit (CTK) Screening

Cancer Tool Kit lentivirus expression vectors were provided by Kris Wood (Duke). Open reading frame (ORF)- or shRNA-expressing lentiviruses were produced and added to six-well plates in the presence of polybrene (7.5 mg/ml). After virus addition, plates were centrifuged at 2200 x g for 1 hr at 37°C. Twenty-four hr after infection, puromycin (2 mg/ml) was added for selection, and cells were incubated for 48 hr. Cells were then trypsinized, counted, and seeded in 96-well plates at 2000 cells per well. Twentyfour hr later, DMSO or concentrated serial dilutions of the indicated drugs (in DMSO) were added to cells. The viability was calculated as the percentage of control (vehicle-treated uninfected parental cells) after background subtraction with a minimum of three replicates for each cell line/ORF (or shRNA)/drug/concentration.

Table 2.1.

Table 2.1 Mutant *KRAS* PDAC cell lines

Cell Line	*KRAS*	*CDKN2A*	*TP53*	*SMAD4*
MIA PaCa-2	G12C*	Del*	R248W*	WT
HPAF-II	G12D/WT	R29fs*	P151S*	WT
HPAC	G12D*	Stop/Stop	WT	WT
Panc10.05	G12D*	WT	I255N/WT	WT
HuP-T3	G12R/WT	Del*	R282W*	WT
SW-1990	G12D*	Del*	WT	WT
PANC-1	G12D*	Del*	R273H*	WT
Capan-1	G12V*	Del*	A159V*	S343ns*
Capan-2	G12V/WT	WT	WT	WT
AsPC-1	G12D*	WT	C135fs*35/WT	R100T*
CFPAC-1	G12V/WT	WT; methylation	C242R*	Del*

Compiled from COSMIC. *Homozygous; All WT for *BRAF*, *PIK3CA* and *PTEN*; fs, frameshift mutation; Del, deletion

Table 2.1. Mutant *KRAS* PDAC cell lines

Figure 2.1.

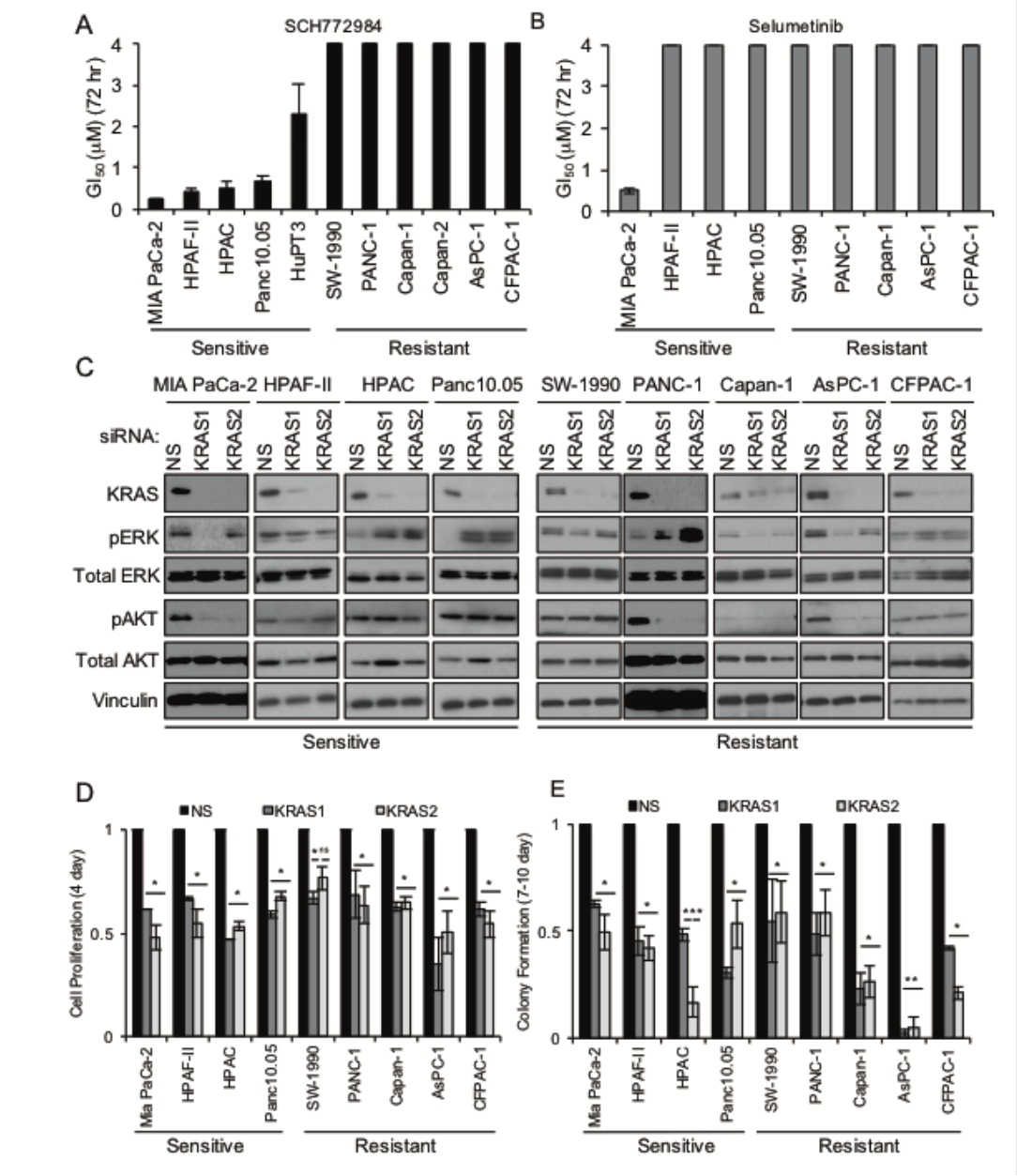

Figure 2.1. PDAC Cell Line Sensitivity to the ERK-Selective Inhibitor SCH772984 Is Not Associated with KRAS Dependency. (A) KRAS-mutant PDAC cell lines were maintained on plastic in growth medium with DMSO vehicle or SCH772984 (3.9 nM-4 μM). Proliferation was monitored by MTT assay to assess growth inhibition after 72 hr treatment. GI_{50} values were determined using CalcuSyn. Data are representative of three independent experiments. Bars indicate standard deviation from triplicate samples for each cell line. (B) SCH772984-sensitive and -resistant PDAC cell lines were maintained on plastic in growth medium with vehicle or the MEK inhibitor selumetinib (3.9 nM-4 μM). MTT assays were performed and GI_{50} values were determined as in (A). (C) Cells were transfected with scrambled (NS) or one of two individual siRNAs targeting KRAS (designated KRAS1 or KRAS2) for 48 hr, followed by western blot for

total K-Ras4B, ERK1/2 (ERK), AKT1-3 (AKT) and for vinculin to verify equivalent loading of total protein. Phospho-specific antibodies were used to monitor phosphorylation and activation of ERK (T202/Y204; pERK) and AKT (S473; pAKT). Data are representative of two independent experiments. (D) Cells transfected with NS or KRAS siRNAs were monitored for proliferation on plastic at 6 days post-transfection by MTT assay. Error bars represent the standard error of the mean. Data are representative of three independent experiments. Asterisks represent statistical significance using one-way ANOVA analysis, where * = $p < 0.05$, ** = $p < 0.001$, and ns = not significant. (E) Cells transfected with NS or KRAS siRNAs were plated at low density and clonogenic growth was monitored at 9-12 days post-transfection. Error bars represent standard error of the mean. Data are representative of three independent experiments. Asterisks represent statistical significance using one-way ANOVA analysis, where * = $p < 0.05$, ** = $p < 0.001$, and ns = not significant.

Figure 2.2.

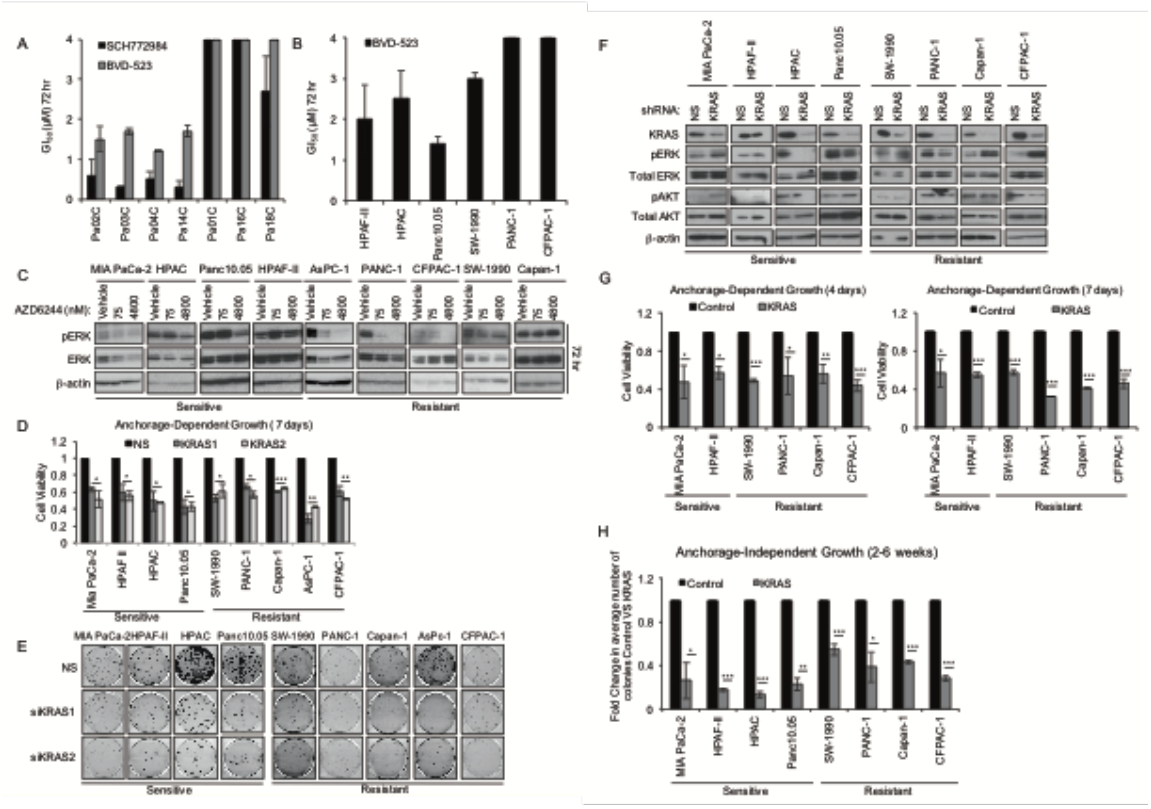

Figure 2.2. Related to Figure 2.1. (A) *KRAS*-mutant PDX cell lines grown on plastic were maintained in growth medium supplemented with vehicle (DMSO) or with BVD-523 or SCH772984 at concentrations ranging from 3.9 nM to 4 μM. Proliferation was monitored by MTT viability assay to assess growth inhibition after 72 hr treatment. GI_{50} values were determined using CompuSyn. All data shown in this figure are representative of three independent experiments. Bars indicate standard deviation from triplicate samples for each cell line. (B) *KRAS*-mutant PDAC cell lines grown on plastic were maintained in growth medium supplemented with vehicle (DMSO) or with BVD-523 at concentrations ranging from 3.9 nM to 4 μM. Proliferation was monitored by MTT viability assay to assess growth inhibition after 72 hr treatment. GI_{50} values were determined using CompuSyn. All data shown in this figure are representative of three independent experiments. Bars indicate standard deviation from triplicate samples for each cell line. (C) Western blot analysis of ERK activation following treatment with selumetinib (AZD6244) at 75 and 4800 nM for 72 hr. Blot analysis of β-actin was done to verify equivalent loading of total cellular protein. Data shown are representative of three independent experiments. (D) The consequences of siRNA *KRAS* suppression on anchorage-dependent growth was monitored on plastic 7 days post-transfection. Error bars represent the standard error of the mean. Asterisks represent statistical significance using one-way ANOVA analysis, where * $p < .05$, ** $p < .001$, and *** $p < .0001$. (E) The consequences of siRNA *KRAS* suppression on clonogenic growth with the indicated PDAC cell lines was determined by colony formation on plastic 9-12 days post-transfection. Shown are photomicrographs (scale bar, 100 μm) of representative dishes after staining with 2 mg/ml crystal violet after 9-12 days post-siRNA transfection. (F) Western blot analysis following shRNA-mediated *KRAS* knockdown showing the effects on K-Ras4B protein expression, phosphorylation status of ERK and AKT, and β-actin as a loading control for total

cellular protein. (G) Anchorage-dependent growth assay following shRNA-mediated *KRAS* ablation using one verified *KRAS*-directed shRNA sequence in a panel of *KRAS*- mutant PDAC cell lines. Anchorage-dependence was measured 4 and 7 days post-selection. Error bars represent the standard error of the mean of two independent experiments. Asterisks represent statistical significance using a paired *t*-test analysis, where * $p < 0.05$, ** $p < 0.001$, and *** $p < 0.0001$. (H) Anchorage-independent growth assay in soft agar following shRNA-mediated *KRAS* ablation using one verified *KRAS*-directed shRNA sequence (1) in a panel of *KRAS*- mutant PDAC cell lines. Anchorage-independent growth was measured post selection. Cell lines were allowed 2-4 weeks of growth. Error bars represent the standard error of the mean of two independent experiments. Asterisks represent statistical significance using a paired *t*-test analysis, where * $p < 0.05$, ** $p < 0.001$, and *** $p < 0.0001$.

Table 2.2.

Table 2.2 PDX-derived PDAC cell lines

Cell Line	SCH772984 sensitive	*KRAS*	*CDKN2A*	*TP53*	*SMAD4*	Tissue of Origin
Pa02C	Y	Q61H*	Del*	L247P*	Del*	Liver metastasis
Pa03C	Y	G12D/WT	WT	L244P*	WT	Liver metastasis
Pa04C	Y	G12V*	Del*	Del*	WT	Liver metastasis
Pa14C	Y	G12D*	Del*	Del*	fs-indel*	Primary tumor
Pa01C	N	G12D/WT	WT	T155P*	Del*	Liver metastasis
Pa16C	N	G12D/WT	WT	I255N	WT	Primary tumor
Pa18C	N	G12D/WT	Del*	WT	Del*	Primary tumor

*Homozygous; fs, frameshift; indel, in frame insertion, deletion, or duplication change affecting more than a single codon

Table 2.2. PDX-derived PDAC cell lines

Figure 2.3.

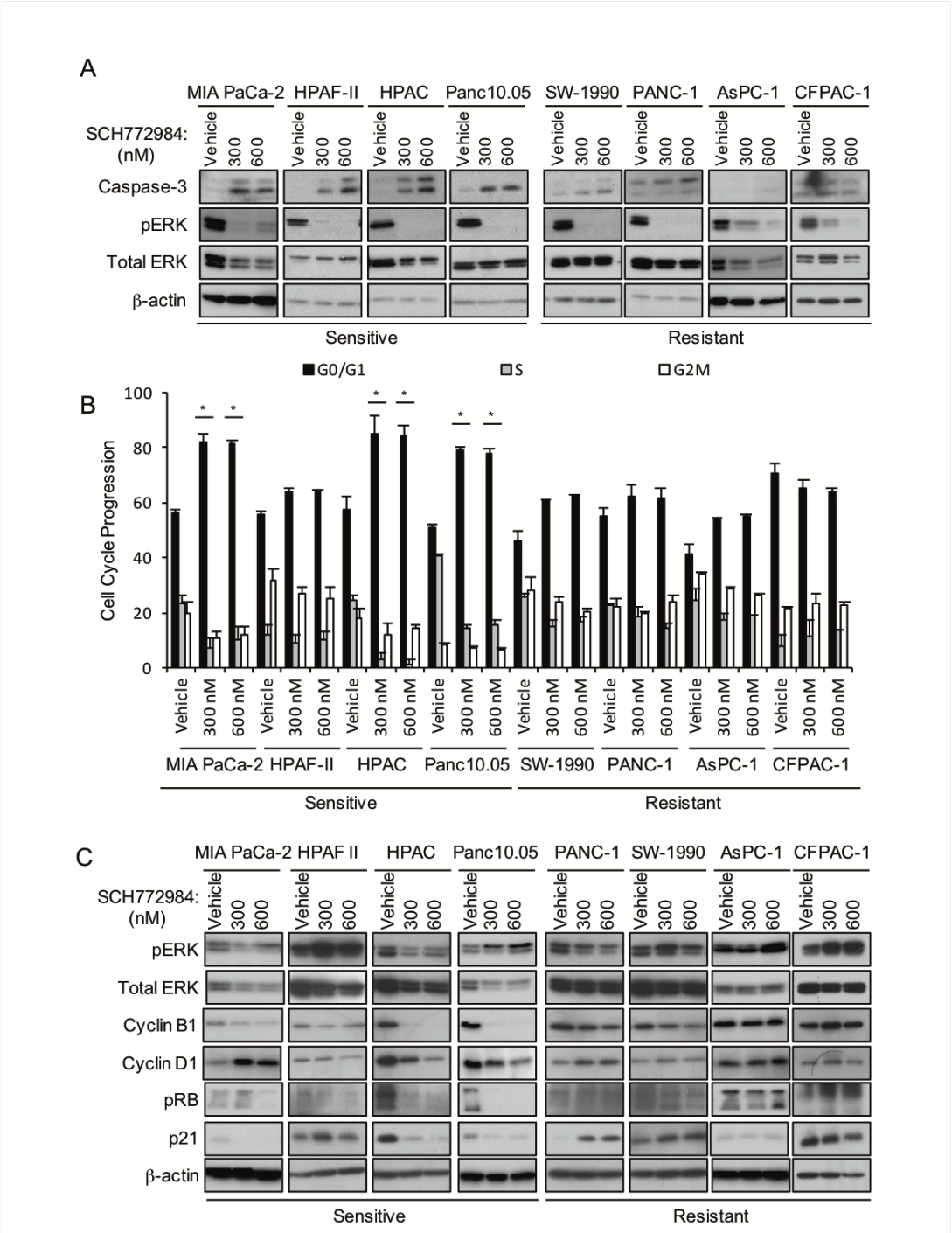

Figure 2.3. Short-term SCH772984 Treatment Induces Apoptosis and Altered Cell Cycle Progression. (A) SCH772984-sensitive or -resistant cell lines were treated for 72 hr with DMSO vehicle or SCH772984. Non-adherent cells were collected and monitored for apoptosis by western blot for cleaved caspase-3. Data are representative of three independent experiments. (B) Cells treated as above were stained with propidium iodide followed by flow cytometry. Error

bars represent standard error of the mean. Asterisks represent statistical significance using one-way ANOVA analysis, where * = $p < 0.05$. (C) Cells treated as above were collected for western blot for total cyclin B1, cyclin D1 and p21, and of phosphorylated, inactivated RB (S807/811; pRB). Western blot for pERK was done to verify SCH772984 inhibition; β-actin was the loading control.

Figure 2.4.

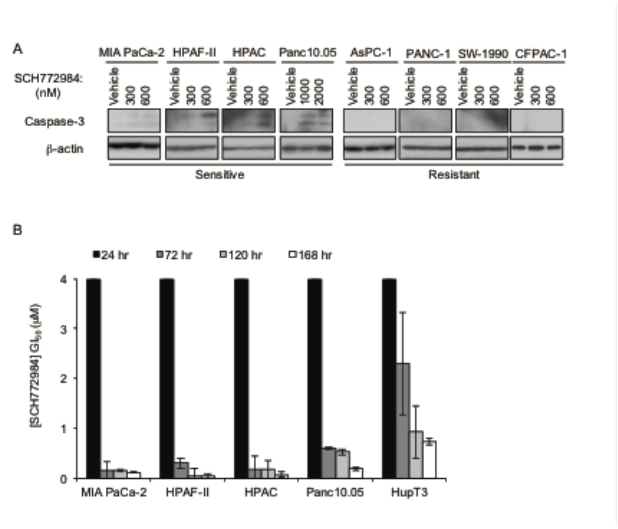

Figure 2.4. Related to Figure 2.3. (A) SCH772984 sensitive or resistant cell lines were treated with vehicle or the indicated concentrations of SCH772984 for 72 hr and adherent cells were then collected for blot analyses to monitor apoptosis by formation of the cleaved activated caspase-3 fragment. Blot analysis for β-actin was done to verify equivalent loading of total cellular protein. Data shown are representative of three independent experiments. (B) SCH772984-sensitive PDAC cell lines were maintained on plastic in growth media supplemented with vehicle or a range of concentrations from 3.9 nM to 4 μM of the SCH772984 for 24, 72, 120, and 168 hr. MTT assays were performed and GI_{50} values were determined. Error bars represent the standard error of the mean of three independent experiments.

Figure 2.5

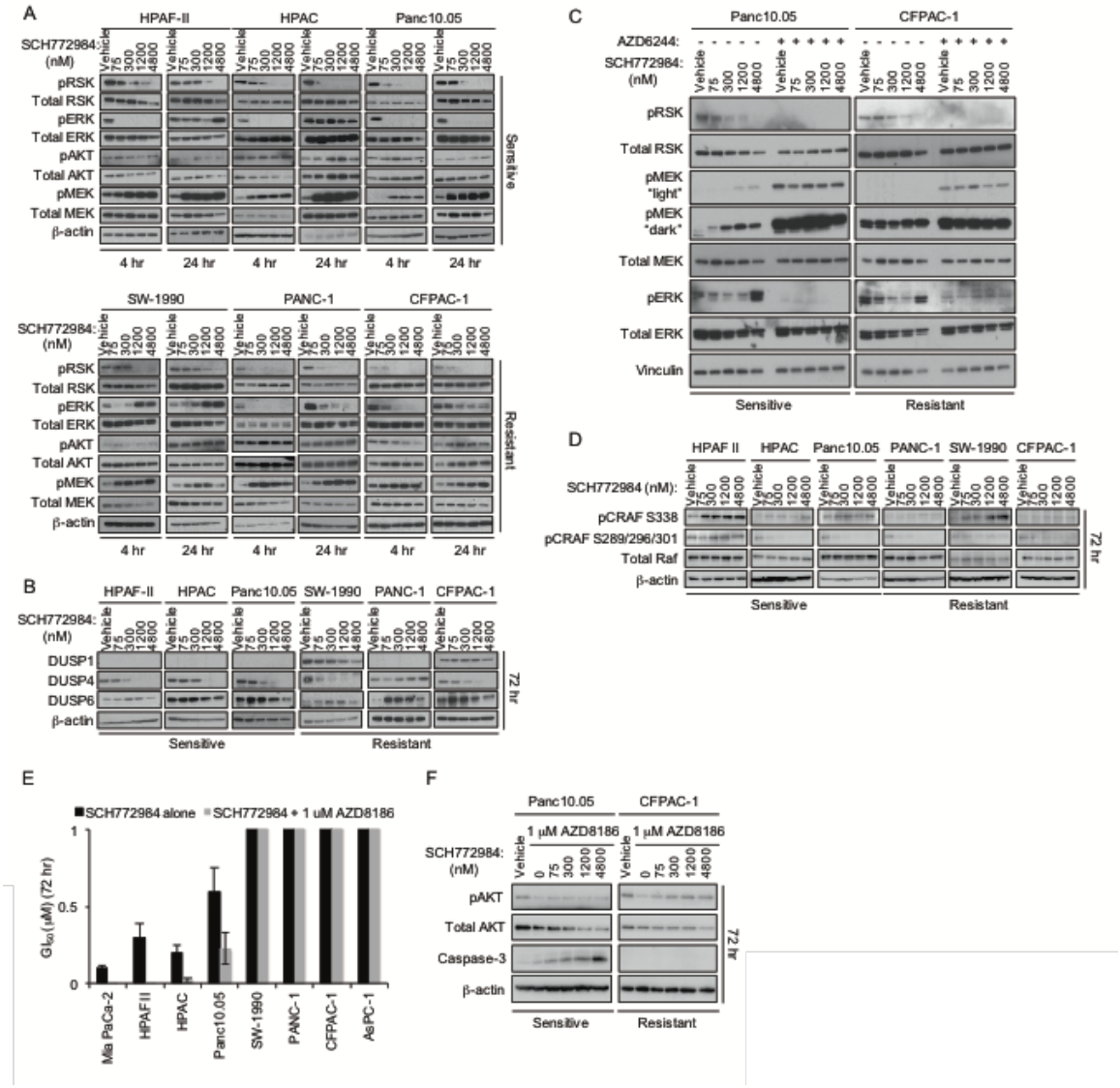

Figure 2.5 SCH772984 Sensitivity Is Associated with Treatment-Induced AKT Phosphorylation. (A) Cells were treated for 4 or 24 hr with DMSO vehicle or SCH772984, then evaluated by western blot with phospho-specific antibodies for RSK (T395/S363; pRSK), MEK1/2 (S217/221; pMEK), AKT (S473; pAKT), and ERK (T202/Y204; pERK). Total RSK, ERK, AKT, MEK and β-actin were also analyzed. Data are representative of three independent experiments. (B) Cells were treated as in (A) for 72 hr and evaluated by western blot for DUSP1, DUSP4, DUSP6 and β-actin. (C) SCH772984-sensitive (Panc10.05) and -resistant (CFPAC-1) cell lines were treated concurrently with selumetinib (5 μM) and either vehicle or the indicated concentrations of SCH772984. Phosphorylated and total RSK, MEK, ERK and vinculin were evaluated by western blot. (D) Cells were treated as above and collected for western blot for pCRAF (S338), pCRAF (S289/296/301), total CRAF and β-actin. (E) Cells were maintained in growth medium with vehicle or SCH772984 (3.9 nM-4 μM), with or without the PI3K inhibitor AZD8186 (1 μM). MTT was used to assess growth inhibition after 72 hr. Data are representative of three independent experiments. Bars indicate standard deviation from triplicate samples for

each cell line. (F) Cells were co-treated with SCH772984 and AZD8186. Western blots were performed for pAKT (S473) and total AKT, caspase-3 and β-actin.

Figure 2.6.

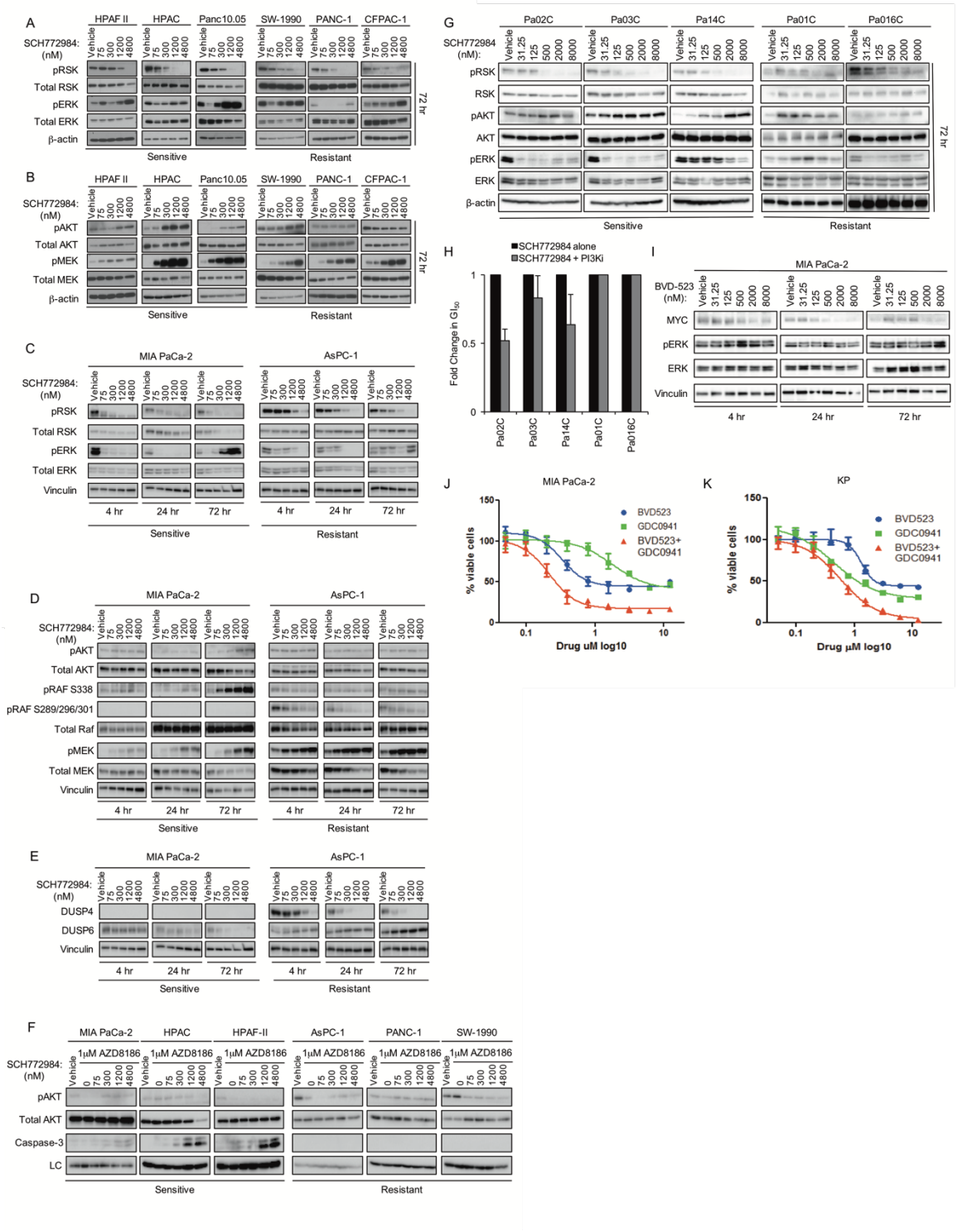

Figure 2.6 Related to Figure 2.5. (A) Sensitive or resistant cell lines maintained on plastic with complete serum-supplemented growth media were treated for 72 hr with vehicle or the indicated concentration of SCH772984, then evaluated by blot analysis with phospho-specific antibodies

for RSK (T395/S363; pRSK) and ERK. Blot analyses for total RSK, ERK, and β-actin to verify equivalent loading of total cellular protein were also done. Data shown are representative of three independent experiments. (B) Sensitive or resistant cell lines maintained on plastic with complete growth media were treated for 72 hr with vehicle or the indicated concentration of SCH772984, then evaluated by blot analysis with phospho-specific antibodies for MEK1/2 and AKT. Blot analyses for total AKT and MEK, and for β-actin to verify equivalent loading of total cellular protein were also done. (C) Sensitive or resistant cell lines maintained on plastic with complete growth media were treated for 4, 24, and 72 hr with vehicle or the indicated concentration of SCH772984, then evaluated by western blot analysis with phospho-specific antibodies for RSK (T395/S363; pRSK) and ERK. Blot analyses for total RSK, ERK, and vinculin to verify equivalent loading of total cellular protein were also done. Data shown are representative of three independent experiments. (D) Sensitive or resistant cell lines maintained on plastic with complete growth media were treated for 4, 24, and 72 hr with vehicle or the indicated concentration of SCH772984, then evaluated by blot analysis with phospho-specific antibodies for CRAF, MEK1/2 and AKT. Blot analyses for total CRAF, AKT and MEK, and for vinculin to verify equivalent loading of total cellular protein were also done. (E) Cells were treated as described above (A-D) for 4, 24 and 72 hr and then evaluated by blot analyses for DUSP4 and DUSP6 protein levels, with vinculin as the loading control. (F) Sensitive or resistant cell lines were co-treated with SCH772984 and AZD8186. Blot analysis was performed for phospho-AKT (S473), caspase-3 and total AKT. β-actin or vinculin served as a loading control (LC). (G) Sensitive or resistant cell lines maintained on plastic with complete serum-supplemented growth media were treated for 72 hr with vehicle or the indicated concentration of SCH772984, then evaluated by blot analysis with phospho-specific antibodies for RSK, pRSK, AKT, pAKT, pERK and ERK. Blot analyses for total RSK, ERK, AKT and β-actin to verify equivalent loading of total cellular protein were also done. Data shown are representative of two independent experiments. (H) Sensitive or resistant cell lines grown on plastic were maintained in growth medium supplemented with vehicle or with SCH772984 at concentrations ranging from 3.9 nM to 4 μM, with and without the addition of 1 μM AZD8186. Proliferation was monitored MTT viability assay to assess growth inhibition after 72 hr treatment. Data shown are representative of two independent experiments. (I) MIA PaCa-2 cells were maintained on plastic with complete serum-supplemented growth media were treated for 72 hr with vehicle or the indicated concentration of BVD-523, then evaluated by blot analysis with phospho-specific antibodies for pERK and total antibodies for MYC and ERK. Vinculin was used to verify equivalent loading of total cellular protein. (J) MIA PaCa-2 cells were grown on plastic were maintained in growth medium supplemented with vehicle or with BVD-523 at concentrations ranging from 100 nM to 10 μM, with and without the addition of GDC-0941. Proliferation was monitored by MTT viability assay to assess growth inhibition after 72 hr treatment. (K) KP mouse cells were grown on plastic were maintained in growth medium supplemented with vehicle or with BVD-523 at concentrations ranging from 100 nM to 10 μM, with and without the addition of GDC-0941. Proliferation was monitored by MTT viability assay to assess growth inhibition after 72 hr treatment.

Figure 2.7.

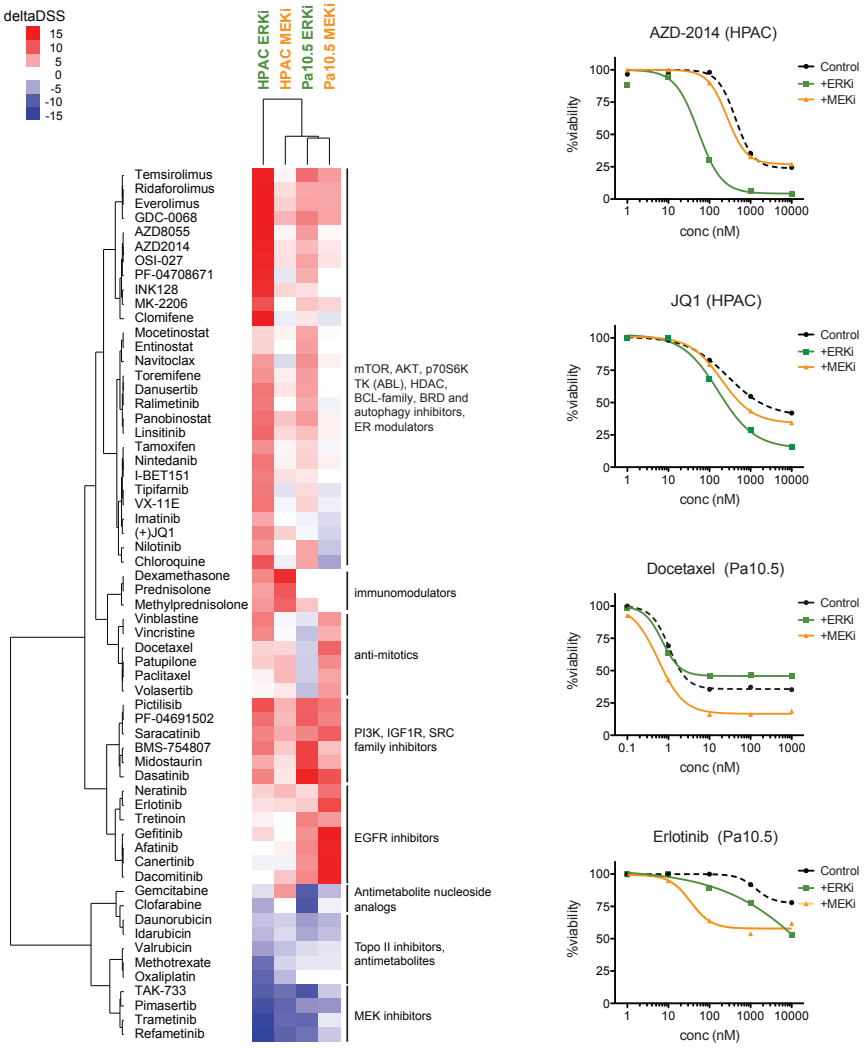

Figure 2.7. Distinct Patterns of Drug Synergies in ERK versus MEK Inhibitor Combinations. HPAC and Panc10.05 cells were exposed to dose-dependent drug sensitivity testing (DSRT) against 309 oncology-related compounds in the presence or absence of the ERK inhibitor SCH772984 (2 μM) or the MEK inhibitor AZD6244/selumetinib (1 μM). Cell viability was measured using CellTiter-Glo and drug responses were calculated as drug sensitivity scores (DSS). Plotted in the heatmap are the deltaDSS values (DSS in the presence of ERK/MEK inhibitor – DSS in the absence of overlaid inhibitor) for each condition, where red signifies potential synergies and blue indicates negative interactions between the two drugs. Drugs where the deltaDSS remained between -5 and 5 for all four conditions were excluded from the heatmap.

Figure 2.8.

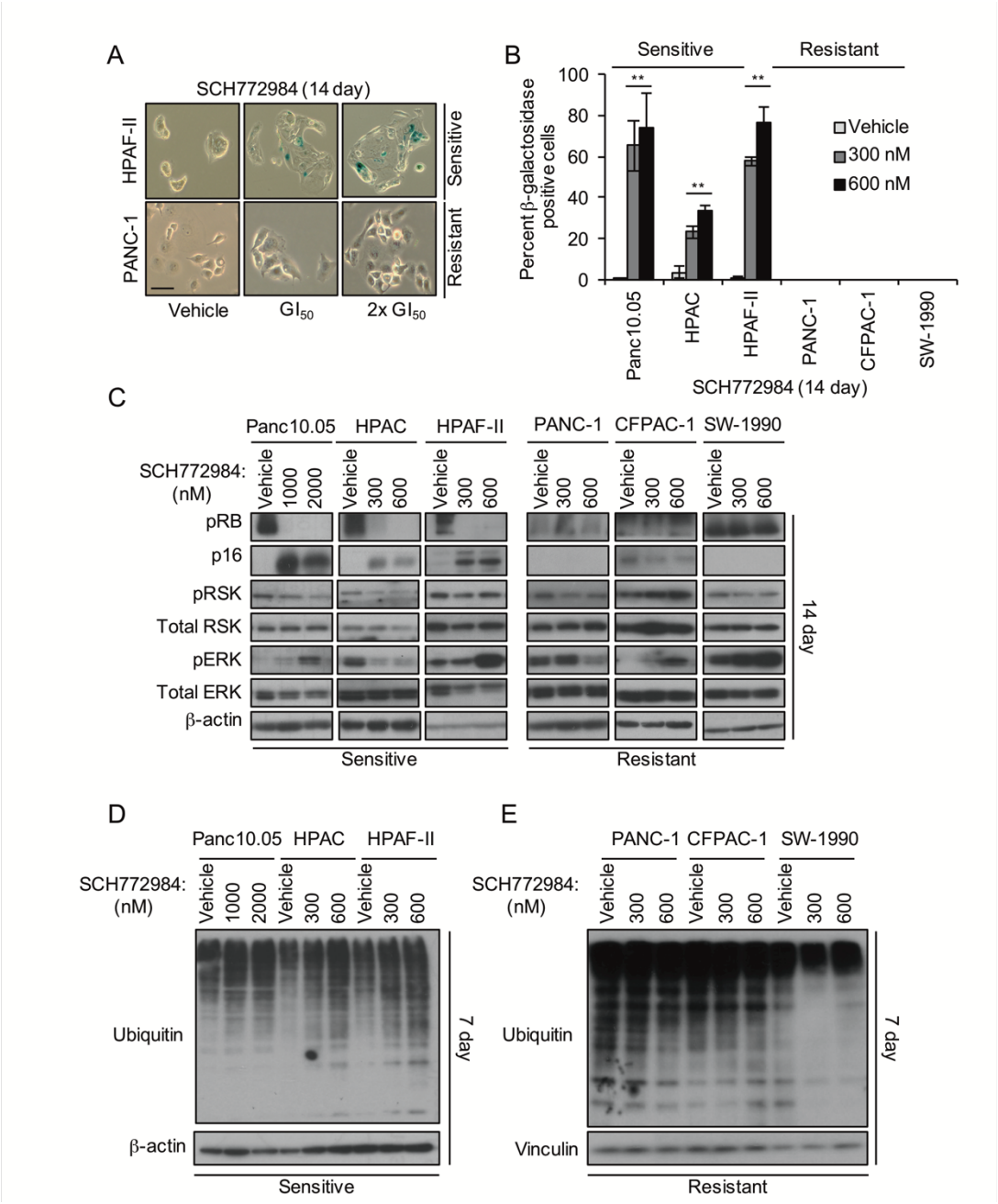

Figure 2.8. Long-term SCH772984 Treatment Induces Markers of Senescence and Ubiquitination in Sensitive but Not Resistant Cell Lines. (A and B) Cells were treated with SCH772984 at GI_{50} or at 2x GI_{50} concentrations for 14 days and stained for β-galactosidase. Representative images (scale bar, 50 μm) are shown in the left panel, with quantitation in the right panel. Error bars represent standard error of the mean. Data are representative of three independent experiments. Asterisks represent statistical significance using one-way ANOVA analysis, where * = $p < 0.05$ and ** = $p < 0.001$. (C) Cells were treated with SCH772984 for 14

days on plastic, followed by western blot for pRB, pRSK and pERK, and for total p16, RSK and ERK; β-actin was a loading control. (D and E) Cells were treated with vehicle or SCH772984 for 7 days, and then immunoblotted for ubiquitin or for β-actin.

Figure 2.9.

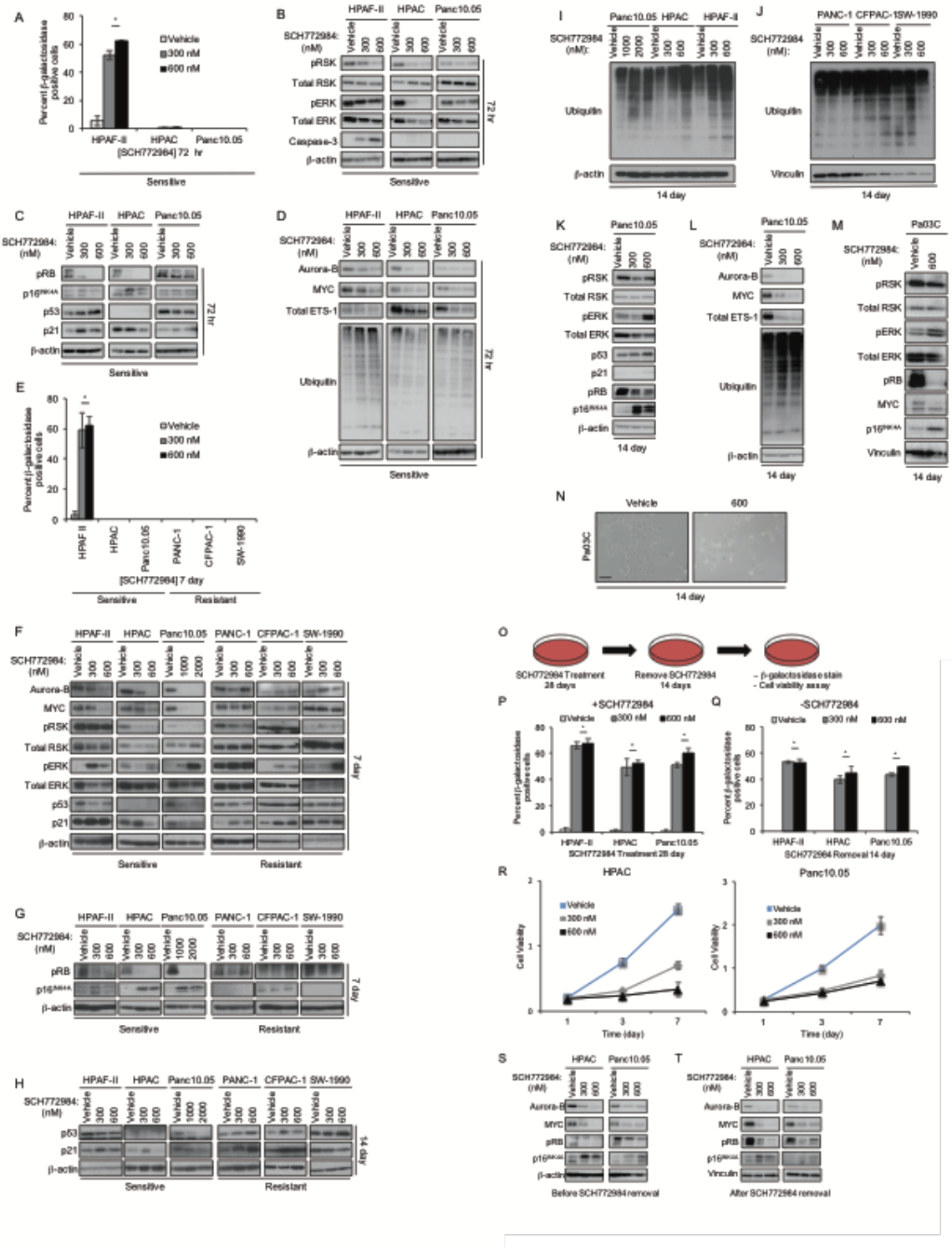

Figure 2.9. Related to Figure 2.8. (A) Senescence associated β-galactosidase stain of sensitive and resistant cell lines after 72 hr of SCH772984 treatment. Error bars represent the standard error of the mean for three independent experiments. Asterisks represent statistical significance

using one-way ANOVA analysis, where * $p < 0.05$. (B) Blot analysis of RSK, ERK, and caspase-3 following 72 hr of SCH772984 treatment. β-actin is a loading control. Data shown are representative of three independent experiments. (C) Blot analysis of pRb, $p16^{INK4A}$, p53, and p21 following 72 hr of SCH772984 treatment. β-actin is a loading control. Data shown are representative of three independent experiments. (D) Blot analysis of Aurora kinase B, MYC, ETS1 and total ubiquitin following 72 hr of SCH772984 treatment. β-actin is a loading control. Data shown are representative of three independent experiments. (E) Senescence associated β-galactosidase stain of sensitive and resistant cell lines after 7 days of SCH772984 treatment. Error bars represent the standard error of the mean for three independent experiments. Asterisks represent statistical significance using one-way ANOVA analysis, where * $p < 0.05$. (F) Blot analysis of Aurora kinase B, MYC, RSK, ERK, p53, and p21 following 7 days of SCH772984 treatment. β-actin is a loading control. Data shown are representative of three independent experiments. (G) Blot analysis of pRB and $p16^{INK4A}$ following 7 days of SCH77984 treatment. Blot analysis for β-actin was done to verify equivalent loading of total cellular protein. (H) Blot analysis of p53 and p21 following 14 days of SCH77984 treatment. Blot analysis for β-actin was done to verify equivalent loading of total cellular protein. (I, J) Sensitive (I) or resistant (J) cell lines maintained on plastic were treated with vehicle or the indicated concentration of SCH772984 for 14 days, and then blotted for ubiquitin or β-actin to verify equivalent loading of total cellular protein. (K) Blot analysis of RSK, ERK, p53, p21, pRB, $p16^{INK4A}$, and total ubiquitin following 14 days of 300 nM and 600 nM SCH772984 treatment in Panc10.05. β-actin is a loading control for total cellular protein. Data shown are representative of three independent experiments. (L) Blot analysis of Aurora B, MYC, ETS1 and total ubiquitin following 14 days of 300 nM and 600 nM SCH772984 treatment in Panc10.05. β-actin is a loading control. Data shown are representative of three independent experiments. (M) Blot analysis of pRSK/RSK, pERK/ERK, pRB, MYC, and p16 following 14 days of 600 nM SCH772984 treatment in Pa03C. Blot analysis for vinculin was done to verify equivalent loading of total cellular protein. (N) Pa03C cell line was treated with SCH772984 at 600 nM for 14 days and then stained for β-galactosidase expression (scale bar, 100 μm). (O) Schematic of SCH772984 removal assay. (P) β-galactosidase staining of sensitive cell lines after 28 days of SCH772984 treatment. Error bars represent the standard error of the mean for three independent experiments. Asterisks represent statistical significance using one-way ANOVA analysis, where * $p < 0.05$. (Q) β-galactosidase staining of sensitive cell lines after 14 days of SCH772984 removal. Error bars represent the standard error of the mean for three independent experiments. Asterisks represent statistical significance using one-way ANOVA analysis, where * $p < 0.05$. (R) The consequences of SCH772984 removal on anchorage-dependent growth were monitored on plastic at 1, 3, and 7 days. Error bars represent the standard error of the mean. (S) Blot analysis of Aurora B, MYC, pRB, and p16 following long-term treatment with SCH772984. β-actin is a loading control. Data shown are representative of three independent experiments. (T) Blot analysis of Aurora B, MYC, pRB, and p16 following removal of SCH772984 after long-term treatment with SCH772984. Vinculin is a loading control. Data shown are representative of three independent experiments.

Figure 2.10.

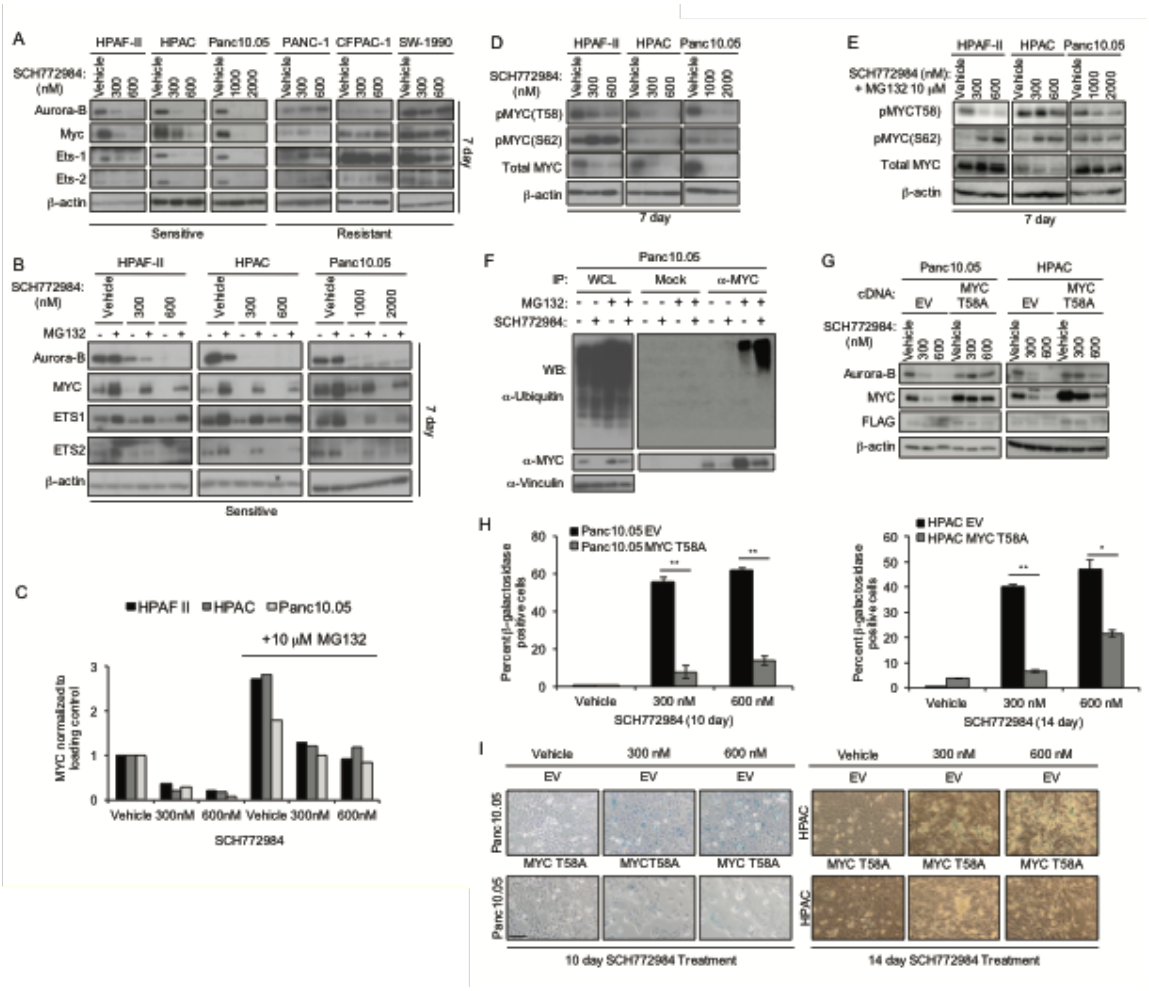

Figure 2.10. Induction of Senescence Is Dependent on Proteasomal Degradation of cMYC. (A) Cells were treated with vehicle or SCH772984 for 7 days, then immunoblotted for Aurora B, MYC, ETS1 or ETS2, and β-actin. Data are representative of three independent experiments. (B) Sensitive cell lines were treated with vehicle or the indicated concentrations of SCH772984 for 7 days, and then co-treated with either vehicle (-) or MG132 (10 μM, +) for an additional 8 hr, followed by western blots for Aurora-B, MYC, ETS-1, and ETS-2. β-actin is the loading control. (C) Densitometry analysis of MYC protein levels from (B). (D) Sensitive cell lines were treated with vehicle or SCH772984 for 7 days, and then immunoblotted with phospho-specific antibodies for Myc residues T58 or S62 (pMYC), or for total MYC and β-actin. (E) Cells were treated as in (D) and then MG132 (10 μM) was added for 8 hr. (F) Sensitive Panc10.05 cells maintained on plastic were treated with either vehicle (-) or SCH772984 (1,000 nM, +) for 7 days, then co-treated with either vehicle (-) or MG132 (10 μM, +) for an additional 8 hr. Whole cell lysates (WCL) were then subjected to control normal serum (mock) or to anti-MYC immunoprecipitation (IP), resolved by SDS-PAGE and then immunoblotted for ubiquitin or for MYC, and for vinculin to verify equivalent loading of total cellular protein. (G) Sensitive Panc10.05 and HPAC cells stably infected with either the empty pMSCV retrovirus vector (EV) or pMSCV encoding a FLAG epitope-tagged ubiquitination-deficient MYC T58A mutant were treated with vehicle or SCH772984 for 10 or 14 days. Western blot was performed to determine levels of Aurora-B, MYC, and FLAG.

Asterisk denotes band of interest. β-actin is the loading control. (H) Panc10.05 and HPAC cells expressing either EV or MYC T58A were treated with SCH772984 for 10 or 14 days, then stained for β-galactosidase. The percentage of β-galactosidase-positive cells was determined. Error bars represent standard error of the mean. Asterisks represent statistical significance using an unpaired *t*-test, where ** = $p < 0.01$ and * = $p < 0.05$. (I) Images (scale bar, 100 μm) of β-galactocidase-positive cell staining in Panc10.05 and HPAC cells, stably infected with the empty pMSCV puro retrovirus vector (EV) or pMSCV encoding MYC T58A, after 10 or 14 days of SCH772984 treatment.

Figure 2.11.

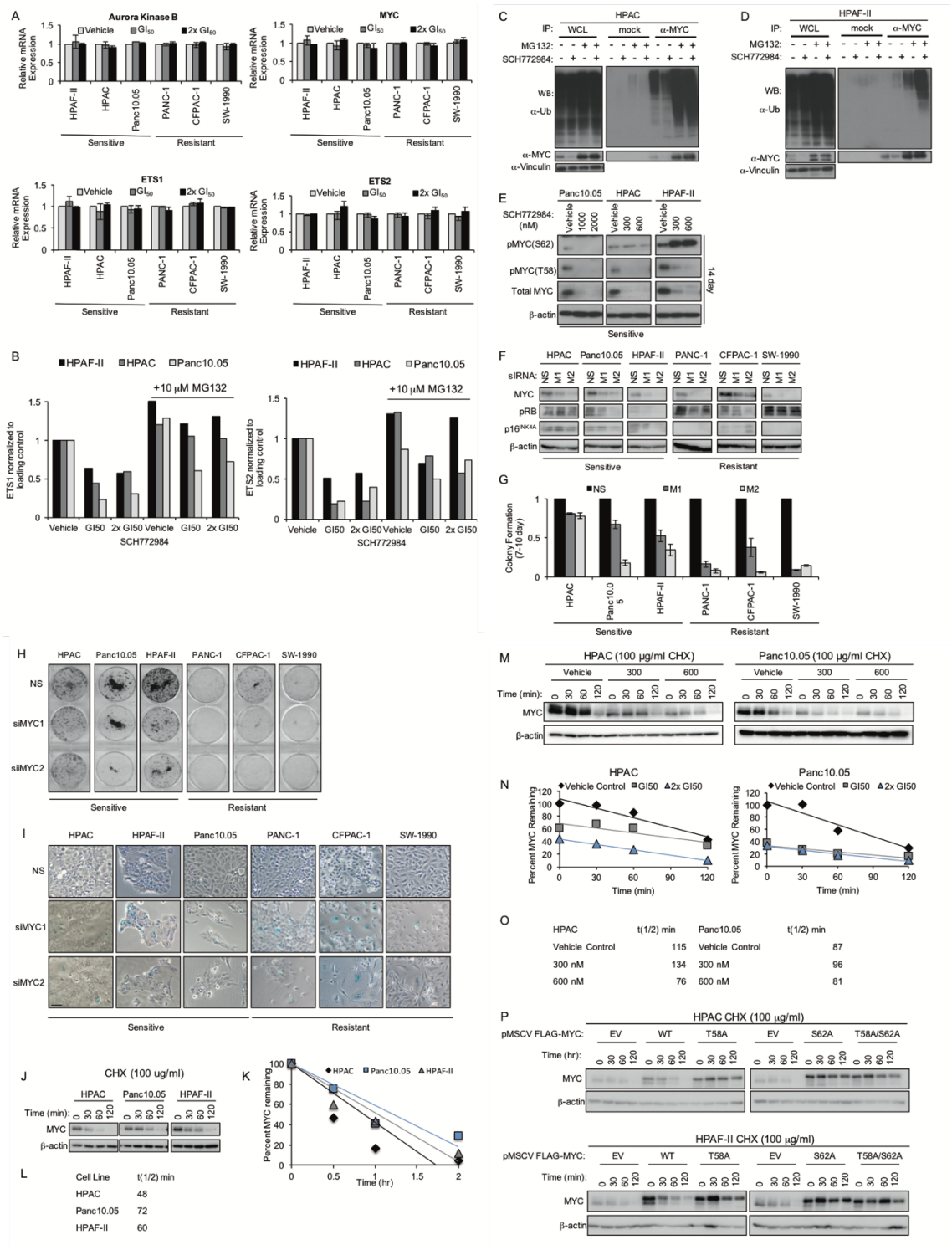
A
Aurora Kinase B
MYC
ETS1
ETS2
Vehicle
GI50
2x GI50
Relative mRNA Expression
HPAF-II
HPAC
Panc10.05
PANC-1
CFPAC-1
SW-1990
Sensitive
Resistant
B
HPAF-II
HPAC
Panc10.05
+10 μM MG132
ETS1 normalized to loading control
ETS2 normalized to loading control
Vehicle
GI50
2x GI50
SCH772984
C
HPAC
IP:
WCL
mock
α-MYC
MG132:
SCH772984:
WB:
α-Ub
α-MYC
α-Vinculin
D
HPAF-II
E
Panc10.05
HPAC
HPAF-II
SCH772984: (nM)
Vehicle
1000
2000
300
600
pMYC(S62)
pMYC(T58)
Total MYC
β-actin
t4 day
Sensitive
F
HPAC
Panc10.05
HPAF-II
PANC-1
CFPAC-1
SW-1990
siRNA:
NS
M1
M2
MYC
pRB
p16INK4A
β-actin
Sensitive
Resistant
G
NS
M1
M2
Colony Formation (7-10 day)
HPAC
Panc10.05
HPAF-II
PANC-1
CFPAC-1
SW-1990
Sensitive
Resistant
H
HPAC
Panc10.05
HPAF-II
PANC-1
CFPAC-1
SW-1990
NS
siMYC1
siMYC2
Sensitive
Resistant
I
HPAC
HPAF-II
Panc10.05
PANC-1
CFPAC-1
SW-1990
NS
siMYC1
siMYC2
Sensitive
Resistant
J
CHX (100 ug/ml)
HPAC
Panc10.05
HPAF-II
Time (min):
MYC
β-actin
K
HPAC
Panc10.05
HPAF-II
Percent MYC remaining
Time (hr)
L
Cell Line
t(1/2) min
HPAC
48
Panc10.05
72
HPAF-II
60
M
HPAC (100 μg/ml CHX)
Panc10.05 (100 μg/ml CHX)
Vehicle
300
600
Time (min):
MYC
β-actin
N
HPAC
Panc10.05
Vehicle Control
GI50
2x GI50
Percent MYC Remaining
Time (min)
O
HPAC
t(1/2) min
Vehicle Control
115
300 nM
134
600 nM
76
Panc10.05
t(1/2) min
Vehicle Control
87
300 nM
96
600 nM
81
P
HPAC CHX (100 μg/ml)
pMSCV FLAG-MYC:
EV
WT
T58A
S62A
T58A/S62A
Time (hr):
MYC
β-actin
HPAF-II CHX (100 μg/ml)
pMSCV FLAG-MYC:
EV
WT
T58A
S62A
T58A/S62A
Time (min):
MYC
β-actin

Figure 2.11.

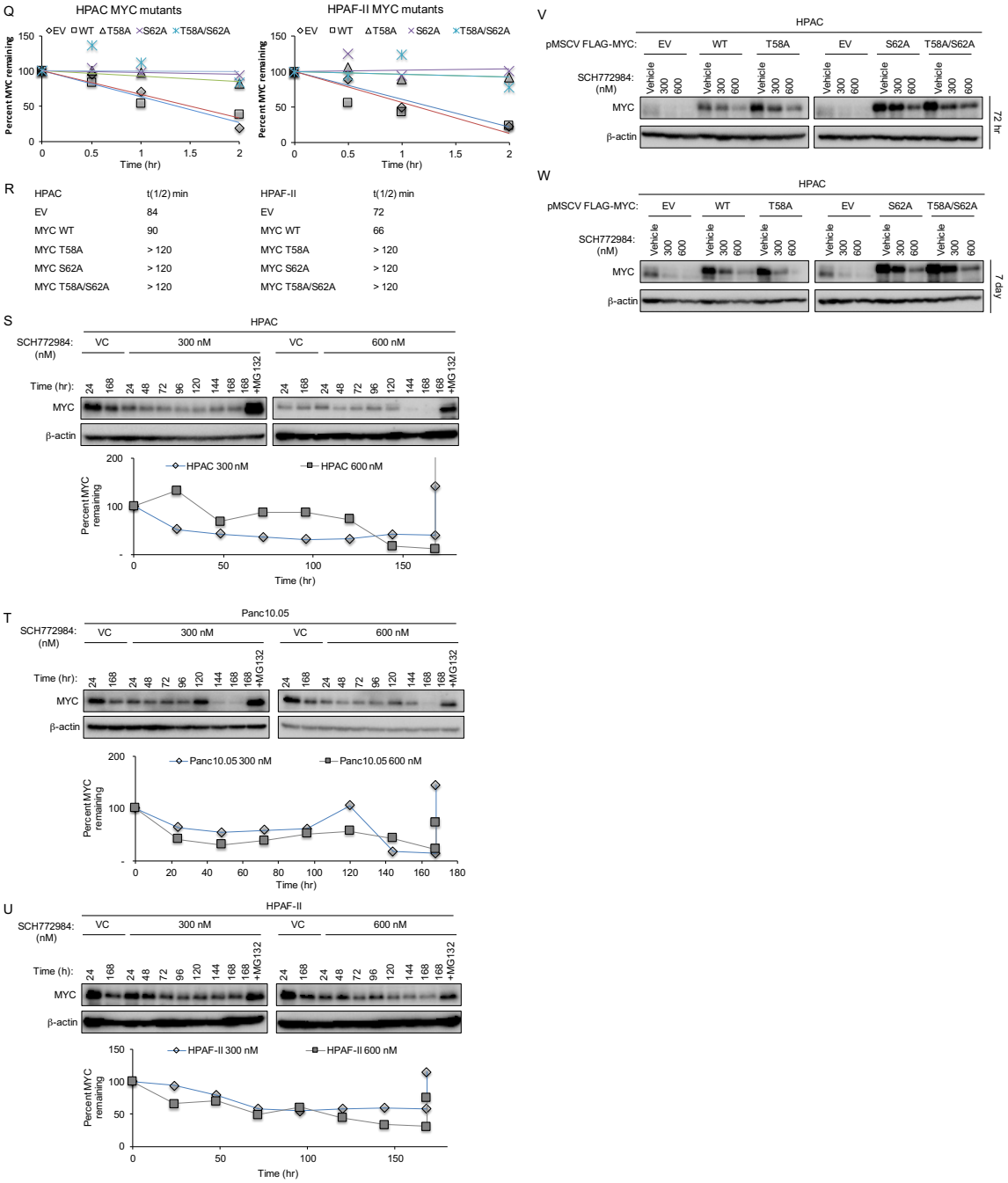

Figure 2.11. Related to Figure 2.10. (A) RT-PCR analysis of mRNA levels of *AURKB*, *MYC*, *ETS1*, and *ETS2*. Sensitive and resistant cell lines were treated with SCH772984 for 7 days on plastic. Error bars represent the standard error of the mean for three independent experiments. (B) Densitometry analysis of ETS1 and ETS2 protein levels from Figure (2.10B). (C) HPAC cells maintained on plastic were treated with either vehicle (-) or 300 nM SCH772984 (+) for 7 days, and then together with either vehicle (-) or 10 μM MG132 (+) for an additional 8 hr. Whole cell lysates (WCL) were then subjected to control normal serum (mock) or to anti-MYC immunoprecipitation (IP), resolved by SDS-PAGE and then blotted for ubiquitin and MYC, and

vinculin to verify equivalent loading of total cellular protein. (D) HPAF-II cells maintained on plastic were treated as described in panel (C). (E) Blot analysis of MYC phosphorylation and total protein expression. Sensitive cell lines were treated with SCH772984 for 14 days. MYC phosphorylation at residues T58 and S62 was determined by phospho-specific antibodies. Blot analysis for β-actin was done to verify equivalent loading of total cellular protein. (F) Cells were transfected with scrambled (NS) or two individual siRNAs targeting *MYC* (designated M1 or M2) for 48 hr, followed by western blot analysis of total MYC, pRB, $p16^{INK4A}$, and β-actin to verify equivalent loading of total protein. Data shown are representative of three independent experiments. (G) Cells transfected with NS or *MYC* siRNA were plated at low density and clonogenic growth was monitored by quantitation of colony formation at 9-12 days post-transfection. Error bars represent the standard error of the mean. Data shown are representative of three independent experiments. (H) The consequences of siRNA *MYC* suppression on clonogenic growth of the indicated PDAC cell lines was determined by colony formation on plastic 9-12 days post-transfection. Shown are photomicrographs (scale bar, 100 μm) of representative dishes after staining with 2 mg/ml crystal violet after 9-12 days post-siRNA transfection. (I) Cells treated as in (H). Shown are photomicrographs (scale bar, 100 μm) of representative fields after staining with β-galactosidase after 9-12 days post-siRNA transfection. (J) Sensitive cell lines were treated with 100 g/ml cycloheximide (CHX) for 0, 30, 60, and 120 min. Blot analysis depicts endogenous MYC loss as a consequence of CHX treatment. β-actin serves as a loading control. (K) Quantitation of blot data from (J) for percentage of MYC remaining after CHX treatment. (L) Half-life calculations (min) of MYC protein in sensitive cell lines. (M) Blot analysis depicts endogenous MYC loss as a consequence of CHX treatment with cells previously treated with SCH772984 at the indicated concentrations for 72 h. β-actin serves as a loading control. (N) Quantitation of blot data from (M) for percentage of MYC remaining after CHX treatment in cells previously treated with SCH772984. (O) Half-life calculations (min) of MYC protein in SCH772984-treated sensitive cell lines. (P) HPAC and HPAF-II cell lines expressing either empty vector (EV), MYC wild-type (WT), MYC T58A, MYC (S62A), and MYC (T58A/S62A), were treated with CHX as in (J). Blot analysis depicts exogenous MYC loss a consequence of CHX treatment. β-actin serves as a loading control. (Q) Quantitation of blot data from (P) for percentage of MYC remaining after CHX treatment. (R) Half-life calculations (min) of MYC in HPAC and HPAF-II expressing empty vector (EV), MYC WT, MYC T58A, MYC (S62A), and MYC (T58A/S62A). (S) HPAC cell line treated with SCH772984 for 24, 48, 72, 96, 120, 144, 168, and 168 hr plus 10 μM MG132. Blot analysis depicts endogenous loss of MYC. β-actin serves as a loading control. Graph depicts densitometry of percentage MYC remaining. (T) Panc10.05 cell line was treated as in (S). (U) HPAF-II cell line was treated as in (S). (V) HPAC cell lines expressing either empty vector (EV), MYC WT, MYC T58A, MYC (S62A), and MYC (T58A/S62A) were treated SCH772984 for 72 hr. Western blot analysis depicts exogenous MYC loss as a consequence of SCH772984 treatment. β-actin serves as a loading control. (W) Cells treated as in (M) for 7 days.

Figure 2.12.

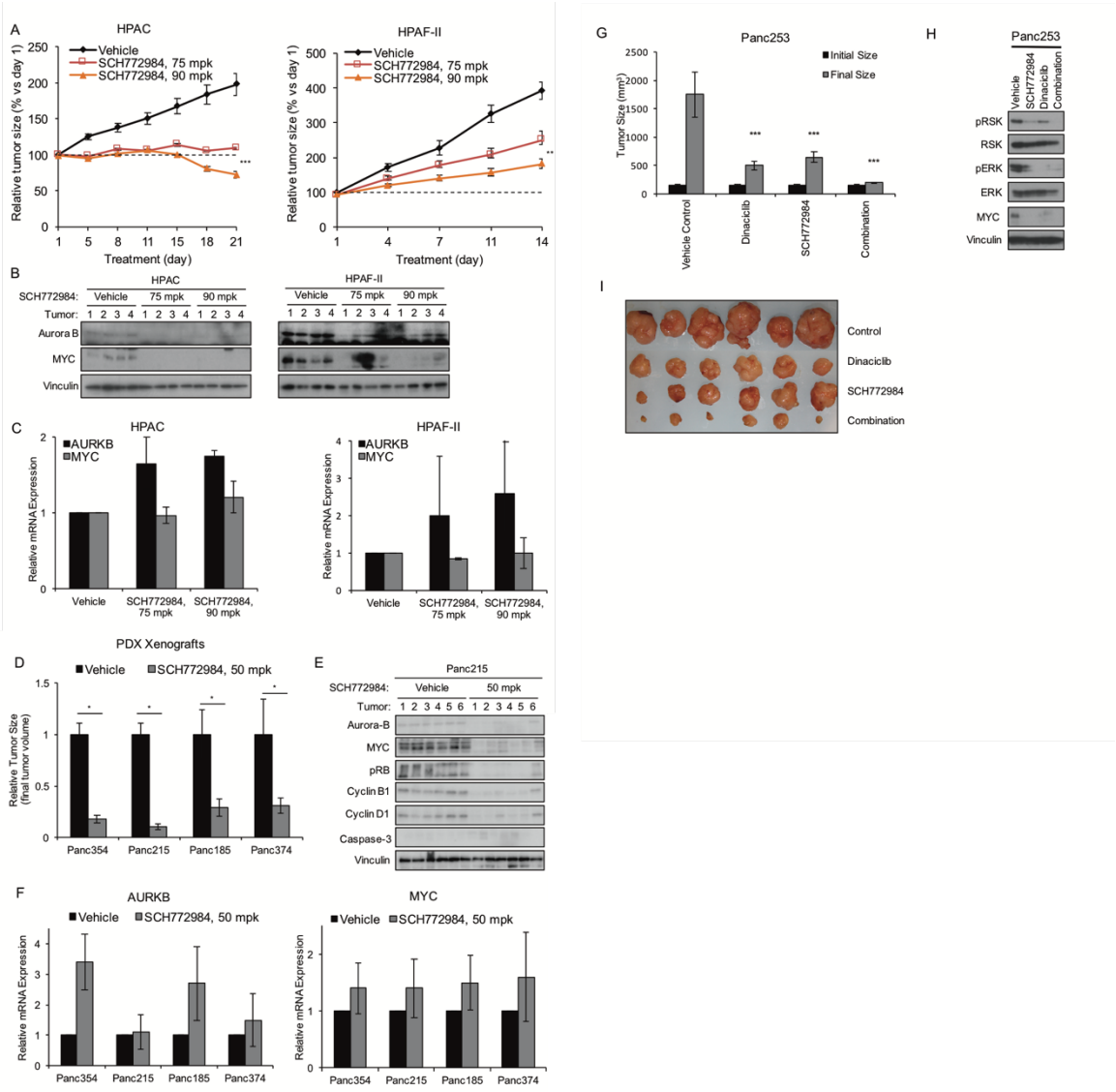

Figure 2.12. SCH772984 Inhibition of Tumor Growth Is Associated with Suppression of Myc and Aurora B Abundance. (A) HPAC or HPAF-II cells were injected subcutaneously into the flanks of nude mice. Tumors were allowed to reach 300-450 mm^3, then mice were treated i.p. daily with vehicle (20% hydroxypropyl beta-cyclodextrin or HPBCD) or with SCH772984 at 75 or 90 mpk for 21 or 14 days, respectively. Error bars represent standard error of the mean (n=10). (B) Tumors from mice treated as in (A) were harvested after 21 days and lysates were analyzed by blotting for Aurora B and MYC protein. (C) Tumors from mice treated as in (A) were harvested after 21 days and analyzed by RT-PCR for *AURKB* and *MYC* mRNA. (D) *KRAS*-mutant pancreatic cancer patient-derived xenograft (PDX) cell lines (Panc354, Panc215, Panc185, and Panc374) were injected subcutaneously into the flanks of nude mice. Tumors were allowed to reach 200 mm^3, then mice were treated with vehicle (10% HPBCD) or SCH772984 at 50 mpk b.i.d. for 14 days. Error bars represent standard error of the mean (n=10). Asterisks represent statistical

significance using two-way ANOVA, where * = $p < 0.05$. (E) Panc215 xenograft tumors treated as in (B) were harvested after 14 days and lysates were analyzed by blotting for Aurora B, MYC, pRB, cyclin B1, cyclin D1, caspase-3 and vinculin. (F) Panc215 xenograft tumors treated as in (C) were harvested after 14 days and lysates were analyzed by RT-PCR for *AURKB* and *MYC* mRNA. (G) Panc253 tumors were orthotopically implanted in nude mice and allowed to grow to a mean size of 200 mm^3, as measured by ultrasound. Mice were treated i.p. with SCH772984 at 25 mpk three times per week or with dinaciclib at 20 mpk twice weekly. After 25 days, tumors were harvested and weighed. All data represent mean ± SE (n= 7); ***, $p < 0.001$, each arm versus vehicle control. (H) Tumors harvested from mice treated as in (B) were analyzed by western blot for phospho-RSK and -ERK, and total RSK, ERK, and MYC. Vinculin is a loading control. (I) Images of Panc253 tumors treated as described in (G).

Figure 2.13.

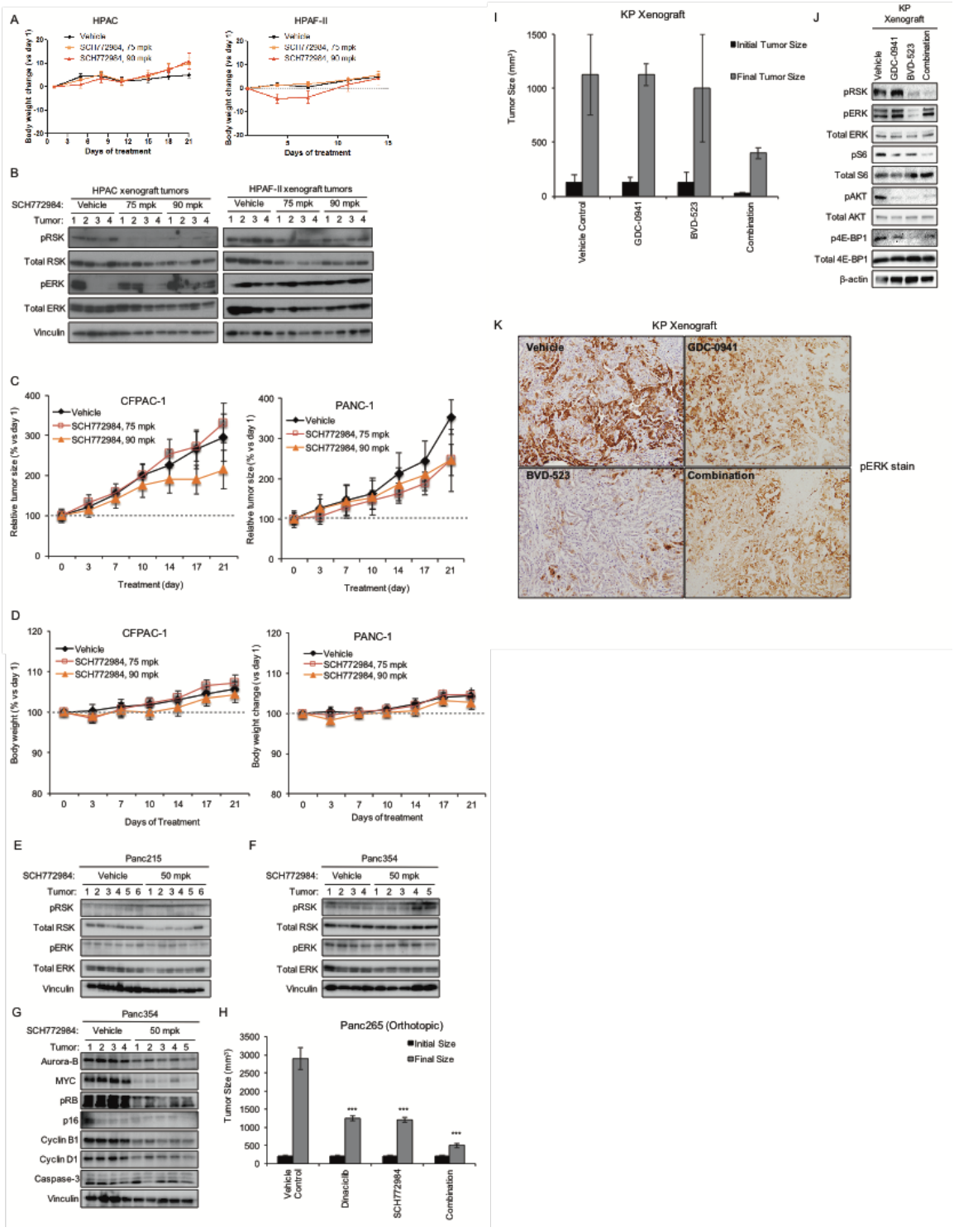

Figure 2.13. Related to Figure 2.12. (A) Body weight change after treatment with SCH772984 in sensitive HPAC and HPAF-II xenografts. (B) Western blot analysis of phosphorylated and total RSK and ERK in HPAC and HPAF-II tumors. Tumors were treated for either 18 (HPAF-II) or 21

(HPAC) days. (C) CFPAC-1 and PANC-1 cells were injected subcutaneously into the flanks of nude mice. Tumors were allowed to reach 300-450 mm^3 and mice were then treated i.p. daily with vehicle (20% HPBCD) or with SCH772984 at 75 or 90 mpk. Error bars represent the standard error of the mean. (D) Body weight change after treatment with SCH772984 in resistant CFPAC-1 and PANC-1 xenografts. (E) Western blot analysis of phosphorylated and total RSK and ERK in Panc215 tumors. Tumors were treated for either with SCH772984 at 50 mpk for 14 days. (F) Western blot analysis of phosphorylated and total RSK and ERK in Panc354 tumors. Tumors were treated for 14 days either with vehicle control or SCH772984 at 50 mpk. (G) Western blot analysis of Aurora B, MYC, pRB, p16, cyclin B1, cyclin D1, and caspase-3 in Panc354 tumors. Tumors were treated as in (F). (H) Panc265 tumors were orthotopically implanted in nude mice and allowed to grow to a mean size of 200 mm^3, as measured by ultrasound. Mice were treated i.p. with SCH772984 at 25 mpk three times per week or with dinaciclib at 20 mpk twice weekly. After 25 days, tumors were harvested and weighed. All data represent mean ± SE (n= 7); ***, $p < 0.001$, each arm versus vehicle control. (I) KP mouse cells were injected subcutaneously into the flanks of C57BL/6J mice. Mice received vehicle (0.5% methylcellulose /0.2% Tween-20 and 1% carboxymethyl-cellulose), 50 mg/kg GDC-0941 daily, 100 mg/kg BVD-523 BID, or 50 mg/kg GDC-0941 daily plus 100 mg/kg BVD-523 twice daily, orally for 14 days. Data are presented as mean ± SEM. (J) Western blot analysis of pRSK, pERK/total ERK, pS6/total S6, pAKT/total AKT, and p4E-BP1/total 4E-BP1 in KP cells. β-actin serves as a loading control (K) Immunohistochemical staining of pERK (rabbit polycolonal antibody) in KP xenografts from mice after 2 hr of oral gavage with 2 mg BVD-523, 1 mg GDC-0941 and combination of BVD-523 and GDC-0941 (1 mg BVD-523 + 0.5 mg GDC-0941).

Figure 2.14.

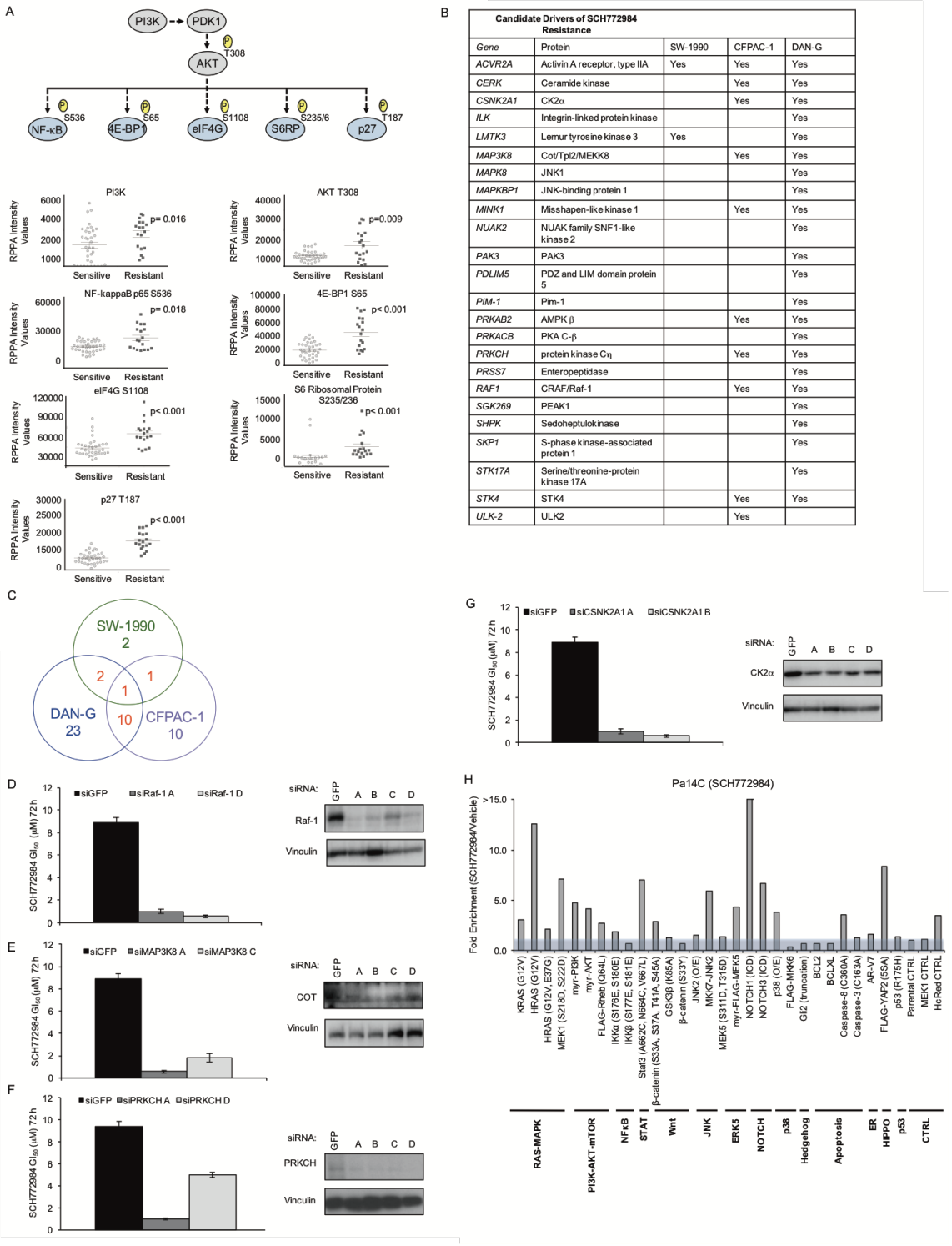

Candidate Drivers of SCH772984 Resistance				
Gene	Protein	SW-1990	CFPAC-1	DAN-G
ACVR2A	Activin A receptor, type IIA	Yes	Yes	Yes
CERK	Ceramide kinase		Yes	Yes
CSNK2A1	CK2α		Yes	Yes
ILK	Integrin-linked protein kinase			Yes
LMTK3	Lemur tyrosine kinase 3	Yes		Yes
MAP3K8	Cot/Tpl2/MEKK8		Yes	Yes
MAPK8	JNK1			Yes
MAPKBP1	JNK-binding protein 1			Yes
MINK1	Misshapen-like kinase 1		Yes	Yes
NUAK2	NUAK family SNF1-like kinase 2			Yes
PAK3	PAK3			Yes
PDLIM5	PDZ and LIM domain protein 5			Yes
PIM-1	Pim-1			Yes
PRKAB2	AMPK β		Yes	Yes
PRKACB	PKA C-β			Yes
PRKCH	protein kinase Cη		Yes	Yes
PRSS7	Enteropeptidase			Yes
RAF1	CRAF/Raf-1		Yes	Yes
SGK269	PEAK1			Yes
SHPK	Sedoheptulokinase			Yes
SKP1	S-phase kinase-associated protein 1			Yes
STK17A	Serine/threonine-protein kinase 17A			Yes
STK4	STK4		Yes	Yes
ULK-2	ULK2		Yes	

Figure 2.14.

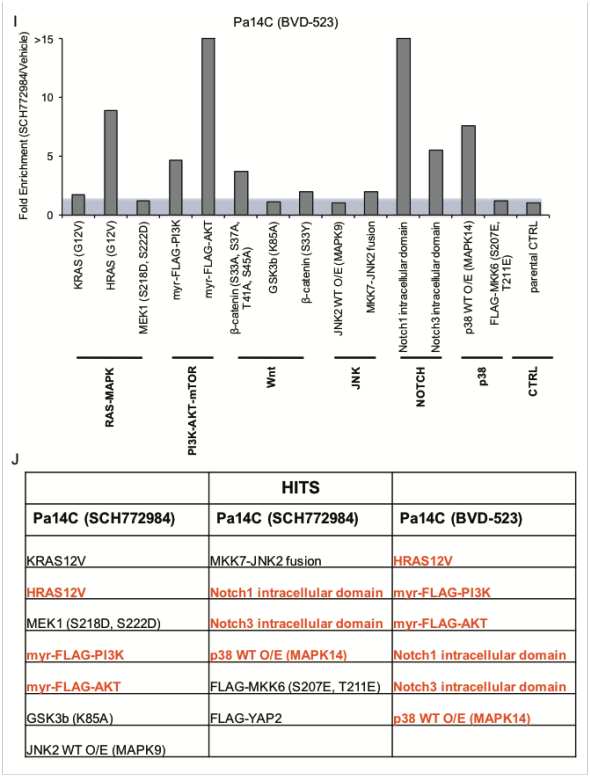

J

	HITS	
Pa14C (SCH772984)	**Pa14C (SCH772984)**	**Pa14C (BVD-523)**
KRAS12V	MKK7-JNK2 fusion	HRAS12V
HRAS12V	Notch1 intracellular domain	myr-FLAG-PI3K
MEK1 (S218D, S222D)	Notch3 intracellular domain	myr-FLAG-AKT
myr-FLAG-PI3K	p38 WT O/E (MAPK14)	Notch1 intracellular domain
myr-FLAG-AKT	FLAG-MKK6 (S207E, T211E)	Notch3 intracellular domain
GSK3b (K85A)	FLAG-YAP2	p38 WT O/E (MAPK14)
JNK2 WT O/E (MAPK9)		

Figure 2.14. Related to Figure 2.15. (A) PI3K-AKT-mTOR network (top) activation signature in SCH772984-treated established and PDX PDAC cell lines. Scatter plots (bottom) are shown for each network component that was significantly elevated in ERK inhibitor-resistant lines compared to ERK sensitive lines. (B) List of genes whose knockdown in resistant PDAC cell lines by at least two independent siRNAs caused a 5-fold increase in sensitivity to the ERK-inhibitor SCH772984. (C) Venn diagram displaying overlapping hits among ERK inhibitor resistant cell lines. (D) CFPAC-1 cells were transfected with siRNA targeting green fluorescent protein (GFP) or RAF-1, then exposed to varying concentrations of SCH772984 for 72 hr. CompuSyn software was used to generate GI_{50} values. Western blot analysis of RAF-1 and vinculin (total cellular protein loading control) after siRNA knockdown. (E) Cells were treated as in (D) with siRNA targeting GFP or COT/TPL2. CompuSyn Software was used to generate GI_{50} values. Western blot analysis of COT/TPL2 (encoded by *MAP3K8*) and vinculin (total cellular protein loading control) after siRNA knockdown. (F) Cells were treated as in (D) with siRNA targeting GFP or protein kinase eta (PRKCH). CompuSyn software was used to generate GI_{50} values. Western blot analysis of PRKCH and vinculin (total cellular protein loading control) after siRNA knockdown. (G) Cells were treated as in (D) with siRNA targeting GFP or CK2α. CompuSyn Software was used to generate GI_{50} values. Western blot analysis of CKα (encoded by *CSNK2A1*) and vinculin (total cellular protein loading control) after siRNA knockdown. (H) and (I) Pa14C cells were transduced with individual lentiviral constructs and cultured in the presence of vehicle or either SCH772984 or BVD-0523. Bars show the fold increase in sensitivity relative to vehicle-treated samples. Transparent blue shading marks threshold fold enrichment score of 1.0. (J) Common hits between SCH772984 and BVD-523.

Figure 2.15.

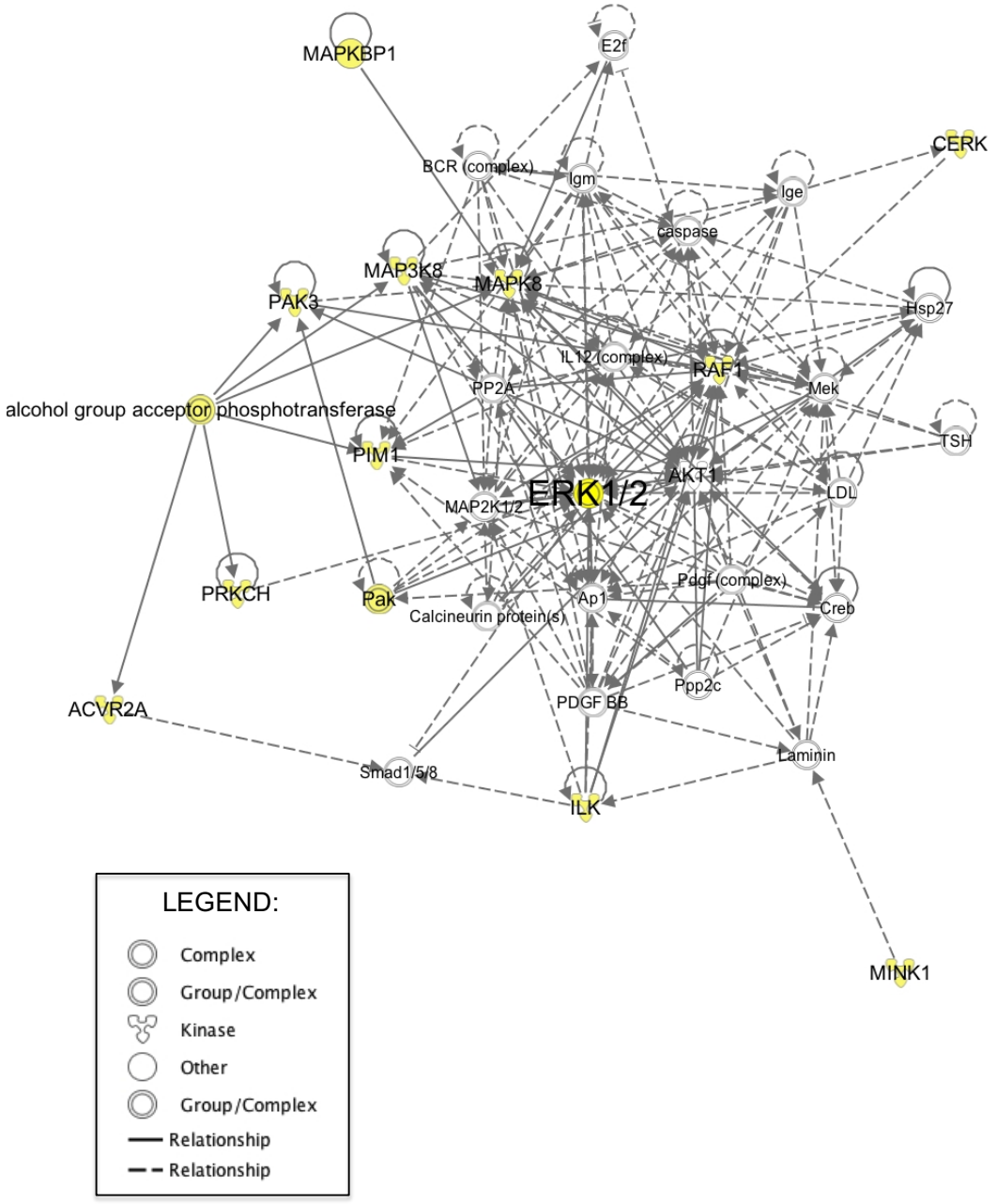

Figure 2.15. Identification of Protein Kinases That Regulate Resistance of PDAC Cell Lines to SCH772984. Pathway analysis based on Ingenuity Pathway Knowledge Base. The highest scoring networks (Post-translational Modification, Cell Morphology, Cellular Assembly and Organization; score 29, p-values < 0.05) were obtained from the proteins identified in our kinome-wide siRNA SCH772984 resistance screen. A black solid line represents a direct relationship between two nodes. A dotted line represents an indirect interaction between two nodes. Shaded nodes are the genes identified in our screen.

REFERENCES

Alagesan, B., Contino, G., Guimaraes, A.R., Corcoran, R.B., Deshpande, V., Wojtkiewicz, G.R., Hezel, A.F., Wong, K.K., Loda, M., Weissleder, R., et al. (2015). Combined MEK and PI3K Inhibition in a Mouse Model of Pancreatic Cancer. Clin Cancer Res *21*, 396-404.

Bardeesy, N., Aguirre, A.J., Chu, G.C., Cheng, K.H., Lopez, L.V., Hezel, A.F., Feng, B., Brennan, C., Weissleder, R., Mahmood, U., et al. (2006). Both p16(Ink4a) and the p19(Arf)-p53 pathway constrain progression of pancreatic adenocarcinoma in the mouse. Proc Natl Acad Sci USA *103*, 5947-5952.

Bonet, C., Giuliano, S., Ohanna, M., Bille, K., Allegra, M., Lacour, J.P., Bahadoran, P., Rocchi, S., Ballotti, R., and Bertolotto, C. (2012). Aurora B is regulated by the mitogen-activated protein kinase/extracellular signal-regulated kinase (MAPK/ERK) signaling pathway and is a valuable potential target in melanoma cells. J Biol Chem *287*, 29887-29898.

Bryant, K.L., Mancias, J.D., Kimmelman, A.C., and Der, C.J. (2014). KRAS: feeding pancreatic cancer proliferation. Trends Biochem Sci *39*, 91-100.

Caldwell, M.E., DeNicola, G.M., Martins, C.P., Jacobetz, M.A., Maitra, A., Hruban, R.H., and Tuveson, D.A. (2012). Cellular features of senescence during the evolution of human and murine ductal pancreatic cancer. Oncogene *31*, 1599-1608.

Campisi, J. (2013). Aging, cellular senescence, and cancer. Annu Rev Physiol *75*, 685-705.

Cox, A.D., Fesik, S.W., Kimmelman, A.C., Luo, J., and Der, C.J. (2014). Drugging the undruggable RAS: Mission possible? Nat Rev Drug Discov *13*, 828-851.

Deschenes-Simard, X., Gaumont-Leclerc, M.F., Bourdeau, V., Lessard, F., Moiseeva, O., Forest, V., Igelmann, S., Mallette, F.A., Saba-El-Leil, M.K., Meloche, S., et al. (2013). Tumor suppressor activity of the ERK/MAPK pathway by promoting selective protein degradation. Genes Dev *27*, 900-915.

Dougherty, M.K., Muller, J., Ritt, D.A., Zhou, M., Zhou, X.Z., Copeland, T.D., Conrads, T.P., Veenstra, T.D., Lu, K.P., and Morrison, D.K. (2005). Regulation of Raf-1 by direct feedback phosphorylation. Mol Cell *17*, 215-224.

Duncan, J.S., Whittle, M.C., Nakamura, K., Abell, A.N., Midland, A.A., Zawistowski, J.S., Johnson, N.L., Granger, D.A., Jordan, N.V., Darr, D.B., et al. (2012). Dynamic reprogramming of the kinome in response to targeted MEK inhibition in triple-negative breast cancer. Cell *149*, 307-321.

Eser, S., Reiff, N., Messer, M., Seidler, B., Gottschalk, K., Dobler, M., Hieber, M., Arbeiter, A., Klein, S., Kong, B., et al. (2013). Selective requirement of PI3K/PDK1 signaling for Kras oncogene-driven pancreatic cell plasticity and cancer. Cancer cell *23*, 406-420.

Farrell, A.S., and Sears, R.C. (2014). MYC Degradation. Cold Spring Harb Perspect Med *4*.

Feldmann, G., Mishra, A., Bisht, S., Karikari, C., Garrido-Laguna, I., Rasheed, Z., Ottenhof, N.A., Dadon, T., Alvarez, H., Fendrich, V., et al. (2011). Cyclin-dependent kinase inhibitor

Dinaciclib (SCH727965) inhibits pancreatic cancer growth and progression in murine xenograft models. Cancer Biol Ther *12*, 598-609.

Feldmann, G., Mishra, A., Hong, S.M., Bisht, S., Strock, C.J., Ball, D.W., Goggins, M., Maitra, A., and Nelkin, B.D. (2010). Inhibiting the cyclin-dependent kinase CDK5 blocks pancreatic cancer formation and progression through the suppression of Ras-Ral signaling. Cancer Res *70*, 4460-4469.

Germann, U., Furey, B., Roix, J., Marklan, W., Hoover,R., Aronov, A., Hale, M., Chen,.G., Martinez-Botella, G., Alargova, R., Fan, B., Sorrell,D., Meshaw,K., Shapiro, P., Wick,M., Benes,C., Garnett, M.,DeCrescemzp, G., Namchuk, M., Saha, S., Welsch, D (2015). The selective ERK inhibitor BVD-523 is active models of MAPK pathway-dependent cancers, including those with intrinsic and acquired drug resistance. Proceedings of the 106th Annual Meeting of the American Association for Cancer Research.

Goetz, E.M., Ghandi, M., Treacy, D.J., Wagle, N., and Garraway, L.A. (2014). ERK mutations confer resistance to mitogen-activated protein kinase pathway inhibitors. Cancer Res *74*, 7079-7089.

Hancox, U., Cosulich, S., Hanson, L., Trigwell, C., Lenaghan, C., Ellston, R., Dry, H., Crafter, C., Barlaam, B., Fitzek, M., et al. (2015). Inhibition of PI3Kbeta Signaling with AZD8186 Inhibits Growth of PTEN-Deficient Breast and Prostate Tumors Alone and in Combination with Docetaxel. Mol Cancer Ther *14*, 48-58.

Hatzivassiliou, G., Liu, B., O'Brien, C., Spoerke, J.M., Hoeflich, K.P., Haverty, P.M., Soriano, R., Forrest, W.F., Heldens, S., Chen, H., et al. (2012). ERK inhibition overcomes acquired resistance to MEK inhibitors. Mol Cancer Ther *11*, 1143-1154.

Hidalgo, M., Amant, F., Biankin, A.V., Budinska, E., Byrne, A.T., Caldas, C., Clarke, R.B., de Jong, S., Jonkers, J., Maelandsmo, G.M., et al. (2014). Patient-derived xenograft models: an emerging platform for translational cancer research. Cancer Discov *4*, 998-1013.

Johannessen, C.M., Boehm, J.S., Kim, S.Y., Thomas, S.R., Wardwell, L., Johnson, L.A., Emery, C.M., Stransky, N., Cogdill, A.P., Barretina, J., et al. (2010). COT drives resistance to RAF inhibition through MAP kinase pathway reactivation. Nature *468*, 968-972.

Junttila, M.R., Devasthali, V., Cheng, J.H., Castillo, J., Metcalfe, C., Clermont, A.C., Otter, D.D., Chan, E., Bou-Reslan, H., Cao, T., et al. (2015). Modeling targeted inhibition of MEK and PI3 kinase in human pancreatic cancer. Mol Cancer Ther *14*, 40-47.

Kapoor, A., Yao, W., Ying, H., Hua, S., Liewen, A., Wang, Q., Zhong, Y., Wu, C.J., Sadanandam, A., Hu, B., et al. (2014). Yap1 activation enables bypass of oncogenic Kras addiction in pancreatic cancer. Cell *158*, 185-197.

Lim, K.H., O'Hayer, K., Adam, S.J., Kendall, S.D., Campbell, P.M., Der, C.J., and Counter, C.M. (2006). Divergent roles for RalA and RalB in malignant growth of human pancreatic carcinoma cells. Curr Biol *16*, 2385-2394.

Liotta, L.A., Espina, V., Mehta, A.I., Calvert, V., Rosenblatt, K., Geho, D., Munson, P.J., Young, L., Wulfkuhle, J., and Petricoin, E.F., 3rd (2003). Protein microarrays: meeting analytical challenges for clinical applications. Cancer Cell *3*, 317-325.

Lito, P., Rosen, N., and Solit, D.B. (2013). Tumor adaptation and resistance to RAF inhibitors. Nat Med *19*, 1401-1409.

Martz, C.A., Ottina, K.A., Singleton, K.R., Jasper, J.S., Wardell, S.E., Peraza-Penton, A., Anderson, G.R., Winter, P.S., Wang, T., Alley, H.M., et al. (2014). Systematic identification of signaling pathways with potential to confer anticancer drug resistance. Sci Signal *7*, ra121.

Morris, E.J., Jha, S., Restaino, C.R., Dayananth, P., Zhu, H., Cooper, A., Carr, D., Deng, Y., Jin, W., Black, S., et al. (2013). Discovery of a novel ERK inhibitor with activity in models of acquired resistance to BRAF and MEK inhibitors. Cancer Discov *3*, 742-750.

Nardella, C., Clohessy, J.G., Alimonti, A., and Pandolfi, P.P. (2011). Pro-senescence therapy for cancer treatment. Nature Rev Cancer *11*, 503-511.

Nissan, M.H., Rosen, N., and Solit, D.B. (2013). ERK pathway inhibitors: how low should we go? Cancer Discov *3*, 719-721.

Ohtani, N., Zebedee, Z., Huot, T.J., Stinson, J.A., Sugimoto, M., Ohashi, Y., Sharrocks, A.D., Peters, G., and Hara, E. (2001). Opposing effects of Ets and Id proteins on p16INK4a expression during cellular senescence. Nature *409*, 1067-1070.

Pemovska, T., Kontro, M., Yadav, B., Edgren, H., Eldfors, S., Szwajda, A., Almusa, H., Bespalov, M.M., Ellonen, P., Elonen, E., et al. (2013). Individualized systems medicine strategy to tailor treatments for patients with chemorefractory acute myeloid leukemia. Cancer Discov *3*, 1416-1429.

Samatar, A.A., and Poulikakos, P.I. (2014). Targeting RAS-ERK signalling in cancer: promises and challenges. Nat Rev Drug Discov *13*, 928-942.

Shao, D.D., Xue, W., Krall, E.B., Bhutkar, A., Piccioni, F., Wang, X., Schinzel, A.C., Sood, S., Rosenbluh, J., Kim, J.W., et al. (2014). KRAS and YAP1 converge to regulate EMT and tumor survival. Cell *158*, 171-184.

Shimizu, T., Tolcher, A.W., Papadopoulos, K.P., Beeram, M., Rasco, D.W., Smith, L.S., Gunn, S., Smetzer, L., Mays, T.A., Kaiser, B., et al. (2012). The clinical effect of the dual-targeting strategy involving PI3K/AKT/mTOR and RAS/MEK/ERK pathways in patients with advanced cancer. Clin Cancer Res *18*, 2316-2325.

Singh, A., Greninger, P., Rhodes, D., Koopman, L., Violette, S., Bardeesy, N., and Settleman, J. (2009). A gene expression signature associated with "K-Ras addiction" reveals regulators of EMT and tumor cell survival. Cancer Cell *15*, 489-500.

Stephen, A.G., Esposito, D., Bagni, R.K., and McCormick, F. (2014). Dragging Ras Back in the Ring. Cancer cell *25*, 272-281.

Tolcher, A.W., Khan, K., Ong, M., Banerji, U., Papadimitrakopoulou, V., Gandara, D.R., Patnaik, A., Baird, R.D., Olmos, D., Garrett, C.R., et al. (2015). Antitumor Activity in RAS-Driven Tumors by Blocking AKT and MEK. Clin Cancer Res *21*, 739-748.

Villanueva, J., Vultur, A., Lee, J.T., Somasundaram, R., Fukunaga-Kalabis, M., Cipolla, A.K., Wubbenhorst, B., Xu, X., Gimotty, P.A., Kee, D., et al. (2010). Acquired resistance to BRAF inhibitors mediated by a RAF kinase switch in melanoma can be overcome by cotargeting MEK and IGF-1R/PI3K. Cancer Cell *18*, 683-695.

Vogel, C.J., Smit, M.A., Maddalo, G., Possik, P.A., Sparidans, R.W., van der Burg, S.H., Verdegaal, E.M., Heck, A.J., Samatar, A.A., Beijnen, J.H., et al. (2015). Cooperative induction of apoptosis in NRAS mutant melanoma by inhibition of MEK and ROCK. Pigment Cell Melanoma Res *28*, 307-317.

Waddell, N., Pajic, M., Patch, A.M., Chang, D.K., Kassahn, K.S., Bailey, P., Johns, A.L., Miller, D., Nones, K., Quek, K., et al. (2015). Whole genomes redefine the mutational landscape of pancreatic cancer. Nature *518*, 495-501.

Wee, S., Jagani, Z., Xiang, K.X., Loo, A., Dorsch, M., Yao, Y.M., Sellers, W.R., Lengauer, C., and Stegmeier, F. (2009). PI3K pathway activation mediates resistance to MEK inhibitors in KRAS mutant cancers. Cancer Res *69*, 4286-4293.

Wu, C.H., van Riggelen, J., Yetil, A., Fan, A.C., Bachireddy, P., and Felsher, D.W. (2007). Cellular senescence is an important mechanism of tumor regression upon c-Myc inactivation. Proc Natl Acad Sci USA *104*, 13028-13033.

Yeh, E., Cunningham, M., Arnold, H., Chasse, D., Monteith, T., Ivaldi, G., Hahn, W.C., Stukenberg, P.T., Shenolikar, S., Uchida, T., et al. (2004). A signalling pathway controlling c-Myc degradation that impacts oncogenic transformation of human cells. Nat Cell Biol *6*, 308-318.

Yoon, S., and Seger, R. (2006). The extracellular signal-regulated kinase: multiple substrates regulate diverse cellular functions. Growth Factors *24*, 21-44.

CHAPTER 3: DISCUSSION

The use of targeted small molecule inhibitors has greatly impacted the treatment of human diseases, from cancer to genetic disorders. Inhibitors, such as imatinib (Gleevec) have proven to be curative, while others, vemurafinib (Zelboraf) for example, have generated new fields of study. Unlike genetic tools, such as siRNA, shRNA, or CRISPR/Cas9, inhibitors have both significantly impacted our understanding of the complexities of signaling networks and provided a therapeutic benefit for patients. Having said that, there are several current studies evaluating use of siRNA as a therapy, however, that therapeutic option is far from the clinic.

The use of small-molecule inhibitors has revealed many complexities associated with signal transduction networks, yet there are still many unanswered questions. Today, generating protein kinase inhibitors is commonplace; however, not all proteins are as easily targeted. GTPases and transcription factors, for example, remain elusive, though there has been an intensive effort to develop direct small molecule inhibitors for each. Ras (GTPase) and Myc (transcription factor) proteins represent the two most frequently mutated oncogenes in cancer, yet they cannot be directly targeted (Yokota et al., 1986). To that end, genetic manipulation remains the best option to investigate the regulation and function of such proteins. Using a combination of inhibitors and genetic manipulations has significantly enhanced our current understanding of signal transduction in mutant *RAS* driven cancers. Since we cannot directly inhibit mutant *RAS*, indirect inhibition remains the best available option. Targeting effector cascades associated with mutant *RAS* dependency are likely the best therapeutic option for disruption of mutant *RAS* signaling.

Chapter II assessed the effectiveness of ERK inhibition in mutant *KRAS* cancers. In my studies, we identified a bi-modal action of the ERK inhibitor SCH772984 where short and long-term treatment resulted in differential consequences. Current inhibitor studies generally focus on the effects of short-term treatment, from 24-72 h, however patient treatments are rarely, if ever, that acute. Our studies suggest that the long-term phenotype is likely the more relevant for patient treatment. Furthermore, we identified novel mechanisms of resistance to ERK inhibition that will likely drive future combination treatments in PDAC. In this chapter, I will consider how these observations as well as others can guide future investigations.

3.1 Mutant *RAS* Dependency

It has been well established that KRAS is the most frequently mutated oncogene in cancer, however, whether mutant *KRAS* cancers are still dependent on the continued expression of mutant *KRAS* for growth/survival remains partially unanswered. We know from mouse models that mutant *RAS* is essential for initiation, progression, and maintenance (Chin et al., 1999; Johnson et al., 2001; Lim and Counter, 2005). However, recent studies have suggested that not all mutant *KRAS* cancers are dependent on the continued expression of mutant *KRAS* (Singh et al., 2009). Most of these analyses have been carried out using an *in vitro* tumor cell line culture model.

Our tumor cell line data, in both established and PDX tumor cell lines, suggests that all mutant *KRAS* tumor cell lines are dependent on the continued expression of mutant *KRAS* for growth. Additionally, we have even expanded our findings to include mutant *NRAS* and *HRAS* cancers. Consistent with our observations in mutant *KRAS* tumor cell lines, we find that suppression of either oncogenic *NRAS* or *HRAS* in tumor cell lines containing the respective mutation results in reduced growth (data not shown). We have reproducibly demonstrated this observation using both siRNA and shRNA knockdown of mutant *KRAS*. Importantly, we observed that the degree of sensitivity to loss of mutant *KRAS* varies between tumor cell lines. Furthermore,

sensitivity is also dependent on the effectiveness of knockdown, as might be expected. When mutant *KRAS* is depleted by greater than 90%, the growth rate is markedly reduced.

Defining the notion of sensitivity (or dependence) is a key aspect to understanding what seems to be contradictory data. Our lab has defined sensitivity as growth in either an *in vitro* anchorage-dependent (2D) or -independent (3D) assay. Historically, anchorage-independent growth assays have been the gold standard for predicting *in vivo* efficacy, meaning that observations made under anchorage-independent conditions are more likely to be recapitulated in an *in vivo* system. We, as well as others, find that mutant *KRAS* dependency is equally observable under both 2D and 3D systems (Bryant et al., 2014;Commisso et al., 2013).

However, several other prominent studies have defined sensitivity as induction of apoptosis/survival. In these studies, several groups were able to distinguish between tumor cell lines that were dependent on the continued expression of mutant *KRAS*, and ones that were independent (Fujita-Sato et al., 2015; Singh et al., 2009). Cleaved-caspase-3 and PARP, both markers indicative of apoptosis, were enhanced when mutant *KRAS* tumor cells lines were depleted of K-Ras in one such study. In further support of this observation, ectopic expression of mutant *KRAS* was able to partially reverse the apoptotic phenotype suggesting that it was an on-target effect.

How can these seemingly opposing observations coexist, without disproving either each other? In studies where mutant *KRAS* depletion results in an apoptotic phenotype, there is still a population of attached cells. Though the attached cells are not replicating as fast as the control, they are still viable as marked by uptake of crystal violet or MTT. After time, this population can be characterized by markedly reduced cellular growth compared to the control. In our studies, we find this same cellular population when mutant *KRAS* is depleted. Consistent with this observation, other studies have found that depletion of K-Ras in mutant *KRAS* cells can result in cell cycle arrest as measured by Propidium Iodine (P.I.) staining (Halilovic et al., 2010). Together, both the reduced growth and apoptotic observations suggest that the total population of cells is

quite heterogenous. This notion partially reconciles the multiple phenotypes observed with the depletion of mutant *KRAS.* However, which phenotype is most relevant remains unresolved.

Future Studies

To effectively investigate the oncogene dependency question, I would propose to use both *in vitro* and *in vivo* techniques. First, I would make a confetti (or rainbow) cell line expressing GFP, RFP, CFP, and YFP fluorophores in order to follow individual clones. We would first take a Ras mutant tumor cell line (either established and PDX) and isolate a large number of individual clones. These clones would then be infected with a different fluorophore; once infected I would set up various mixtures of clones from that cell line. Then we would deplete Ras, using a combination of siRNA, shRNA, and CRISPR/Cas9 techniques, from these cells to determine the effect on each subpopulation. I would measure the effects using standard growth assays in combination with a fluorescent scope to follow each subpopulation. Additionally, we would use flow cytommetry to isolate each subpopulation. After isolation of each subpopulation, markers of apoptosis and cell cycle would be analyzed. After demonstrating proof of concept, I would expand this system to include many mutant *RAS* (K-Ras, H-Ras, and N-Ras) tumor cell lines.

Furthermore, we would characterize these populations by investigating changes in effector usage after Ras depletion. We would accomplish this using reverse-phase protein array (RPPA), which would determine changes in phosphorylated and total proteins downstream of mutant *RAS* in each subpopulation. In Chapter II, we effectively used RPPA to distinguish between basal signaling in ERK inhibitor sensitive and resistant cell lines. From there, we were able to reveal a ERK inhibitor resistance signature that was associated with PI3K signaling in the ERK inhibitor resistant cell lines. This was an interesting and somewhat confusing observation, in that we also observed that PI3K signaling was important in ERK inhibitor sensitive cell lines. The difference being that basal PI3K signaling was elevated in resistant cell lines even before the ERK inhibitor was administered. This was in opposition to ERK inhibitor sensitive cell lines, which only activated PI3K signaling after ERK inhibitor treatment. Collectively, those observations suggest that

activating PI3K signaling has the same effect in both cell line conditions, where in sensitive cell lines it prevents apoptosis in a portion of the cellular population and in resistant cell lines it prevents apoptosis in the entire cellular population.

In combination with RPPA, we would use MiB M/S (multiplex-inhibitor beads), as this would tell us about the changes in kinase activity. I have already generated data demonstrating that loss of K-Ras leads to marked changes in total tyrosine, threonine, and serine phosphorylation levels (Fig. 3.1A-C). Based on our initial observations, it is likely that RPPA and MiB M/S analysis will reveal promising hits. These observations would then be validated in our cell lines. To delve deeper into the heterogeneous nature of tumor cell lines, we would use capillary electrophoresis to separate and quantify nonphosphorylated and phosphorylated proteins in single cells (Proctor et al., 2014). Additionally, we would perform RNAseq on each subpopulation as well as RNAseq on several single cells from each subpopulation in Ras depleted cells (Bose et al., 2015). We would also perform whole genome sequencing in the same manner as above. Together, these data would give us a vast understanding of the genomic landscape of Ras dependency.

While unraveling the genomic landscape associated with Ras dependency is important, the methodology behind the experimental design is equally as important. Molecular signaling is a dynamic process that brings together numerous protein networks that are constantly modulated. Generally, assessing changes in genomic landscapes are investigated at single time points. Experiments of this nature are really snapshots of molecular signaling. What is becoming ever more clear is that signaling networks have a propensity to rewire upon perturbations, in sometimes unexpected manners. Given that observation, we would investigate Ras depletion at various time points using all the methods mentioned above. This would give us a partial understanding of the dynamics that characterize Ras dependency.

Next, we would expand our anaylsis' to include dependency on other known oncogenes in Ras related pathways, such as Myc, B-Raf, and PI3K. After compiling all the data, we would

be in a position to address questions of similarities and distinctions between various oncogene addictions and the complexities that drive them. As the data are generated we will need to use bioinformatics and computational analysis to build/design a platform to organize the data in a meaningful way. From there we would take a systems biology approach to design software, through a collaboration, that could predict vulnerabilities in oncogene addiction. After a prediction has been made, we would validate the observation in tumor cell lines. Our system would then be expanded to include additional oncogenes and tumor suppressors in pathways unrelated to mutant *RAS* function.

To support our *in vitro* efforts, we would develop a confetti mouse model, which marks stem cells in the pancreas (Snippert et al., 2010). Then we would cross this mouse to the KPC mouse model (Hingorani et al., 2005). Once tumors have formed, I would deliver siRNA, targeting mutant *KRAS* (Pecot et al., 2014; Yuan et al., 2014). Then we would collect tumor tissue from the animals using surgical techniques at various time points, where only a portion of the tumor was collected, while the rest remained unaltered. That tissue would be subjected to the same genomic analysis mentioned above (RPPA, RNAseq, DNAseq, etc). After demonstrating success in this initial model, we would cross other mutant *RAS* GEMM mouse models to our confetti mouse. From there we would create another database chronicling the dynamic changes associated with mutant *RAS* oncogene addiction *in vivo*.

Our major goal with these studies would be to identify commonalities in oncogene addiction between tumor cell lines and mouse models. We would hypothesize that these commonalities might represent novel vulnerabilities, which might result in new therapies for mutant *RAS* cancers. This is a key point as mutant *RAS*, currently, is not targetable. Therefore, it is imperative that we find other potential targets. Determining the underlying mechanisms of oncogene addiction will help to identify these potential targets.

3.2 ERK inhibitors in mutant Ras cancer

It was not until recently that ERK inhibitors started to gain traction as a potential alternative to either Raf or MEK inhibition (Nissan et al., 2013). Numerous studies have identified reactivation of ERK as a common mechanism of resistance to Raf and MEK inhibition suggesting that direct targeting of ERK could be a superior approach (Hatzivassiliou et al., 2010; Johannessen et al., 2010; Poulikakos et al., 2010). Furthermore, several other ERK inhibitors, in addition to SCH772984, have been rigorously tested in pre-clinical models and show efficacy, with some making it to the clinic (Infante et al, 2015, J Clin Oncol 33; abstract 2506, Hatzivassiliou et al., 2012; Herrero et al., 2015; Morris et al., 2013).

Future Studies

Currently, there are a number of ERK inhibitors under development. Our first investigations would involve characterizing/comparing the different ERK inhibitors and determining the mechanisms of action of each both *in vitro* and *in vivo*. In Chapter II, we investigated the mechanism of action and signaling changes associate with BVD-523, as it is already in the clinic for AML (Acute Myelogenous Luekemia and Myelodysplastic Syndromes (clinicaltrials.gov), and will likely be moving to the clinic for pancreatic cancer. Interestingly, we found that SCH772984 and BVD-523 have a similar profile of sensitivity in mutant *KRAS* cell lines, meaning that cell lines that are sensitive to SCH772984 are also sensitive to BVD-0523. Furthermore, the SCH772984 resistant cell lines are also resistant to BVD-0523. To date, the most significant difference between SCH772984 and BVD-523 seems to be potency, where SCH772984 sensitive cell lines have a significantly lower GI_{50}. Though there is a difference in potency, the is resulting phenotypes associated with each inhibitor seem to comparable in short-term studies. These observations are consistent with the manner in which the inhibitor works. SCH772984 is both an allosteric and ATP-competitive inhibitor, while BVD-523 is an ATP-competitive inhibitor. Moving forward, a proteomics approach will be employed to help distinguish between BVD-523 sensitive and resistance cell lines, as this inhibitor is moving into in clinical

trials. Furthermore, it would be important to know whether BVD-523 has a bi-modal action similar to that of SCH772984. Finally, BVD-523 long-term treatment phenotypes will need to be evaluated.

Importantly, our *in vivo* studies were performed in the absence of gemcitabine, the current standard of care for PDAC. It would be necessary to perform a combination treatment with ERK inhibitor plus gemcitabine, though our *in vitro* data suggest that ERK inhibition might not synergize with gemcitabine treatment. This experiment is important to conduct because it is unlikely that ERK inhibitor would be given to patients as a stand alone drug. Furthermore, there are two other cytotoxic regimens that have demonstrated promise for the treatment of PDAC, nab-paclitaxel and FOLFORINOX. Future experiments might include combining ERK inhibition with either of these two treatment options. Though toxicities will likely be a hurdle to their success and implementation.

Another difficulty associated with PDAC treatment regimens involves delivery. Even if there was a miracle drug for PDAC, there would still be the obstacle of getting the drug to the desired tissue. PDAC is characterized by a dense stroma, which reduces the likelihood of any treatment reaching the pancreas. Given this observation, it is likely that ERK inhibitors will run into the same difficulties. Currently, there are a number of methods under evaluation to solve this problem (Yu et al., 2010). Carbon nanotubes and nanoparticles are two promising directions for addressing the delivery issue; therefore, I would collaborate with a chemistry lab with expertise in nano-style delivery to optimize the conditions necessary for transport of ERK inhibitor. This serves an additional purpose in that not all tissue and cells would be exposed to ERK inhibition, as would be the case if ERK was administered directly. This is an significant point, as the ERK inhibitors block wild-type proteins and numerous cell types use ERK signaling to mediate growth. Using a nano-style delivery system might reduce ERK inhibitor toxicities.

Another interesting direction would be to assess the efficacy of ERK inhibition in other mutant *RAS* cancers. Our lab already has promising preliminary data in mutant *KRAS* lung cancer

and mutant *NRAS* melanoma (data not shown). There are a number of mutant *RAS* cancers to chose from, we would likely start with lung and colon cancer as they are among the top causes of cancer related deaths in the United States and they possess a high frequency of KRAS mutations. We would investigate the same ERK inhibitor phenotypes as we observed in PDAC. Then we would expand our studies to include mutant *HRAS* and *NRAS* cancers.

A key observation from our studies was the bi-modal action of ERK inhibition. When performing inhibitor studies, many within the field stick to short time points to determine sensitivity and target inhibition, favoring investigations at 24 h and/or earlier. However, in patients, drugs are never prescribed for that length of time. In our studies, we found distinct mechanisms of action between short- and long-term treatments. It is unlikely this observation is specific to ERK inhibition, however studies with other inhibitors have not included long-term treatment. Generally, the only long-term studies performed with inhibitors tend to involve the unraveling of potential resistance mechanisms. This is unlike our studies, where we observe distinct mechanisms of action after short- and long-term ERK inhibitor treatment. Based on our observations, future inhibitor studies should be expanded to include longer treatment regiments. Our studies also raise a key question as to which phenotype is most relevant for the treatment of a potential patient: apoptosis (short-term) or cell cycle arrest/senescence (long-term) in a tumor cell line model? Our *in vivo* observations suggest that the later phenotype (long-term treatment) is more relevant. While we were unable to observe senescence *in vivo*, there was a pronounced cell cycle defect that was marked by reductions in pRB and cyclin B1 and D1. Consistent with our *in vitro* studies, we did not observe any changes in apoptosis (short-term phenotype) after extended treatment.

Interestingly, we noticed that treatment with SCH772984 (short and long-term) in mutant *KRAS* tumor cell lines resulted in widespread protein ubiquitination. To our knowledge, this is the first reported instance where MAPK inhibition has been linked to widespread protein ubiquitination. While, I was able to identify and link the degradation of Myc to senescence associated beta-galactosidase staining, there were still a number of proteins that were

independently degraded. It would be interesting to unravel the mechanisms that govern the stability of ERK substrates. In order to determine the identity of those proteins, we would use Mass Spectrometry (MS) analysis.

In parallel we would deplete mutant *KRAS* from tumor cell lines to look for a similar degradation pattern. We would then extend these analyses to include genetic and pharmacological inhibition of other components of the MAPK pathway (Raf and MEK), as well as components from other pathways such as PI3K or RalA/B. This would add a level of specificity in terms of effectors modulating this phenotype. If widespread ubiquitination seems to rely heavily on the Raf-MEK-ERK MAPK signaling cascade, it would be interesting to investigate the other MAPK (p38 and JNK) signaling cascades. Once proteins have been identified and validated, we would investigate degradation mechanisms in proteins where none have been previously determined.

In support of a degradation phenotype, our lab has preliminary data showing that SCH772984 treatment results in degradation of Ets-1 and Ets-2 (also discussed in Chapter II). We have data showing that Ets-1 is directly ubiquitinated after treatment (Fig 3.2A-B). However, the mechanism, which allows for Ets protein degradation has not been determined. We would start investigations with a combination of tandem mass spectrometry (MS/MS) and scan site to identify possible phosphorylation sites and protein binding motifs. From there we would make mutants and use the Global Protein Stability (GPS) and Quantitative Ubiquitylation Interrogation (QUAINT) platforms assess the stability of our Ets-1 mutants (Emanuele et al., 2011; Kim et al., 2011). A similar methodology would be employed with other identified proteins.

Finally, we would investigate why subsets of proteins are degraded after inhibition of Ras signaling. We would start investigations with whether mutant *HRAS*, *KRAS*, and *NRAS* yield a similar degradation pattern with different perturbations, both figenetic and pharmacologic. Perhaps specific patterns of protein degradation could be linked to the numerous cancer

phenotypes associated with Ras dependency. This could reveal novel unknown dependencies necessary for Ras proteins.

3.3 Ras effectors and ERK inhibition

Ras is thought to regulate at least 11-catalytically distinct effectors. Of those 11 effectors, 4 of them have been directly linked to mutant *RAS* oncogensis (Raf, PI3K, Tiam1, and RalGEF). All four of these effector signaling cascades have targetable kinases, some of which already have potent inhibitors specifically targeting them. Since mutant *RAS* has been shown to signal through multiple effectors, it is likely that collectively blocking effectors will yield more promising results. In Chapter II, we performed a drug sensitivity screen (DSS) where we combined over 500 inhibitors with the SCH772984 ERK inhibitor in two sensitive cell lines. Interestingly, we identified a number of combinations, including multiple Ras effector targeting strategies.

Future Studies

While, we have already addressed the significance of combination treatments with PI3K inhibition and ERK inhibition, we have only preliminarily investigated combination treatments with the other lesser studied Ras effectors. Tiam1 and RalGEF are the lesser studied effectors because they are not mutated in cancers, though they have both been shown to be critical for mutant *RAS* oncogenesis. Though, Tiam1 and RalGEF are not themselves targetable, there are targetable kinases in their downstream cascades. Downstream of Tiam1 are the PAK kinases and downstream of RalGEF is TBK1, both which are important for PDAC oncogenesis (data not shown). The DSS screen we performed did not contain inhibitors targeting either Tiam1 or RalGEF, therefore, I would propose to gather validated TBK1/PLD and PAK/JNK inhibitors to assess the significance of RalGEF and Tiam1 inhibition in combination with ERK inhibition *in vitro*. If these experiments yielded promising hits, we would move to an *in vivo* model of PDAC. Finally, we would expand these observations to other mutant *RAS* cancers.

3.4 ERK inhibitors in Myc amplified cancers

Alterations in Myc are found in nearly 20% of cancers, which makes Myc the second most commonly altered oncogene behind Ras (Nilsson and Cleveland, 2003). Like mutant *RAS* oncogenes, Myc oncogenes are also considered to be undruggable. Direct targeting of transcription factors is not a viable option, currently; therefore, indirect targeting remains the best method. While we have yet to determine changes in Myc targeted gene expression in relation to Myc protein stability in our cell lines, we do know from our data and others that Myc half-life is significantly enhanced in mutant *KRAS* cells compared to what has been reported for normal cells (Sears et al., 2000). In tumor cells, Myc is known to accumulate in promoter regions of active genes and causes transcriptional amplification (Lin et al., 2015). We also know that ERK is a well-established modulator of Myc stability (Farrell and Sears, 2014), data from our lab shows that depletion of ERK with siRNA leads to reduction of total Myc protein levels and a growth defect (Figure 3.3A-B). Furthermore, in Chapter II we observed that ERK inhibition leads to reduction of total Myc protein level, both endogenous and exogenous. Therefore, I would hypothesize that Myc amplification driven cancers might be sensitive to ERK inhibition.

Future Studies

To test this hypothesis, I would focus on cancers with Myc amplifications. Based on publicly data available from cbioportal (www.cbioportal.org), there are several cancers that exhibit amplified Myc. Ovarian cancer is characterized by ~43% alteration frequency, which is twice as frequent as the next Myc amplified cancer in the sample set used (Figure 3.4). I would employ similar assays as those mentioned in Chapter II to determine a sensitivity profile to ERK inhibition. From there, we would delve into the mechanism and determination of Myc protein stability/half-life. Should ERK inhibition prove to beneficial for ovarian cancer, we would expand our studies to include other cancers and move into Myc amplification driven mouse models, of which there are several (Morton and Sansom, 2013).

3.5 Resistance mechanisms for ERK inhibition in mutant *RAS* cancer

Targeted therapy and resistance mechanisms, in today's climate, go hand-in-hand, as there are few curative drugs on the market. Consequently, understanding and predicting rewiring of signaling networks has become a large focus of pre-clinical and clinical inhibitor evaluations. There are two types of resistance, innate and acquired. Both instances have been intensively studied in recent years. In our studies, we have attempted to identify and understand both innate and acquired resistance mechanisms to ERK inhibition.

3.5.1 Acquired Resistance Mechanisms

Since we observed a cytostatic response to inhibition with SCH772984 induction of senescence, we sought to identify combinations that would turn our cytostatic effect to a cytotoxic effect. We observed a number of combinations that made SCH772984 toxic, as measured by a reduction in growth. A significant number of hits from our SCH772984 drug sensitivity screen were members of the PI3K-AKT-mTOR signaling cascade. We found that co-treatment with PI3K (AZD8186) and SCH772984 resulted in enhanced apoptosis. Additionally, we found co-treatment with an AKT (AZD5363) inhibitor and SCH772984 synergized (Fig 3.5). This observation is not as surprising considering there have been a number of studies involving MEK inhibition in combination with PI3K or mTOR inhibition (Engelman et al., 2008; Faber et al., 2009; Liu and Xing, 2008; Sos et al., 2009; Yu et al., 2008). Furthermore, there is data suggesting that PI3K can mediate resistance to MEK inhibitors in mutant *KRAS* cancers (Wee et al., 2009). There are/have been a number of clinical trials featuring MEK and PI3K combination treatments, which have demonstrated efficacy, at the expense of greater toxicity than inhibition of either pathway alone (Shimizu et al., 2012). It is likely that co-treatment with an ERK inhibitor plus a PI3K inhibitor in patients will have similar toxicity issues.

Future Studies

Outside of PI3K-AKT-mTOR signaling toxicities, we identified a number of interesting combination treatments with SCH772984. For example, we observed a novel synergy with chloroquine. This observation was reproducible in a number of cell lines suggesting it could be a widespread vulnerability. This is an interesting finding, as it has been well established by Kimmelman and colleagues that PDAC, a mutant *KRAS* cancer, is dependent on autophagy for tumor growth (Yang et al., 2011). Furthermore, there are a number of other mutant *RAS* cancers that are at least partially dependent on autophagy, which enhances its attractiveness as a target. The next direction for these studies would be to use a mouse model (KPC, orthotopic xenograft, etc) to determine the efficacy of co-treatment with chloroquine and SCH772984. Should the study yield promising results, the combination would be taken to clinical trials for patients with mutant *KRAS* cancers. Another direction would be to determine whether either mutant *HRAS* or *NRAS* are dependent on autophagy, as this combination could be expanded for the treatment of other mutant *RAS* cancers.

Long-term inhibitor treatment is a common method for identifying acquired resistance mechanisms. Surprisingly, we were unable to identify resistant clones to SCH772984 treatment in sensitive cell lines after months of treatment. We observed that long-term treatment resulted in a senescence-like phenotype, marked by beta-galactosidase staining, loss of pRB levels and increased p16 levels. However, the beta-galactosidase stained cells did not represent the entire population of treated cells. When we removed the inhibitor after long-term treatment, we observed a outgrowth of cells; however, this outgrowth grew slower than the vehicle control population. Additionally, a significant portion of the population remained senescent as marked by beta-galactosidase staining, loss of pRB levels and increased p16 levels. Based on our data it seems that long-term ERK inhibition with SCH772984 induces either senescence or quiescence. Unfortunately, there are not decisive markers to discern quiescence, which make it difficult to isolate that population. However, I would hypothesize that the quiescent cell population is the

outgrowth population seen after removal of SCH772984. Moving forward, it would interesting to develop a live cell senescence maker that could be used to distinguish between senescent and quiescent cell populations.

Though we did not observe significant outgrowth after prolonged treatment in sensitive cell lines, this does not mean that SCH772984 will be immune to acquired mechanisms of resistance. If anything, recent history has shown us that perturbing signaling networks, especially with small molecule inhibitors, invariably results in kinome reprogramming. To address this concern, we turned to Wood and colleagues, as they have developed a platform that allows for the identification of acquired resistance mechanisms (Martz et al., 2014; Winter et al., 2014).

In Chapter II, we identified several acquired mechanisms of resistance for both SCH772984 and BVD-0523. Using both inhibitors, we have implicated PI3K, Notch, p38, and Hippo signaling pathways as potential acquired mechanisms of resistance in our studies. While this platform is somewhat artificial, there is evidence (direct and indirect) that ERK interacts with the implicated pathways (Bose et al., 2015; Izrailit et al., 2013; Lin et al., 2015; Mendoza et al., 2011). However, p38, PI3K, Notch, and Hippo signaling have already been implicated with Raf and MEK as mechanisms of resistance (Lin et al., 2015; Martz et al., 2014; Rudalska et al., 2014; Wee et al., 2009). Of these pathways, Notch, PI3K, and p38 are targetable with small molecule inhibitors. We have previously shown that PI3K and AKT combinations with SCH772984 have displayed synergy. Consistent with previous observations, we also find that co-treatment with SCH772984 and SB203580 (tool p38 compound) synergizes in KRAS mutant cell lines (Fig 3.6). Future studies would entail determining the mechanism by which PI3K, Notch, p38, and Hippo signaling determines ERK inhibitor resistance.

3.5.2 De Novo Resistance Mechanisms

We observed that a portion of mutant *KRAS* cell lines were innately resistant to SCH772984 and BVD-523. Therefore, we performed a siRNA kinome library screen to identify targeted mechanisms of innate resistance. From our screen we found a number of novel kinases

that have not been linked to MAPK inhibitor resistance. Additionally, we identified several kinases that are known mechanisms of resistance to Raf and MEK inhibition, which provide some validation that our screen yielded real hits. Next, we plan to determine how our identified hits modulate SCH772984 sensitivity.

Future Studies

In Chapter II, we identified PRKCH (protein kinase eta) as a potential modulator of ERK inhibitor sensitivity. This hit is interesting as it was also validated in a separate screen using the Raf inhibitor, vemurafinib. Collectively, the data suggests that PRKCH might be acting as modulator of Raf-MEK-ERK signaling pathway. Future studies would entail designing a specific drug for a novel interacting kinase, like PRKCH, and then testing a combination treatment *in vivo* with ERK-inhibitor resistant cell lines.

3.6 Inhibitor Dosing

Regimented inhibitor dosing is an important feature of patient treatment. How often, what time of day, and how many days in a row should a drug be taken? These are all extremely important questions that, as molecular biologists, many us fail to incorporate into our studies. More importantly, how should we design regimens when combining inhibitors? In this section I will discuss use of circadian rhythm and dosing schedules to as tools to yield optimal inhibitor regimens. Circadian clock (rhythm) research is gaining traction in small molecule inhibitor studies seeing as most organisms from single cells to humans follow some sort of circadian rhythm. Most cellular processes are somehow connected to a circadian rhythm, from cell cycle progression to changes in gene expression. Signal transduction is no exception as there are numerous studies highlighting this observation (Zhang et al., 2014). This becomes important when considering dosing strategies for small molecule inhibitors. We want to treat patients at the best time to get an optimal outcome.

Future Studies

ERK kinase activity has known circadian oscillation patterns, where ERK activity peaks during the middle of the light cycle (Eckel-Mahan et al., 2008; Fu and Lee, 2003). Using this observation, we would design future studies to determine when ERK is most active in mutant *RAS* tumors using an *in vivo* system. Given the previous result, we would design a regimen that best blocks ERK signaling at its activity climax using an *in vivo* system. Should this method yield significant improvements in tumor reduction, we would move to human patients to determine to determine ERK activity climaxes. While determining climaxes in ERK kinase output would be difficult in solid tumors, hematopoietic cancers (Leukemias, etc), driven by amplified MYC, would be an ideal system as attaining multiple patient samples would be feasible.

Furthermore, other Ras effectors are likely to have circadian rhythms which may or may not differ from ERK. Identifying circadian rhythms of these effectors and designing regimens to take advantage of the point at which activity is highest would be an important future direction. Given sufficient supporting data, we could also set up regimens where we treat with one inhibitor for a selected time and then treated with another inhibitor for a selected time (alternate dosing). This might allow for combination treatments (ie PI3Ki and MEKi) that otherwise would be too toxic if given at the same time for extended periods. Finally, regimen design is not only relevant for ERK inhibitor studies, but can be expanded to any targeted molecule in any cancer.

3.7 Concluding Remarks

While targeted small molecule inhibitors have expanded our understanding of many signaling cascades and how they are intertwined, there are still many limitations to their effectiveness as therapeutic treatments. Very few targeted inhibitors actually target an altered protein (ie a mutated kinase), most of them target a wild-type protein. Targeting an unaltered protein is very similar to using a chemotherapy reagent in sense that the inhibitor is blocking its given target in a number of tissues, which could result in toxicities and reduced potency for the

target tissue. Though targeting specific alterations has proven successful, there are still limitations, namely induction of resistance mechanisms that limit inhibitor efficacy. Resistance mechanisms also occur when using inhibitors that block wild-type proteins limiting their therapeutic value. Furthermore, both types of inhibitors rarely become successful clinical standards. So many inhibitors enter the clinic and fail to improve patient outcome, which most attribute to poor preclinical investigation. I tend to agree with this point of view, we need to implement more standardized and rigorous preclinical experimentation and evaluation before proceeding to the clinic with small molecule inhibitors.

Figure 3.1.

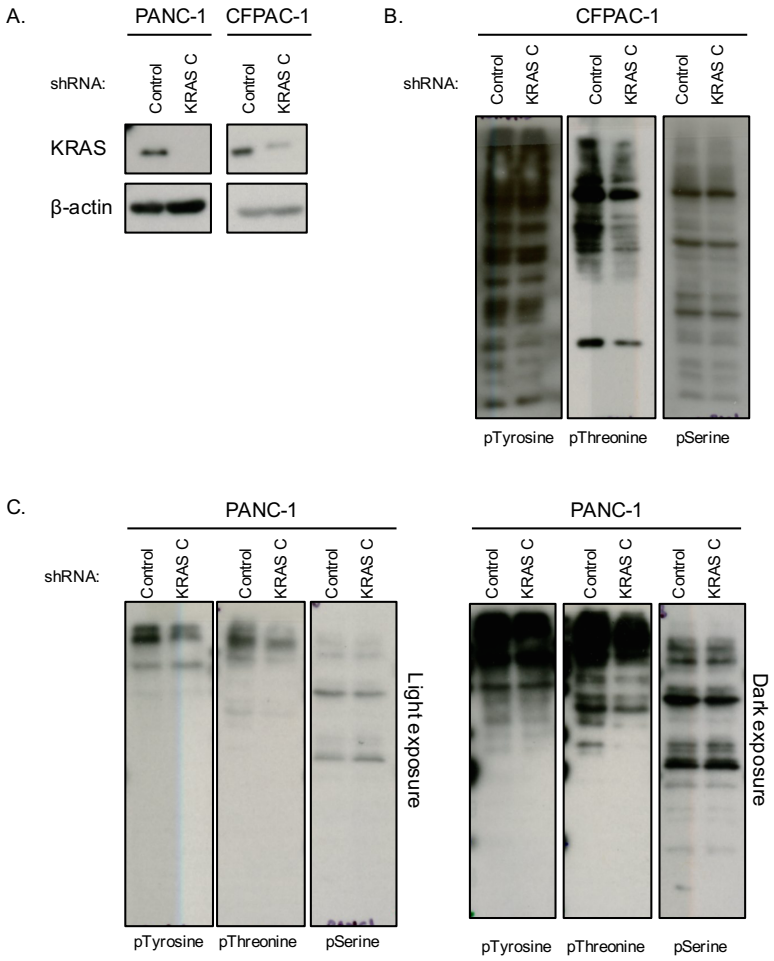

Figure 3.1. KRAS stable knockdown leads to changes in phospho-tyrosine, threonine, and serine. (A) Western blot analysis following shRNA-mediated *KRAS* knockdown showing the effects on K-Ras protein expression in PANC-1 and CFPAC-1. (B and C) Cells were treated as in (A). Western blot analysis of phospho-tyrosine, threonine, and serine in CFPAC-1 (B) and PANC-1 (C) cell lines.

Figure 3.2.

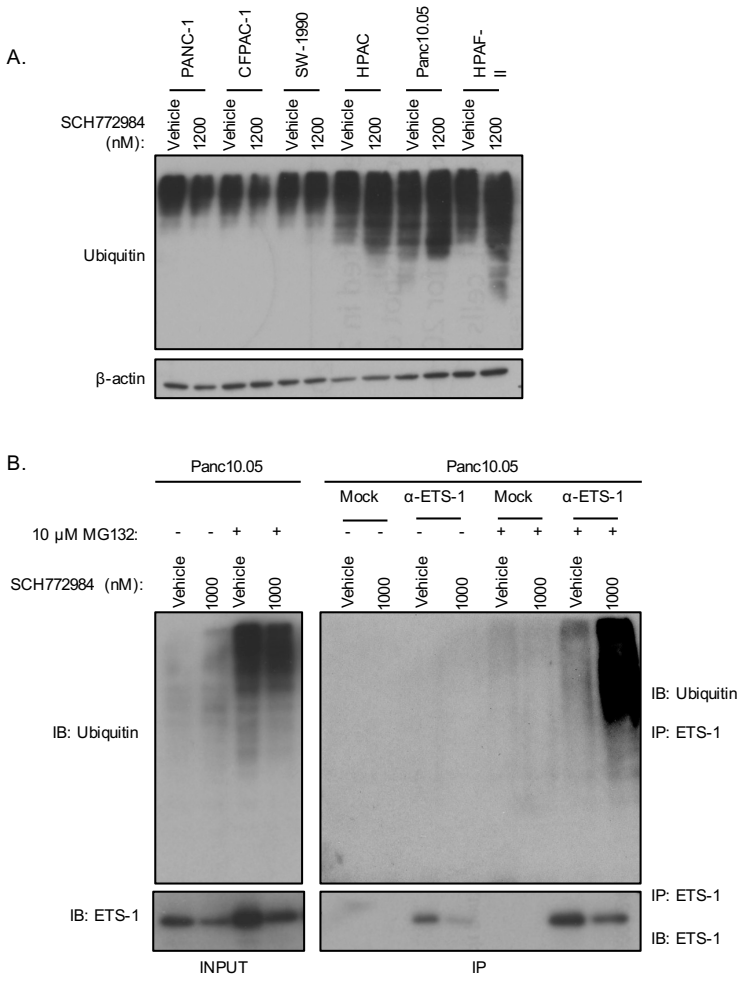

Figure 3.2. ERK-inhibitor treatment in PDAC cell lines causes widespread ubiquitination. (A) Sensitive and resistant cell lines maintained on plastic were treated with vehicle or the indicated concentration of SCH772984 for 72 h, and then blotted for ubiquitin or β-actin to verify equivalent loading of total cellular protein (B) Panc10.05 cells maintained on plastic were treated with either vehicle (-) or 1000 nM SCH772984 (+) for 72 h, and then together with either vehicle (-) or 10 μM MG132 (+) for an additional 8 hr. Whole cell lysates (WCL) were then subjected to control normal serum (mock) or to anti-Ets-1 immunoprecipitation (IP), resolved by SDS-PAGE and then blotted for ubiquitin and Ets-1.

Figure 3.3

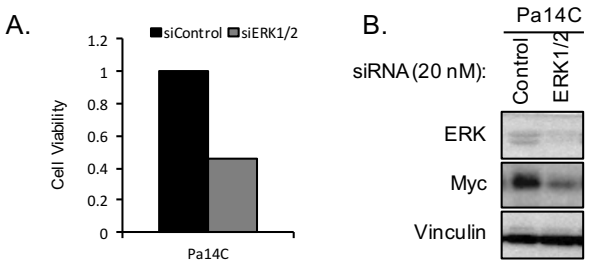

Figure 3.3. ERK siRNA silencing in Pa14C cell line. (A) Pa14C anchorage-dependent growth is reduced following siRNA-mediated *ERK1/2*. Anchorage-dependent growth was measured by MTT 4 days post-selection. (B) Myc protein is reduced with ERK1/2 suppression. Western blot analysis following siRNA-mediated *ERK1/2* knockdown for total ERK, Myc and vinculin to verify equivalent total cellular protein.

Figure 3.4

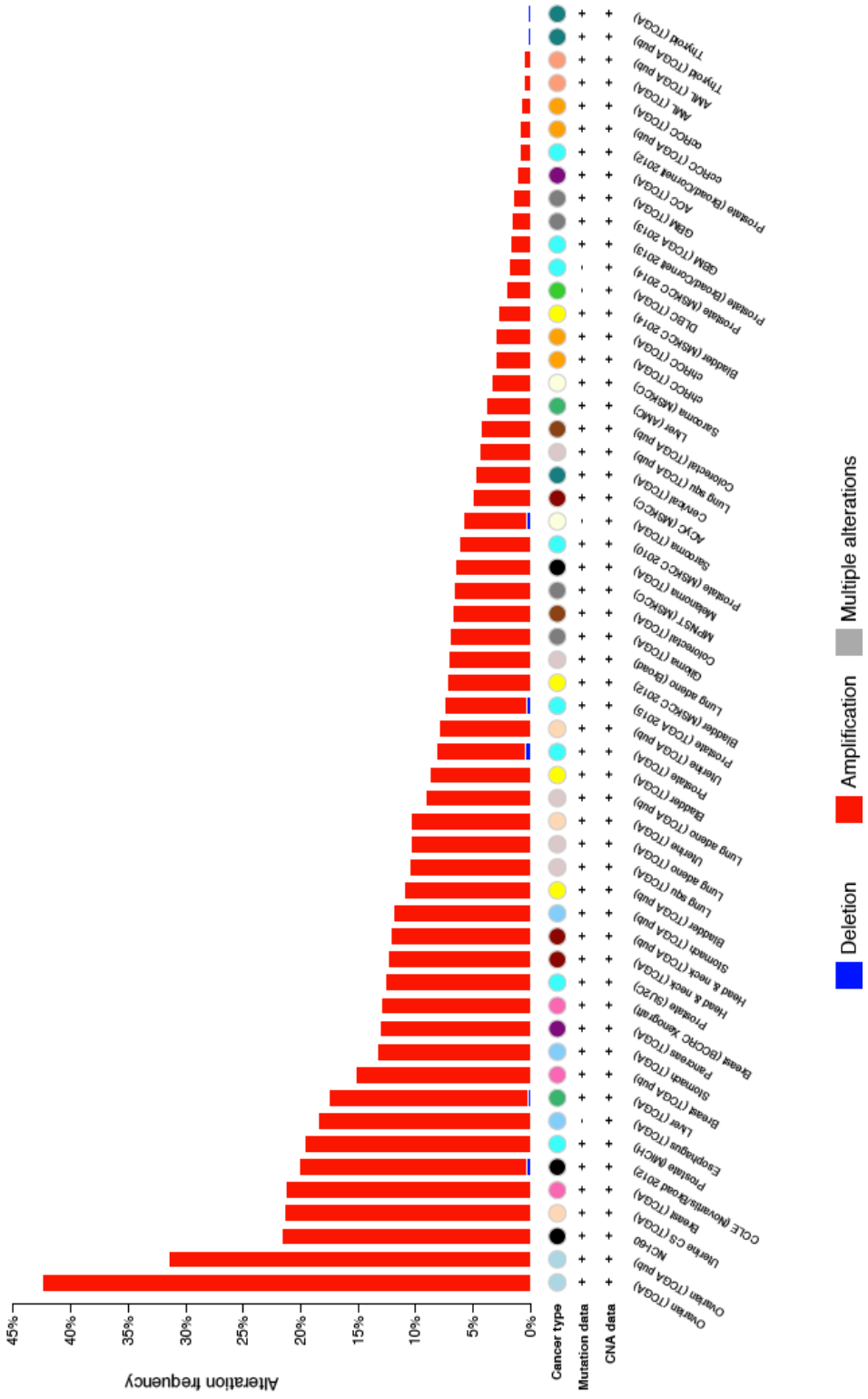

Figure 3.4. MYC amplification in cancer. MYC amplification data compiled from www.cbioportal.org.

Figure 3.5.

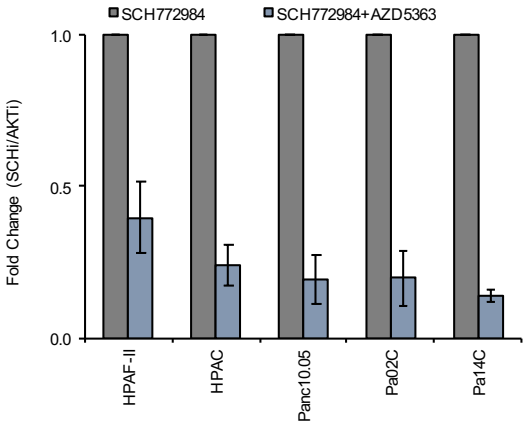

Figure 3.5. SCH772984 combination treatment with AZD5363 (AKT inhibitor). Combination treatment with SCH772984 and AZD5363 (AKTi) reduces GI_{50} in SCH772984 sensitive but not resistant cell lines. *KRAS*-mutant PDX cell lines grown on plastic were maintained in growth medium supplemented with vehicle (DMSO), SCH772984, or SCH772984 + .5 μM AZD5363 (AKTi) at concentrations ranging from 7.8 nM to 4 μM. Proliferation was monitored by MTT viability assay to assess growth inhibition after 72 h treatment. GI_{50} values were determined using CompuSyn.

Figure 3.6.

A.

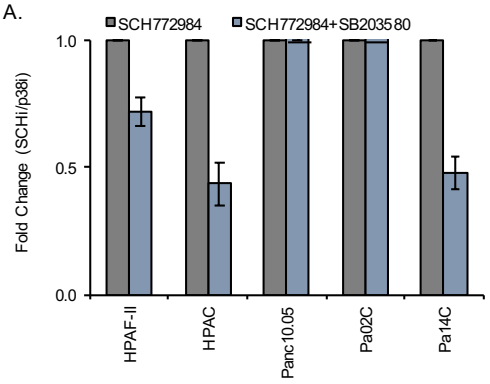

B.

Cell Line	p38-related alteration
HPAF-II	Over-expression of MAP3K13
HPAC	Over-expression of MAP3K8 (COT)
Panc10.05	None
Pa02C	Over-expression of MAPK13
Pa14C	Mutations in MAP2K6, MAP4K2, MAP4K4

Figure 3.6. SCH772984 combination treatment with SB203580 (p38 inhibitor). (A) Combination treatment with SCH772984 and SB203580 (p38i) reduces GI_{50} in SCH772984 sensitive but not resistant cell lines. *KRAS*-mutant PDX cell lines grown on plastic were maintained in growth medium supplemented with vehicle (DMSO), SCH772984, or SCH772984 + 1 μM SB203580 (p38i) at concentrations ranging from 7.8 nM to 4 μM. Proliferation was monitored by MTT viability assay to assess growth inhibition after 72 h treatment. GI_{50} values were determined using CompuSyn. (B) p38-related pathway alterations.

REFERENCES

Bose, S., Wan, Z., Carr, A., Rizvi, A.H., Vieira, G., Pe'er, D., and Sims, P.A. (2015). Scalable microfluidics for single-cell RNA printing and sequencing. Genome Biol *16*, 120.

Bryant, K.L., Mancias, J.D., Kimmelman, A.C., and Der, C.J. (2014). KRAS: feeding pancreatic cancer proliferation. Trends Biochem Sci *39*, 91-100.

Chin, L., Tam, A., Pomerantz, J., Wong, M., Holash, J., Bardeesy, N., Shen, Q., O'Hagan, R., Pantginis, J., Zhou, H., et al. (1999). Essential role for oncogenic Ras in tumour maintenance. Nature *400*, 468-472.

Commisso, C., Davidson, S.M., Soydaner-Azeloglu, R.G., Parker, S.J., Kamphorst, J.J., Hackett, S., Grabocka, E., Nofal, M., Drebin, J.A., Thompson, C.B., et al. (2013). Macropinocytosis of protein is an amino acid supply route in Ras-transformed cells. Nature *497*, 633-637.

Eckel-Mahan, K.L., Phan, T., Han, S., Wang, H., Chan, G.C., Scheiner, Z.S., and Storm, D.R. (2008). Circadian oscillation of hippocampal MAPK activity and cAmp: implications for memory persistence. Nat Neurosci *11*, 1074-1082.

Emanuele, M.J., Elia, A.E., Xu, Q., Thoma, C.R., Izhar, L., Leng, Y., Guo, A., Chen, Y.N., Rush, J., Hsu, P.W., et al. (2011). Global identification of modular cullin-RING ligase substrates. Cell *147*, 459-474.

Engelman, J.A., Chen, L., Tan, X., Crosby, K., Guimaraes, A.R., Upadhyay, R., Maira, M., McNamara, K., Perera, S.A., Song, Y., et al. (2008). Effective use of PI3K and MEK inhibitors to treat mutant Kras G12D and PIK3CA H1047R murine lung cancers. Nat Med *14*, 1351-1356.

Faber, A.C., Li, D., Song, Y., Liang, M.C., Yeap, B.Y., Bronson, R.T., Lifshits, E., Chen, Z., Maira, S.M., Garcia-Echeverria, C., et al. (2009). Differential induction of apoptosis in HER2 and EGFR addicted cancers following PI3K inhibition. Proc Natl Acad Sci U S A *106*, 19503-19508.

Farrell, A.S., and Sears, R.C. (2014). MYC Degradation. Cold Spring Harb Perspect Med *4*.

Fu, L., and Lee, C.C. (2003). The circadian clock: pacemaker and tumour suppressor. Nat Rev Cancer *3*, 350-361.

Fujita-Sato, S., Galeas, J., Truitt, M., Pitt, C., Urisman, A., Bandyopadhyay, S., Ruggero, D., and McCormick, F. (2015). Enhanced MET Translation and Signaling Sustains K-Ras-

Driven Proliferation under Anchorage-Independent Growth Conditions. Cancer Res *75*, 2851-2862.

Halilovic, E., She, Q.B., Ye, Q., Pagliarini, R., Sellers, W.R., Solit, D.B., and Rosen, N. (2010). PIK3CA mutation uncouples tumor growth and cyclin D1 regulation from MEK/ERK and mutant KRAS signaling. Cancer Res *70*, 6804-6814.

Hatzivassiliou, G., Liu, B., O'Brien, C., Spoerke, J.M., Hoeflich, K.P., Haverty, P.M., Soriano, R., Forrest, W.F., Heldens, S., Chen, H., et al. (2012). ERK inhibition overcomes acquired resistance to MEK inhibitors. Mol Cancer Ther *11*, 1143-1154.

Hatzivassiliou, G., Song, K., Yen, I., Brandhuber, B.J., Anderson, D.J., Alvarado, R., Ludlam, M.J., Stokoe, D., Gloor, S.L., Vigers, G., et al. (2010). RAF inhibitors prime wild-type RAF to activate the MAPK pathway and enhance growth. Nature *464*, 431-435.

Herrero, A., Pinto, A., Colon-Bolea, P., Casar, B., Jones, M., Agudo-Ibanez, L., Vidal, R., Tenbaum, S.P., Nuciforo, P., Valdizan, E.M., et al. (2015). Small Molecule Inhibition of ERK Dimerization Prevents Tumorigenesis by RAS-ERK Pathway Oncogenes. Cancer Cell *28*, 170-182.

Hingorani, S.R., Wang, L., Multani, A.S., Combs, C., Deramaudt, T.B., Hruban, R.H., Rustgi, A.K., Chang, S., and Tuveson, D.A. (2005). Trp53R172H and KrasG12D cooperate to promote chromosomal instability and widely metastatic pancreatic ductal adenocarcinoma in mice. Cancer Cell *7*, 469-483.

Izrailit, J., Berman, H.K., Datti, A., Wrana, J.L., and Reedijk, M. (2013). High throughput kinase inhibitor screens reveal TRB3 and MAPK-ERK/TGFbeta pathways as fundamental Notch regulators in breast cancer. Proc Natl Acad Sci U S A *110*, 1714-1719.

Johannessen, C.M., Boehm, J.S., Kim, S.Y., Thomas, S.R., Wardwell, L., Johnson, L.A., Emery, C.M., Stransky, N., Cogdill, A.P., Barretina, J., et al. (2010). COT drives resistance to RAF inhibition through MAP kinase pathway reactivation. Nature *468*, 968-972.

Johnson, L., Mercer, K., Greenbaum, D., Bronson, R.T., Crowley, D., Tuveson, D.A., and Jacks, T. (2001). Somatic activation of the K-ras oncogene causes early onset lung cancer in mice. Nature *410*, 1111-1116.

Kim, W., Bennett, E.J., Huttlin, E.L., Guo, A., Li, J., Possemato, A., Sowa, M.E., Rad, R., Rush, J., Comb, M.J., et al. (2011). Systematic and quantitative assessment of the ubiquitin-modified proteome. Mol Cell *44*, 325-340.

Lim, K.H., and Counter, C.M. (2005). Reduction in the requirement of oncogenic Ras signaling to activation of PI3K/AKT pathway during tumor maintenance. Cancer Cell *8*, 381-392.

Lin, L., Sabnis, A.J., Chan, E., Olivas, V., Cade, L., Pazarentzos, E., Asthana, S., Neel, D., Yan, J.J., Lu, X., et al. (2015). The Hippo effector YAP promotes resistance to RAF- and MEK-targeted cancer therapies. Nat Genet *47*, 250-256.

Liu, D., and Xing, M. (2008). Potent inhibition of thyroid cancer cells by the MEK inhibitor PD0325901 and its potentiation by suppression of the PI3K and NF-kappaB pathways. Thyroid *18*, 853-864.

Martz, C.A., Ottina, K.A., Singleton, K.R., Jasper, J.S., Wardell, S.E., Peraza-Penton, A., Anderson, G.R., Winter, P.S., Wang, T., Alley, H.M., et al. (2014). Systematic identification of signaling pathways with potential to confer anticancer drug resistance. Sci Signal *7*, ra121.

Mendoza, M.C., Er, E.E., and Blenis, J. (2011). The Ras-ERK and PI3K-mTOR pathways: cross-talk and compensation. Trends Biochem Sci *36*, 320-328.

Morris, E.J., Jha, S., Restaino, C.R., Dayananth, P., Zhu, H., Cooper, A., Carr, D., Deng, Y., Jin, W., Black, S., et al. (2013). Discovery of a novel ERK inhibitor with activity in models of acquired resistance to BRAF and MEK inhibitors. Cancer Discov *3*, 742-750.

Morton, J.P., and Sansom, O.J. (2013). MYC-y mice: from tumour initiation to therapeutic targeting of endogenous MYC. Mol Oncol *7*, 248-258.

Nilsson, J.A., and Cleveland, J.L. (2003). Myc pathways provoking cell suicide and cancer. Oncogene *22*, 9007-9021.

Nissan, M.H., Rosen, N., and Solit, D.B. (2013). ERK Pathway Inhibitors: How Low Should We Go? Cancer Discov *3*, 719-721.

Pecot, C.V., Wu, S.Y., Bellister, S., Filant, J., Rupaimoole, R., Hisamatsu, T., Bhattacharya, R., Maharaj, A., Azam, S., Rodriguez-Aguayo, C., et al. (2014). Therapeutic silencing of KRAS using systemically delivered siRNAs. Mol Cancer Ther *13*, 2876-2885.

Poulikakos, P.I., Zhang, C., Bollag, G., Shokat, K.M., and Rosen, N. (2010). RAF inhibitors transactivate RAF dimers and ERK signalling in cells with wild-type BRAF. Nature *464*, 427-430.

Proctor, A., Herrera-Loeza, S.G., Wang, Q., Lawrence, D.S., Yeh, J.J., and Allbritton, N.L. (2014). Measurement of protein kinase B activity in single primary human pancreatic cancer cells. Anal Chem *86*, 4573-4580.

Rudalska, R., Dauch, D., Longerich, T., McJunkin, K., Wuestefeld, T., Kang, T.W., Hohmeyer, A., Pesic, M., Leibold, J., von Thun, A., et al. (2014). In vivo RNAi screening identifies a mechanism of sorafenib resistance in liver cancer. Nat Med *20*, 1138-1146.

Sears, R., Nuckolls, F., Haura, E., Taya, Y., Tamai, K., and Nevins, J.R. (2000). Multiple Ras-dependent phosphorylation pathways regulate Myc protein stability. Genes Dev *14*, 2501-2514.

Shimizu, T., Tolcher, A.W., Papadopoulos, K.P., Beeram, M., Rasco, D.W., Smith, L.S., Gunn, S., Smetzer, L., Mays, T.A., Kaiser, B., et al. (2012). The clinical effect of the dual-targeting strategy involving PI3K/AKT/mTOR and RAS/MEK/ERK pathways in patients with advanced cancer. Clin Cancer Res *18*, 2316-2325.

Singh, A., Greninger, P., Rhodes, D., Koopman, L., Violette, S., Bardeesy, N., and Settleman, J. (2009). A gene expression signature associated with "K-Ras addiction" reveals regulators of EMT and tumor cell survival. Cancer Cell *15*, 489-500.

Snippert, H.J., van der Flier, L.G., Sato, T., van Es, J.H., van den Born, M., Kroon-Veenboer, C., Barker, N., Klein, A.M., van Rheenen, J., Simons, B.D., et al. (2010). Intestinal crypt homeostasis results from neutral competition between symmetrically dividing Lgr5 stem cells. Cell *143*, 134-144.

Sos, M.L., Fischer, S., Ullrich, R., Peifer, M., Heuckmann, J.M., Koker, M., Heynck, S., Stuckrath, I., Weiss, J., Fischer, F., et al. (2009). Identifying genotype-dependent efficacy of single and combined PI3K- and MAPK-pathway inhibition in cancer. Proc Natl Acad Sci U S A *106*, 18351-18356.

Wee, S., Jagani, Z., Xiang, K.X., Loo, A., Dorsch, M., Yao, Y.M., Sellers, W.R., Lengauer, C., and Stegmeier, F. (2009). PI3K pathway activation mediates resistance to MEK inhibitors in KRAS mutant cancers. Cancer research *69*, 4286-4293.

Winter, P.S., Sarosiek, K.A., Lin, K.H., Meggendorfer, M., Schnittger, S., Letai, A., and Wood, K.C. (2014). RAS signaling promotes resistance to JAK inhibitors by suppressing BAD-mediated apoptosis. Sci Signal *7*, ra122.

Yang, S., Wang, X., Contino, G., Liesa, M., Sahin, E., Ying, H., Bause, A., Li, Y., Stommel, J.M., Dell'antonio, G., et al. (2011). Pancreatic cancers require autophagy for tumor growth. Genes & development *25*, 717-729.

Yu, K., Toral-Barza, L., Shi, C., Zhang, W.G., and Zask, A. (2008). Response and determinants of cancer cell susceptibility to PI3K inhibitors: combined targeting of PI3K and Mek1 as an effective anticancer strategy. Cancer Biol Ther *7*, 307-315.

Yuan, T.L., Fellmann, C., Lee, C.S., Ritchie, C.D., Thapar, V., Lee, L.C., Hsu, D.J., Grace, D., Carver, J.O., Zuber, J., et al. (2014). Development of siRNA payloads to target KRAS-mutant cancer. Cancer Discov *4*, 1182-1197.

Zhang, R., Lahens, N.F., Ballance, H.I., Hughes, M.E., and Hogenesch, J.B. (2014). A circadian gene expression atlas in mammals: implications for biology and medicine. Proc Natl Acad Sci U S A *111*, 16219-16224.

Yokota, J., Tsunetsugu-Yokota, Y., Battifora, H., Le Fevre, C., and Cline, M.J. (1986). Alterations of myc, myb, and rasHa proto-oncogenes in cancers are frequent and show clinical correlation. Science *231*, 261-265.

Yu, X., Zhang, Y., Chen, C., Yao, Q., and Li, M. (2010). Targeted drug delivery in pancreatic cancer. Biochim Biophys Acta *1805*, 97-104.